UNIVERSITÀ DEGLI STUDI DI CATANIA

Dipartimento di Ingegneria Elettrica Elettronica e Informatica

Adriano Scibilia

Control Modeling and Intention Estimation in Human-Robot Interaction

Ph.D. Thesis

Supervisor: Prof. Luigi Fortuna
Co-supervisor: Dr. Nicola Pedrocchi

Academic Year 2022 - 2023

Abstract

The study of human-machine interaction as a unique control system has been one of the first research interests in engineering, with almost a century of years since the first works. At the same time, it is a crucial aspect of the most recent technological developments in application fields concerning, for example, collaborative robotics and artificial intelligence.

The cross-domain nature characterizing this field of study can cause difficulties in finding a guiding line that links motor control theory, modeling approaches of physiological control systems, and identifying human-machine general control models in manipulative tasks. For this reason, I chose to start this thesis work by analyzing state-of-the-art linear models, from the first crossover model defined in the frequency domain to the successive optimal control model, to end with models including more detailed descriptions of physiologic subsystems and biomechanics. The motivation behind this effort is to have a complete view of the linear models that could be easily handled both in the time domain and in the frequency domain by using the well-established methodology in the classical linear systems and control theory.

Such model-based approaches aiming to characterize human behavior have been, as said, practically applied in a wide variety of scenarios. Among them, human-robot interaction is one of the most exciting, particularly in tasks where a continuous physical interaction between humans and the controlled plant is present. In this context, the human subject can adapt its control behavior to the external sensed dynamics. This capability significantly affects the control delay, making its characterization and prevision a crucial aspect to understand. I will address this topic in the third chapter of the thesis, where a linear modeling approach that uniquely describes human and robot control actions will be proposed and experimentally validated in a collaborative robotic task. Such manipulation task was performed by ten different healthy subjects with a collaborative low-payload robot.

In Human-Robot interaction, the possibility of increasing the intelligence and adaptability of the controlled plant by imitating human control behav-

ior has been an objective of many research efforts in the last decades. From classical control-theory human control models to modern machine learning, neural networks, and reinforcement learning paradigms, the common denominator is the effort to model complex nonlinear dynamics typical of human activity. This suggests that our analysis can't be limited to the linear models treated above but must proceed with nonlinear dynamics and the efforts that have been made to reproduce them. The fourth chapter investigates state-of-the-art nonlinear modeling techniques from the perspective of human control, considering the different physiological districts involved as the starting point and then proceeding with data-driven and model-based techniques able to describe higher cognitive processes such as decision-making and the creation of long-term strategy.

In the first place, transport systems are presented as an alternative technological scenario in which the discussed techniques have been mainly applied with success recently. Successively, going back to human-robot interaction, I propose a novel nonlinear modeling technique able to predict human force generated during a cooperative task with a controlled robot. The proposed Narmax model was constructed using an artificial neural network as a nonlinear functional approximator and was trained on the same dataset as the one used to validate the previous linear model. The same human model was then tested online with different subjects and, most importantly, on an industrial high-payload robot. This was done to demonstrate that the obtained performance were not derived from data overfitting but that a good generalization capability characterizes the model.

While a deep stability analysis of the system was not in the scope of this work, to avoid unstable and dangerous behavior, the robot has been controlled with an impedance control strategy characterized by a low stiffness value, resulting in compliant and safe movements. Moreover, the framework was controlled with a frequency higher than human motion by more than one order of magnitude.

A further step forward in showing how the proposed modeling technique can be useful can be pointed out by exploiting the partial knowledge that I have of the system, with reference to robot control law and its dynamics, to gain knowledge of the system from raw data in a simple and fast way. The case of study was once again the system delay, which this time was extracted from the human model's output with the aid of simple approximated system identification techniques. This process allows the user to easily extract the delayed information without complicated data processing.

Moreover, by analyzing the characteristics of human response during the proposed cooperative interaction with the controlled robot, a regular presence of peak values is evident, as a first reaction to the external forcing function.

Such peak values represent the most important feature to be known by the robot to anticipate human action, rather than having to estimate the whole force response sample by sample. For this reason, Peak-to-Peak Dynamics have been exploited to obtain a reduced-order model that is able to forecast the peak of human response in a reliable way. The effort in this sense is considerable, given that such techniques have been used in the past with different kinds of chaotic systems characterized by known attractors, but not to Narmax models.

Contents

List of Figures

List of Tables

Chapter 1

Introduction

In any system characterized by a close human-machine physical interaction, providing controlled elements with the ability to identify and understand what the human operator is doing is crucial to increase efficacy and safety. While this is an ability that humans naturally learn over time, machines need to be explicitly trained on how to do this. Such recognition problem is heightened by the dissimilarities between humans and controlled plants from a mental, computational, and physical point of view. These differences imply that, when faced with the uncertainty of the real world, machines cannot always count on humans to behave as expected and cannot always easily anticipate how they will react to an unexpected event [1]. One way this challenge can be addressed is by equipping machines with explicit models of their human teammates. Many different techniques are used to model human cognition and behavior, spanning different timescales and levels.

Modeling of the human control action when interacting with a controlled machine has become almost an independent research field over the years, involving multiple disciplines and approaches. Neurophysiologists and cognitive scientists have improved a lot in the understanding of human perception, information processing, and control strategies with respect to prior approaches, mainly focused on qualitative descriptions of possible human decisions and actions. Since the instrumentation and measurement techniques have dramatically improved, as well as the power of computational calculations, scientists have developed functional maps of neurons and identified deep brain functions [2–4].

Still, the human brain's dexterity and plasticity have a lot of mysteries, and how humans can interact and adapt themselves to unknown external dynamics is an open issue. Therefore, intense research was put into investigating motor control internal dynamics, perception, and learning. With particular reference to the study of input-output characteristics of the motor

apparatus, the concept of the internal model allowed significant advances for describing human adaptation to external dynamics and trajectory planning [5]. The concept underlying the internal model hypothesis found its origin in robot control. In fact, a robot needs knowledge about its internal kinematic model in order to perform any position or velocity control. The same concept was extended to human physiology when Ito [6] proposed that internal models of the limbs and connected brain regions are present in the cerebellum. The acquisition of inverse dynamics of the motor efferent systems, along with the inverse dynamics of the controlled object, helped us to explain how it is possible to perform fast and complex movements even if time delays and low gains characterize biological feedback structures [7]. An opposite approach for the same problem relies on equilibrium-point control models [8], in which the central nervous system is able to control muscle dynamics by simply acting on its threshold level.

Predictive simulations of human movement were also used to dissociate the contributions of neural and musculoskeletal impairments to gait deficits in cerebral palsy [9], evidencing the importance of a precise model of involved body parts and physiological districts to improve the correspondence between simulated and measured data [10]. The same was found in the rehabilitation robotics field, where mechanical impedance control parameters of the upper limbs of a human were identified in order to adapt the rehabilitation robot's training strategy [11,12] accordingly. Modeling approaches of this type linked mathematical descriptions typical of classical control theory with a functional description of physiological systems acting during the control process. This was able to link neurosciences with more practical engineering fields such as robotics and aerospace. Aerospace researchers had the first application scenario, which motivated an interest in this topic in the first decades of the last century. Starting from World War II, engineers' and psychologists' efforts were directed towards the modeling of human behavior as an inanimate feedback controller to improve the performance of pilots and bombardiers [13]. The first approach was to consider the human controller as an inanimate servomechanism, which can be represented in a simple feedback structure as a block with well-defined input(s) and output(s). In a manual human-in-the-loop control problem, the input of the human is an error signal, usually visual. Its output is human control actions, which provide a command to the controlled element (i.e., a gun, an aircraft, a vehicle, etc.). The same consideration is still valid in physical human-robot interaction, especially in those applications involving force or impedance control strategies. Here, continuous and compliant physical contact is required in order to perform cooperative kind of tasks, which can be reduced to mutual movement between humans and robots. In this case, the human operator should be able to

deviate from the robot's initial trajectory and impose a different one.

In such a context, the human operator will act as a proper motor controller by internally deciding the goal trajectory to perform and imposing an external force to achieve such an objective by manipulating the robot. From this point of view, the performance of the human operator can be well approximated as the action of an inanimate controller. This situation results in a simple compensatory manual control system. In [14], Hess explained this concept by giving the example of a human soldier performing a tracking task, attempting to keep a moving target within the gun's field of view. In this case, the angular error between the target and the azimuth of the gun's view fielder can be considered as input, while output control action is a force acting on a simple gear mechanism. Since the soldier is modeled as an inanimate servomechanism, the mathematical representation that was used to describe him should be the same used to describe a linear servomechanism: a set of linear differential equations with constant coefficients, or equivalently, as a transfer function in the frequency domain. The most famous example of this kind of approach is McRuer's crossover model, in which the human is represented as a general quasi-linear describing function. From this first approach, the development of mathematical descriptions of human controllers with a control-theory fashion evolved along with new control techniques. For instance, the development of linear quadratic Gaussian control systems (LQR), when applied to human operator's modeling, led to the "optimal control model." The same concept is valid for recent modeling techniques, such as fuzzy control models or models based on neural networks, which followed the spread of these techniques in systems design.

However, human modeling efforts, which started from this applicative scenario, successively have proved to be useful in many other domains of the engineering field. Classic examples are the design of display and control equipment interface based on man-machine environment system engineering in various types of plants [15, 16], and more recently, service robotics applied to healthcare [17, 18]. The understanding and prevision of human action have been extensively investigated in human-robot interaction (HRI) in the last years, being considered as input information to gather that enables a compliant and adaptive behavior of the robot. In [19], a task-adaptation framework was developed to allow robot compliance with respect to human movements. Similarly, in [20], gesture-based HRI was discussed, allowing an automatic task manager parametrization where the human can help or correct robot choices in collaborative assembly applications. While [21] and [22] tried to analyze the psychological and emotional implications of continuous interaction with a robot in a production setup. Behavioral criteria were also considered in HRI in commercial vehicles [23], where a scheme of mental

state variables can be used to modulate driving velocity and breaking in different moments of the day and night. In a similar context, machine learning techniques can also be applied to HRI intelligent transport systems [24].

Being most of these models the result of a very application-specific effort, their variability causes some difficulties when trying to find common features and divide them into general categories. In other words, every effort put into the definition of human control models originated from the need to describe its behavior in a particular situation. This was done starting from different perspectives and with different levels of abstraction. According to Rasmussen [25], human behavioral models, when interacting with an aircraft, can be grouped into three types: skill-based, rule-based, and knowledge-based. In skill-based models, the human-machine system is continuously controlled following a mission statement. Rule-based models provide a discrete decision-making description of human behavior, which is guided by a stored rule. The last category groups all the control strategies deriving from unexpected events or unfamiliar environments in which the human operator has to avoid dangers and risks. An example can be found once again in the pilot's control of an aircraft. Traditional control models are mainly part of the first category, while the development of modern artificial intelligence techniques has increased the use of models based on the other two. Xu et al. [26] proposed a different classification, identifying human models based on control theory, based on human physiology, and based on intelligence techniques. Classical feedback control models, such as McRuer's crossover model and the optimal control model, fall into the first category.

Successive modeling techniques in which a better description of all the underlying processes that determine the overall human control strategies were the Hess structural model and Hosman's descriptive model. Hess proposed a detailed description of human perception processes and inner loop feedback, while Hosman modeled the interaction between visual and vestibular inputs and their influence on the overall control strategy. Additional models belonging which can be associated with this category are biodynamic models, which try to include biomechanical effects of the body moving into an accelerating environment such as an aircraft or a vehicle. Equivalently to the previously described knowledge-based models, the models based on intelligent techniques include approaches dealing with uncertainty, such as fuzzy logic and neural networks.

In our analysis, the focus will be directed to models based on control theory, including the involved physiological structures. Moreover, human has both linear and non-linear behavior when interacting with a machine. This aspect is reflected in the classifications of control models, where both linear and non-linear dynamics are described.

In the first part of this work, the focus will be mostly on linear models. The second chapter will be structured as follows: In the first section, the main motor control theories will be addressed. Then, the second and third sections will detail the modeling approaches of neuromuscular dynamics and human sensory systems, respectively. The fourth and last section provides a description of the most important human-machine interaction models, in which the dynamics described in the previous sections are represented within a general control structure.

In the third chapter, starting from the state-of-the-art models described before, we propose a linear modeling strategy: the "Precision model of the human-robot complex." As it can be deducible from the given name, such modeling technique described the response of the whole system comprising both the human and the controlled robot. The simulated system response was compared with the measured response and with the response obtainable by simulating the system with a standard Crossover Model. Overall, the main application in relation to which the model was studied was the experimental identification of human reactive delay in a manual guidance task using the small collaborative UR5 robotic arm, where an external virtual reference (acting as a forcing function) was applied.

The second part of this work proceeds with the analysis by going into the details of nonlinear modeling strategies. Despite the successes, linear models lack in representing nonlinearities typical of human control behavior, especially when facing high-complexity scenarios. McRuer and Hess described the evidence of a pulsive behavior of the pilot when the demanded task is too complex, leading to the formulation of Dual Loop control models. They describe human bimodal control behavior, focusing on the error compensation (typical of classical crossover theory) and visual rate sensing (used in pursuit tasks with predictable inputs) [27]. The dual-channel structure proved to be more suitable for capturing nonlinear dynamics in the pilot system during the information processing stage, represented by thresholds and saturation elements, which were used for describing phenomena like Pilot Induced Oscillations (PIO) [28] or Spatial Disorientation (SD) [29].

In such a modeling technique, the human is considered a controller, an element part of the control loop (Human-in-the-loop control). Its sensing elements and muscle actuators' dynamics are related to the external stimuli, the executed task, and the controlled element. While executing a specific task, the human subject tries to optimize its behavior to achieve its goal while reducing efforts. If the difficulty increases, nonlinear dynamics is increasingly observable. Neuromuscular dynamics can be considered one of the primary physiological sources of nonlinearity in human control action. Modeling techniques in this context are often based on optimal control theory,

trying to identify the system's objective function that the human tries to optimize while executing a specific motion.

Aside from classical model-based approaches, a deeper focus on information processing and learning abilities is necessary to have a complete overview of the human as a controller. Different modeling and data-driven approaches have been proposed with this goal in many research efforts, even resulting in a combination of them. The model proposed by Xu et al. [30], for example, studied the origin of nonlinear PIO, proposing a multi-loop human pilot model during a multi-axis control task. Here, the pilot's ability to sense a changing situation, being based on experience and judgment, is represented by a fuzzy logic control element, able to modulate his strategy and, indirectly, the system input/output characteristics (through the variation of model parameters). Apart from multi-loop models, fuzzy logic techniques have been used in association with other nonlinear system modeling approaches and control techniques in order to deal with uncertainties in the external environment [31] or in model parameters tuning [32]. For instance, Fuzzy systems and Artificial Neural Networks (ANN) have been successfully used in hybrid models in the past for human operator tuning [33] or parameter optimization of the controlled plant [34]. The spread of such kind of hybrid models led to the development of neuro-fuzzy systems, which will be discussed in detail in Section 4.3.3.

Due to their simple mathematical structure and low computational cost when implemented, ANNs have been successfully used in the presence of unstructured data in learning, classification, and prediction algorithms in computer vision [35], autonomous driving [36], medical [37, 38], bio-informatics [39], industrial [40] and rehabilitation [41, 42] robotics.

In human-machine interaction, however, it may be important to capture temporal relationships between raw data in order to identify the system model accurately. Special kinds of ANNs, such as the Recurrent Neural Network (RNN) [43,44] and the Long Short-Term Memory network (LSTM) [45], are very common for this purpose, thanks to their internal loops between the hidden layers, which in the case of LSTM allows capturing even long-term temporal relations. Further details on these two architectures will be given in Section 4.4, as well as another data-driven approach, such as Reinforcement Learning, useful to model human decision-making and the generation of its internal goal. Classical supervised, unsupervised, and semi-supervised learning methods are introduced to represent how a "human controller" creates a strategy to achieve a long-term goal, passing through several intermediate steps. There is a wide variety of practical applications exploiting such techniques [46–49]. Remarkably, the optimal control theory modeled the human control action by identifying its internal cost function to minimize, similar

to the reinforcement learning approach. Indeed, in such a case, the human decision-making process is modeled by describing its objective function, which is maximized by the subject during its actions.

The mentioned modeling techniques, from the classical control theory to the modern data-driven approaches, have succeeded in representing a different aspect of the human control strategy when interacting with a machine. Application scenarios such as intelligent transport systems or human-robot collaboration offered many examples of modeling and control techniques, which have been developed by combining two or more of these approaches.

This latter concept has been used to construct a Nonlinear auto-regressive model of the human subject, with moving average and Exogenous input (NARMAX). Narmax models are the nonlinear evolution of the famous linear ARMAX models [50], and became a golden standard on how to construct models from complex and partially unknown systems [51]. The proposed Narmax model was constructed by using an Artificial Neural Network for approximating the nonlinear functional relationship between input data, using the Universal Approximation property of NNs.

In Chapter 5, the human model was defined and trained in the first part using the same dataset acquired in the previous proposed linear model of the third chapter. In the second part of the chapter, the nonlinear human model was applied in a different setup using a high-payload Comau NS16 robotic arm. This way, the model performance with new and different data can be discussed and compared to the ones obtained with the first dataset. Most importantly, the model is now used online, also testing its speed and practical usability. The fact that the Comau arm is not a proper "collaborative robot," built exactly for the purpose of performing tasks with human subjects around, makes this scenario the perfect case in which the controlled plant would have a great benefit on gaining information about the human user, to estimate its intention and better collaborate with him.

In the following chapter, we will see how the proposed model can be used, due to its accuracy, to extract the delay information from data (as previously done with the Precision Model) in a fast and simple way, exploiting the knowledge that we have about the controlled element's dynamics.

In the last chapter of this thesis, the model's ability to forecast the next peak of the output signal was analyzed. The regular presence of peaks in human control output (which corresponds to its applied force) makes really interesting to evaluate such aspect to study the eventual presence of Peak-to-Peak Dynamics (PPD) [52]. As we will see more in detail in the last chapter, PPD have been described and studied extensively in a wide range of chaotic systems and models, being able when observed, to reduce model's order without loss of accuracy.

Chapter 2

Linear Models

2.1 Motor Control in the Central Nervous system

Motor control dynamics in the human nervous system have been widely studied by neurophysiology researchers over the last few years with different approaches. One of the most promising assumes the existence of internal models of sensory-motor output dynamics in the central nervous system (CNS). In [53], it is suggested that the cerebellum forms two different types of internal models. One of them is a forward predictive model of the motor apparatus (e.g., limbs and muscles), providing a rapid prediction of the sensory consequences of each movement. The second is a model of the time delays in the control loop (due to receptor and effector delays, axons, conductances, and cognitive processing delays). This second model delays a copy of the rapid prediction so that it can be compared in the temporal register with actual sensory feedback from the movement. Both models can coexist and form two Smith predictors. In [54], it was experimentally verified that human subjects were able to estimate the hand position without visual feedback and with applied external disturbances, supporting the evidence that the central nervous system internally simulates the dynamic behavior of the motor system in planning, control, and learning. The existence of such internal models of motor dynamics and temporal delays in the central nervous systems has been discussed a lot in cognitive science and neurophysiology fields. The necessity for internal models in motor control has been one of the central issues of debate in relation to other approaches to motor control theory, such as the equilibrium-point control [8].

In the equilibrium-point control or threshold control theory (TCT), motor actions are controlled by changing neuro-mechanical parameters, which

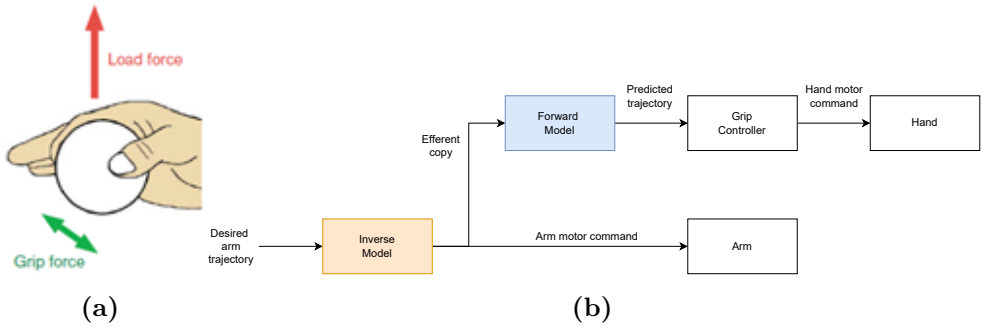

Figure 2.1: Example of how a control structure based on internal models in the Cerebellum can be used to explain human's coordination of load and grip force in a simple grasping task, as studied by Kawato in [55]

establish the steady state (equilibrium point), which is commanded to lower levels (e.g., muscles and limbs) by descendent systems. The neural control variables that determine the equilibrium point are identified in the λ model [56]. As known, muscle activation by efferent neurons and motor units is triggered by a variation in muscle length. When a muscle is quasi-statically stretched, the potential in the motoneuron membrane increases, and after that, a certain threshold value is reached, and the motoneuron starts to be recruited. Physiological data indicates that such threshold length value comprises various factors besides its central component. If the central component is λ, the composite value is:

$$\lambda_c = \lambda - \mu\omega - \rho + \epsilon(t) \tag{2.1}$$

Where μ is a temporal parameter related to the dynamic sensitivity of muscle spindle afferents, ω is the velocity of change in the muscle length, ρ is the shift in the threshold resulting from reflex inputs (such as those responsible for the inter-muscular interaction and cutaneous stimuli) and $\epsilon(t)$ represents temporal changes in the threshold resulting from intrinsic properties of motoneurons. In equation (2.1), the CNS controls both λ and μ parameters. Therefore, according to the position TCT theory, high control levels can control muscular activation minimizing the difference between the actual length and the one established by the threshold. Let's consider a situation in which the human subject is asked to hold an object; according to TCT theory, the gripping force is set in such a way that the difference between the threshold length (established by the physical shape of the object) and the actual, which is set to be virtually inside the object, is minimum. This operation results in the object being held using the minimum quantity of gripping force. The same situation, as shown in Figure 2.1, was considered

from another point of view by Kawato in [55]. Here, the coordination of reaching and grasping, which allows using the minimum grasping force to prevent slip when lifting an object, was considered proof of the existence of the limbs' internal inverse and forward models. When the arm grasps an object, the inverse model of the combined dynamics of the arm, hand, and object computes the necessary motor commands from the desired arm trajectory. Such commands are sent to the arm muscles and to its forward dynamic model, which can predict the future trajectory and establish the grip force necessary to lift it, considering its friction and a certain safety factor.

Actually, alternative explanations of how such predictive capabilities can be possible without internal models also exist. They are linked to biological systems' "strong predictive" and anticipatory properties. In [57], strong predictive systems are defined as those in which predictive properties are inherent in the systems' natural dynamics and thus do not rely on internal models. At the same time, weak predictive systems are based on internal models of themselves. Another motor-control case study that was analyzed to highlight the differences between the two approaches is the formation of an arm trajectory [58]. It is known that muscles and peripheral reflexes control loops have spring-like characteristics, which can pull back the limb's joints to their equilibrium positions. This is done by generating a force directed against the sensed external perturbations. Such viscoelasticity can be considered as the static gain of the peripheral feedback control loop and can be adjusted by properly setting the associated muscle co-contraction level and the reflex gain.

The equilibrium-point control hypothesis implies that through this viscoelasticity, the brain can control the movements of the limbs by simply setting a series of stable equilibrium positions aligned along the desired trajectory [59, 60]. An experimental study of this concept has been presented in [61], where the data of [62] were reinterpreted in an equilibrium control fashion with a straight equilibrium trajectory. However, this approach requires viscoelastic forces to increase proportionally to the movement speed since the dynamic forces exerted on multi-joint links depend on the square of the velocity. Differently, the alternative explanation implying the internal model control allows the realization of accurate and fast movements even considering low viscoelastic forces [63–65]. Experimental evidence of a relatively low stiffness observed during movements performed by a well-trained subject has supported the latter hypothesis [66, 67]. Another step forward was integrating the two approaches, muscle viscoelasticity and internal models, through computational models to learn the behavior and applications of internal models efficiently [68, 69]. For example, in [66], the authors showed

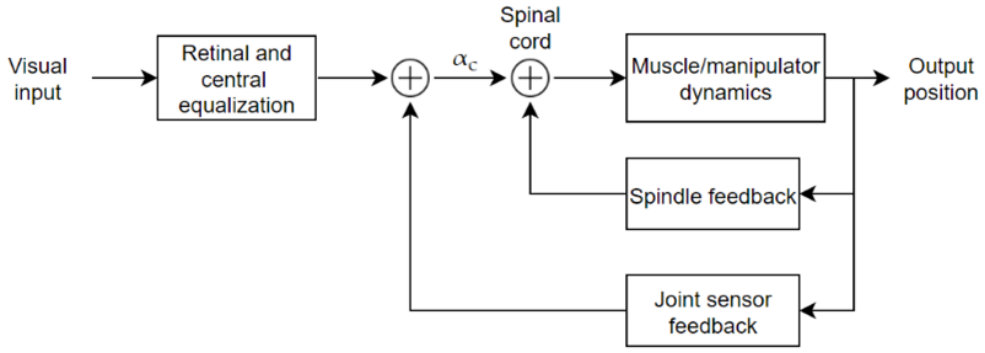

Figure 2.2: Model of subsystems contributing to neuromuscular dynamics in manipulative control tasks, as studied by McRuer et al. [70]

that intrinsic muscle stiffness is not strong enough to stabilize upright posture; using internal models was suggested as an alternative explanation.

2.2 Neuromuscular Dynamics Model

The neuromuscular system dynamics model has been widely investigated in manipulation tasks starting from the early '60s. Typically, muscles and manipulators are considered as a unique function. An example of what can be involved in the muscle-manipulator dynamics was studied in [70]; a simple block scheme of neuromuscular subsystems is shown in Figure 2.2. Retinal and central equalization transfer function changes according to the considered forcing function dynamics. This block was represented by simple gain and delay factors in [70] for a rate stimulus, but changes for other controlled elements. The alpha motor neuron command α_c is the command input from higher centers down to the spinal cord. There, the change in the average firing rate of the alpha motor neurons involved is proportional to the effective driving force. The commanded force signal then goes to the muscle/manipulator block, whose dynamics, as said, are represented by a unique transfer function that consists of a third-order system with one real root and a quadratic pair plus a time delay, being:

$$H_{MM} = \frac{-K_I e^{-\tau_\alpha s}}{(1+\tau_N s)(1+\frac{2\xi_\alpha}{\omega_\alpha}s)+\frac{s^2}{\omega_\alpha^2})} \tag{2.2}$$

The muscle characteristics are functions of the steady-state isometric tension of the muscle system operating point. The changes in this average ten-

sion are caused primarily by changes in the gamma motor neuron system discharge. The effects of the gamma neuron bias signal, while not shown explicitly in Figure 2.1, is used to set up the spindle feedback operating point equalization, whose block also approximates the Golgi ten-don force feedbacks, and the corresponding describing function is:

$$H_{sp} = \frac{K_{sp}(s + Z_{sp})e^{-\tau_{sp}s}}{(s + P_{sp})} \tag{2.3}$$

The effective joint sensor provides A second feedback loop, represented by a gain factor and a time delay $K_j e^{-\tau_j s}$, operating in the frequency region of interest. Therefore, the closed-loop neuromuscular system has third-order dynamics plus a zero due to the spindle pole in the feedback loop. Data obtained by McRuer et al. [27] indicate that the muscle/manipulator dynamics for rudder pedals and hand manipulators are similar in form and numerically, despite the difference in limb size and function. In [71], Van Paassen et al. suggested an extension to the model in which the manipulator and the human arm are not unique blocks anymore, but their interaction is considered. Such kind of analysis is useful in application scenarios in which the human subject is operating while subjected to accelerations (i.e., in a moving vehicle) or it is using active manipulators in which an active servo element is used to provide feedback from the controlled system or from other sources in the environment.

Research efforts have also been addressed towards analyzing the relationship of human performance in manipulative tasks and muscle fatigue dynamics. An example of such muscle fatigue and recovery models is proposed in [72], which links the maximum voluntary contraction (MCV) to the output isometric force in a cycling application. Liang et al. [73] proposed a model in which the muscle capacity after a certain number of contractions is evaluated and put in relation to the external load force. A further extension of this analysis also considered the relationship of MCV with brain effort, distinguishing between fatigued and non-fatigued motor units [74]. Other research activities that rely on different types of modeling techniques were used, such as in [75] and [76], where a bond graph mathematical model was used to describe biomechanical characteristics of upper limbs tendons during grasping. In [77], bond graphs were used to describe the extensor mechanism of a finger, being represented as deformable strings, and assumed to pass through hooks fixed at predetermined points on rigid phalanges.

However, all the descriptive models of neuromuscular dynamics in the literature operate in high frequencies. This consideration leads to the fact that when neuromuscular dynamics are considered as an element of a more general control model, such as the ones that will be analyzed in the next

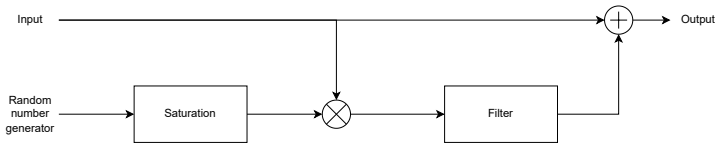

Figure 2.3: Visual cue perception model proposed by Curry [79]

section, often only their low-frequency effects are taken into account. Such effects can be simplified as a delay element.

2.3 Sensory Dynamics

Although all sensory organs are well known individually, as well as their dynamic behavior, their joint role with CNS in perception has been of interest to further investigation even recently [54]. One example that motivates recent interest in sensory dynamics modeling is the operator's disorientation. Although it is commonly taken for granted that reality can be accurately perceived, situations in which a human is subject to continuous rotations may lead to spatial disorientation. Spatial disorientation occurs when the human operator fails to perceive his correct position, motion, or attitude correctly. Research works in this field date back to the latest decades of the eighteenth century, initiated by Ernst Mach and his colleagues with a study on vestibular and acoustic perception. However, true progress will be obtained only after almost a century, in the 1990s, when mathematical modeling of spatial disorientation was proposed [78].

2.3.1 Visual System

The human visual system is our sensory system's primary information source. It was vastly studied as a mathematical model with reference to computer vision techniques or the development of simulators for vehicles or aircraft. The importance of this sensory modality in the last-mentioned application scenario is confirmed by the fact that such a simulator very often relies on a fixed-base structure, thus not stimulating the vestibular system. Human vision can operate mainly in two modalities: ambient or focal mode.

The ambient mode mainly intervenes with human's spatial orientation capabilities and relies on several inputs from the central and peripheral vision systems, such as motion, perspective, texture, and brightness gradients. The most interesting characteristic of this visual mode is its capability to subconsciously process if there is any disturbance over the aforementioned

input signals and provide a stable perception covering a large spatial range. This is done by sending low-frequency, robust signals to the CNS, which uses this information to determine spatial orientation. Oppositely, other sensory systems provide high-frequency transient signals to help stabilize the perceived surrounding environment immediately after motion. The ambient mode is very useful for perceiving distance and the angle between the operator's plane and the ground (i.e., slant). Lone and Cooke well described the possible sources contributing to the spatial disorientation (SD) of a pilot guiding a vehicle [29]. Visual perception of both slant and splay angles, being respectively the relative orientation in the vertical and horizontal plane, can lead to misjudgments about human's estimation of the controlled element's actual position.

The focal mode is linked to object identification and relies mainly on binocular signals coming from the central visual field. It provides very detailed information at high spatial frequencies and is usually represented in conscious states [80]. Figure 2.3 represents the visual perception model that Hess proposed in [79], providing a simple way to model visual observation. Saturation limits can be set by considering two times the value of the variance of the random number generator input. Consequently, the variance determines visual signal quality and is related to the relationship between usable cue environment (UCE) and visual cue rating (VCR) [81, 82]. Its value can be selected between the following ranges:

$$0 < \delta^2_{VIS} < 0.1 \quad \text{if} \quad \text{UCE} = 1 \tag{2.4}$$
$$0.1 < \delta^2_{VIS} < 0.2 \quad \text{if} \quad \text{UCE} = 2 \tag{2.5}$$
$$0.2 < \delta^2_{VIS} < 0.3 \quad \text{if} \quad \text{UCE} = 3\,, \tag{2.6}$$

Such parameter has been extended to task-dependent variance related to vision with multiple axes:

$$\delta^2_{task} = \begin{cases} 0.01n & \text{if} \quad n > 1 \\ 0 & \text{if} \quad n = 0 \end{cases} \quad . \tag{2.7}$$

Being n the number of controlled axes. The two terms can be incorporated into the following factor:

$$f = 1 + 10(\delta^2_{VIS} + \delta^2_{task}) \tag{2.8}$$

Along with the global view of vision modalities, human vision was also studied in relation to object tracking, particularly in computer vision and image processing fields. Nguyen et al. [83] recently developed a tracking model

that utilizes the spa-tial-temporal context information to increase tracking accuracy level. Further improvements in visual tracking research were the widespread adoption of discriminative learning methods [84]. These types of classifiers are tasked with distinguishing between the target and surrounding environment, often used in order to ensure target tracking in the presence of occlusions [85]. The latest trend in the field is multiple object tracking [86]; the challenge, in this case, relies upon locating multiple objects, maintaining their identities, and yielding their individual trajectories given an input video (in the case of computer vision applications). Object to label in this case can be pedestrians [87] or vehicles [88] in the road safety management field.

2.3.2 Vestibular system

The vestibular system is responsible for human equilibrium, postural control, and the proprioceptive sense of body motion. Anatomically, it is housed in the inner ear and can be divided into semicircular and otolith canals. The otoliths perceive a sense of tilt and force, while semicircular canals help provide the sense of angular acceleration. Accurate analysis and estimation of their dynamic response have been crucial for human perception modeling when interacting with any mobile-controlled machine.

Angular motion, characterized by low amplitude, is limited by inherent thresholds, which are a function of the stimulus magnitude and its duration. Mulder's law describes angular accelerations with a duration inferior to 10 seconds as the product of angular acceleration, and its duration is approximately equal to 2.5 deg/s. This means that a weaker acceleration requires more time to be perceived from vestibular canals. In the aerospace domain, experimental studies on human sensory thresholds for angular velocities and accelerations characterized by prolonged duration have been done [89]. It is suggested that such thresholds can vary depending on the nature of the controlled elements. For example, flight can be slightly higher with respect to a car due to more stress and, consequently, the pilot's attention level and allocation. The pilot's experience and training contrast this effect; in this case, the human has an accurate internal model of the machine's dynamics, allowing him to have a certain degree of knowledge in advance and lower the threshold. In summary, the workload, stress level, and training level strongly impact the human sensing abilities of a rotational motion. Being very difficult parameters to quantify, an accurate model of threshold dynamic variation is very hard to obtain. The main role of otoliths relies on the sense of linear accelerations and vertical motions, with threshold levels of 0.1g and 2 degrees. Otolith canals cannot differentiate between acceleration caused by gravity and other linear accelerations. The sensed motion should always

be considered as an apparent vertical motion since there is no difference in the way humans can perceive tilt and linear accelerations.

Further attempts to model the vestibular system led to the development of Hosman's descriptive model, whose main purpose was to integrate visual and vestibular dynamics, which will be better discussed in Section 5.

2.3.3 Proprioceptive systems

One of the first senses to develop in a human being, are without doubts tactile and proprioceptive senses, since they are mandatory for determining the gravity vector and consequently develop the necessary anti-gravity group of muscles, which allow us to walk.

Proprioception, which is also called kinesthesis, refers to such sensory modality which uses muscles spindles to determine the position of body and limbs of the subject, as well as their movements and the joint torques required to start a motion or maintain a steady position against resistive loads. In human-machine interaction, the role of tactile and proprioceptive systems is linked mostly to the force and pressure feedback that the operator has due to the physical contact with an aircraft inceptor, a vehicle steering wheel, or a robot's end-effector.

Pressure receptors are located within the skin all over human body and are of primary interest in the development of modern haptic feedback devices, able for example to provide information about a surface texture belonging to an unknown external environment in teleoperation frameworks.

The modeling of this system is difficult because of the huge number of physical stimuli which trigger its response. Classical factors that trigger an output of the proprioceptive system directed to the CNS are for instance: relative linear and angular velocity, muscle tension and its orientation with respect to the gravity vector. Usually, all these inputs are sensed and elaborated simultaneously. Since, as it is noticeable, some of these factors also stimulate other sensory systems, the CNS combines in case of conflict the multiple received sensory information to develop its own proprioceptive sense. For this reason, proprioception cannot be seen as a unique sensorial system like visual and vestibular ones but should be considered more like a sense developed as a combination of different sources of information. Hess provided a transfer-function representation of proprioceptive dynamics in his "structural model", which will be discussed in detail in Section 5.

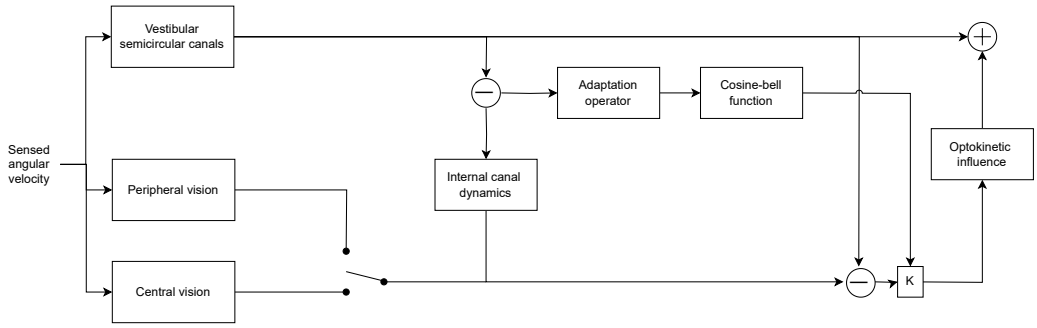

Figure 2.4: Telban and Cardullo's rotational perception model [92]

2.3.4 Inter-sensory models

A relatively recent field of study is the human cognition associated with multi-sensory stimuli. The first steps in this context were provided, once again, by neuroscientists such as Halligan [90] and Lotto [91], even if the considered interaction between senses were limited and focused on forms of synesthesia and go towards a brain function associated with a high level of complexity.

Multi-sensorial perception is mostly modeled as a simple linear summation of inputs, or as a weighted sum, with an almost arbitrary selection of weights. The most complex developed model is Hosman's descriptive model, which has a non-linear combination of visual and vestibular stimuli.

Telban and Cardullo proposed a model able to capture the perception of rotational motion, parametrized in order to match latencies experimentally observed in [93] and [94]. This model is able to analyze inputs coming from peripheral and central visual fields, as well as vestibular inputs. The rotational perception model, which is represented in Figure 2.4, provides the computation of the perceived angular velocity, given the actual inputs coming from the two considered sensory systems, where the semicircular canals represent the vestibular one. A similar model is the translational perception model, in which the perceived velocity and acceleration are obtained given the actual specific force. Vestibular dynamics in the latter case are represented by the otolith canals, which respond to specific force stimuli, while the visual system processes the velocity information, which is mathematically represented as an integrated acceleration. Back to the rotational perception model, peripheral and central vision are considered time delays, respectively set to 90 ms and 150 ms [95]. Further psycho-physical experiments have given evidence that visual perception of self-movements can induce an artificial vestibular response [29]. The opposite process can also happen, even if to a limited degree. This model's main feature is the capability to represent

such influenced esteems of self-movements. Optokinetic influence components provide both a nonlinear gain element and a fist order low pass filter. The gain element is able to represent the weight given to vestibular and visual perceptions and is calculated from a cosine-bell function, which links it to the difference between them. The low-pass filter models the semicircular and otoliths canals, implicitly assuming that the CNS compares the visual stimulus with its estimation of vestibular response. For what concerns vestibular models, a certain degree of correspondence can be noticed between the model proposed by Fernandez et al. [94], Telban et al. [94], and Hosman [95]. In all of these models, the otolith organs respond to a specific force, defined as:

$$f = \hat{g} - a_h \tag{2.9}$$

Here, $\hat{g}$ represents the local gravitational force vector, while a_h is the acceleration of the head of the human operator with respect to a fixed reference frame. Assuming, for the sake of simplicity, that the operator's head is aligned with the fixed frame axes, it is possible to obtain the transfer function between sensed and actual force:

$$\frac{\hat{f}(s)}{f(s)} = \frac{0.4(13.2s+1)}{(5.33s+1)(0.66s+1)} \tag{2.10}$$

While for what concerns the perceived and actual angular rotations, the transfer function can be expressed as:

$$\frac{\hat{\omega(s)}}{\omega(s)} = \frac{456s^2}{(5.7s+1)(80s+1)} \tag{2.11}$$

Providing a reliable representation of vestibular canal dynamics. The adaptation operator element indicates the maximum time for which it is possible to have a conflict between vestibular and visual inputs. This is done by relating the inter-cue error to the washed-out error:

$$\frac{e_w(s)}{|e(s)|} = \frac{\tau_w s}{\tau_w s + 1} \tag{2.12}$$

where τ_w represents a time constant. Simulation results of the model [29] showed that the model is capable of representing the difference between the transient nature of the vestibular response and the constant presence of visual stimuli in human motion perception.

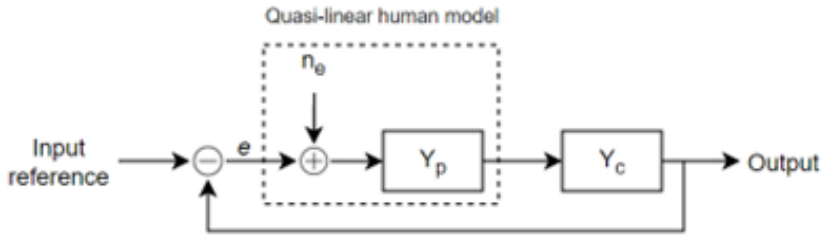

Figure 2.5: Simple feedback structure for a human-machine complex in manipulative compensatory tasks according to crossover model

2.4 Human-machine control models

In this section, human models will be discussed from a global point of view, with a control-theory approach. In the presented models, the human-machine system is described with a task-dependent approach, typical of control science. Here, significant variations can be noticed regarding the contribution of physiological structures described in the previous sections as subsystems in the overall model, as well as the abstraction level of their mathematical representation.

2.4.1 McRuer's Crossover Model

From the very beginning of the studies in this field, McRuer et al. [70] analyzed human control action in compensatory tasks by randomly changing the target reference trajectory which the human had to follow. The result was one of the most common and simple examples of a human control model, McRuer's Crossover (CO) model, also known as the quasi-linear model. The quasi-linear model hints at how humans adapt to different plants to elicit stable and effective control responses.

It can be convinced that such a model exhibits the behavioral invariance of the human in its adaptation to the controlled machine, offering a consistent human-machine behavior where the functional block diagram can be described as a simple compensatory manual control system. Due to its simplicity, the model proposed aim is to avoid common problems related to higher complexity systems.

It was observed that when an external disturbance is introduced in the system, measured human operator responses were different for different transfer functions of the controlled plant, but the combined human-machine behavior is approximately the same for all the experiments. The following equation can describe the transfer function of the combined human-machine

system:

$$Y_p(j\omega)Y_c(j\omega) = \frac{\omega_c}{j\omega}e^{-i\omega\tau} \tag{2.13}$$

Where ω_c is the crossover frequency of the system, and τ is the overall delay in human response. Such an equation indicates that the behavior of the human-machine complex can be described as a simple integrator and a delay in the crossover region. If we isolate the human controller from the controlled element, the whole system relating a voluntary motion can be simplified into three components: a linear controller inside the brain, a neuromuscular dynamic, and a reaction time delay.

After the learning phase of the machine dynamics is sufficiently finished, the human can be considered as a simple feedback controller which moves the controlled element to the target position, in case of a point-to-point- task (PTP), by watching the reference target point.

The neuromuscular dynamics, as said, can often be approximated by a first-order lag, as demonstrated also in [96], and the simplest human controller was modeled as a PD controller in [97]; therefore, the human transfer function $Y_p(s)$ can be described as follows:

$$Y_p(s) = K_p\frac{\tau_L s + 1}{\tau_I s + 1}e^{-\tau_e s} \tag{2.14}$$

where parameter K_p is the pilot's gain, τ_L is the lead time constant, τ_I is the lag time constant, and τ_e is the pilot's reaction time delay. The parameter selection is carried out by using the adjustment rules. According to the model, the reaction time delay should be constant for each human subject [98], with small variabilities due to task and environmental variables.

In the quasi-linear model represented in Figure 2.5, McRuer introduced the remnant noise term n_e to account for the non-stationary effects of the pilot behavior. The remnant was described as a random process, linearly uncorrelated with the control input. Normally, the remnant is related to the error signal $e(t)$. Therefore it is here considered as the observation noise.

Although being born to describe pilot dynamics, the crossover model has become a benchmark in human control models for a variety of applications and controlled elements. For instance, a generalization of the crossover model is proposed in [99], characterizing the human control of systems with both integer and fractional-order plant dynamics. Or, in teleoperated surgical robotic systems [100], it can be used for a detailed characterization of operational delay in order to improve control precision.

2.4.2 Optimal Control Model

The optimal control model has been developed by Kleinman et al. [101, 102] and Wierenga [103] in the first place, in consequence of the advances in optimal control theory, which can be observed between the seventies and the eighties. The main concept behind it is that after a certain level of training and motivation, a human operator can control a machine in an optimal manner, even if it remains subject to physical and psychological limitations. The first observable difference from the crossover model is that the optimal control model was expressed using state space variables, which makes it easier to extend human-machine analysis to multi-loop control tasks.

Figure 2.6a shows the first simple version of the Optimal Control Model (OCM). If we consider a visual input reference y, the first process to consider is the pilot's reactive time delay, while the signal y_p is the perceived input signal, namely the internal image of the actual input y in the CNS of the human pilot.

Neuromuscular dynamics make the pilot execute the optimal control and can be expressed by a first-order lag $\frac{1}{\tau_N s+1}$. Moreover, u is the output human's control action, x is the internal state vector of the controlled element, w is an external disturbance and y is the vector containing external sensed measurements. The elements of estimation and decision consist of the following:

- Kalman filter, which is used to model human's ability to deduce a system state from perceived information
- Kalman predictor, which represents the compensation for inherent time delay
- Optimal feedback, which builds optimal control u_c based on y_p input.

All of these elements require a model of the controlled machine and, therefore, can be considered as the human's internal representation of the machine's dynamics, with all the deriving linearization processes and other psychological limitations [105].

The order of the model is dependent on the human training level and expertise and can include limited models of actuation systems. The validation of OCM can only be performed with a black-box approach, comparing its output to real human control outputs. In systems in which a single input is considered, the performance index reflecting human control strategy can be expressed as the following quadratic cost function:

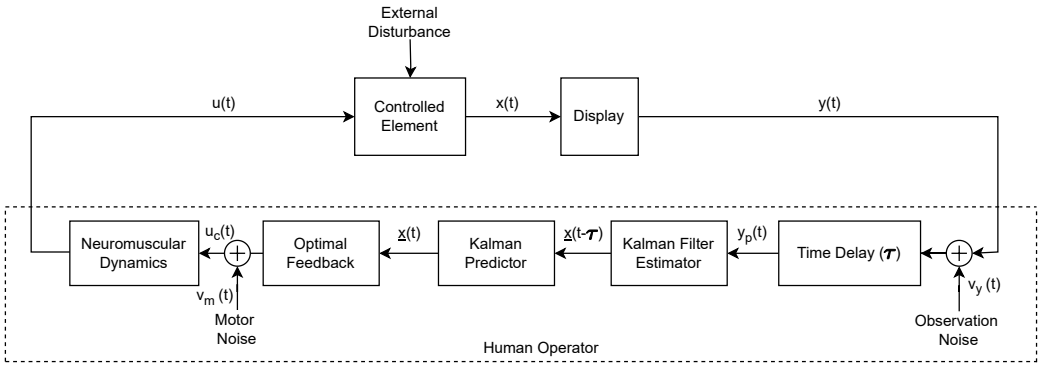

(a)

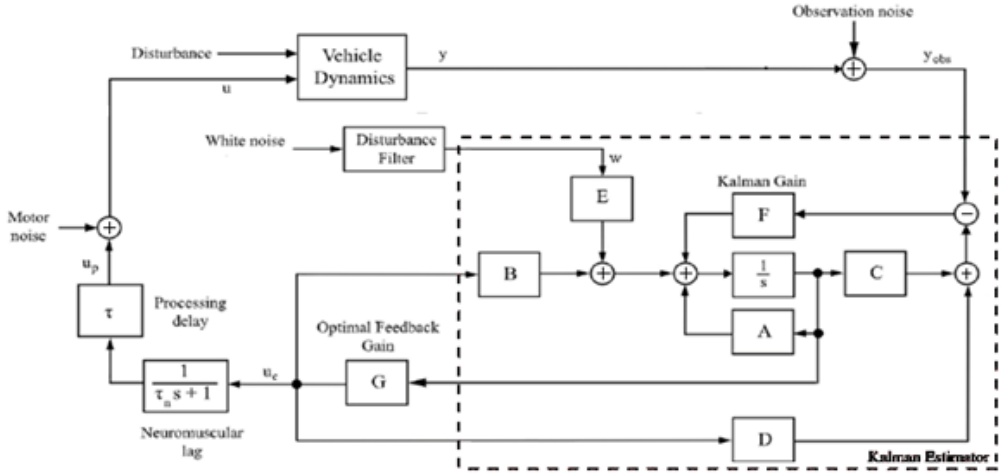

(b)

Figure 2.6: 2.6a Optimal control model of the human operator, as defined by Kleinman et al. in [102] 2.6b Modified version of the Optimal control model for pilot-vehicle dynamics [104]

$$J = \lim_{T\to\infty} \frac{1}{T} E\left\{ \frac{1}{2} \int_0^T (y^T Q y + g\dot{u}^2) dt \right\} \tag{2.15}$$

where E is the expected value, Q is the weight coefficients matrix, while g is a real weigh coefficient chosen so that $g > 0$. In manual control compensatory experiments, the element $y^T Q y$ is usually set in order to minimize mean squared error; here, the determination of Q was performed only by using empirical methods. Moreover, the factor $g\dot{u}^2$ sets a superior threshold on the total energy which can be used in a control task. The inclusion of such a term into the cost functional results in a first-order lag, which is of-

ten associated with neuromuscular dynamics [101]; in fact, given the other parameters of the model, there is a direct proportionality between g and τ_N. Moreover, along with empirical methods, the values of model parameters were also numerically computed by identifying the OCM model in [96] and [106].

However, the model accuracy when matching real data has not been significantly improved with respect to traditional control models, which indicates a certain over-parameterization. For this reason, OCM has been improved to the form of a modified optimal control model (MOCM) developed by Davidson and Schmidt in [104] and represented in Figure 2.6b. Another modification developed in parallel led to the fixed-order OCM [107]. Both of them offer transfer function representations with frequency domain analysis. This work can be considered as the transition phase between the classical frequency domain and more recent time domain approaches. However, the simplification process which motivated their development was contrasted by their complexity. Evidence of this concept is that Schmidt himself chose to use the full parameter model for capturing the effect of aircraft elasticity in his human-in-the-loop simulation and analysis [108].

A revised optimal control model (ROCM) of a pilot, which is based on the aforementioned modified version, was also presented in [109]. This model was later extended for the analysis of different aspects in further research works: human decision-making in [110], its monitoring behavior in [111], the execution of multiloop tasks in [112], and multimodality in [113], where models of semicircular and otolith canals of the vestibular apparatus were provided. Overall, the optimal control model was used to solve a number of applicative control issues, mainly in pilot-aircraft interaction tasks, such as the prediction of flying qualities [81] and the use of such predictive capability in refueling tasks [114]. Other research activities were dedicated to the definition of a relationship between Cooper-Harper ratings and the cost function expressed by equation (2.15) in both single and multi-loop tasks [115, 116]. Moreover, the optimal control model was used for many other applied research activities, such as the simulation of pilot control strategy when encountering wake vortex [117], the assessment of loads in airframe flights [118, 119], or the investigation of display dynamics on the control loop, in order to obtain relationships between display types [120, 121] and ratings of the human operator [106], as well as many other research, works [122–127].

2.4.3 Structural Model

In spite of the successes of linear models described in the previous sections in investigating the relationship between human control dynamics and handling

qualities, as well as their application to analysis/design problems, they both lack an accurate description of the underlying physiological control structure contributing to human pilot dynamics [128]. Moreover, further research done in the same period showed that when the difficulty of a control task increases, the human control behavior becomes highly nonlinear.

Hess's studies were motivated by two main observations: (i) human operator control strategies often seemed to result in discrete or impulsive motions, and (ii) such experimental evidence was not linked to any feature of the classical linear control models. The main assumption of such investigation was that the operator, when associated contemporarily with a high-order-dynamics vehicle and a difficult task, tends to reduce the overall complexity load associated with the time integration of multiple sensory inputs [129]. This simplification is done by simply adopting a nonlinear strategy relying on a limited number of parameters (rather than a linear strategy associated with a high complexity level and the number of parameters).

The first development of these assumptions can be found in the isomorphic model [130], which can be considered the father of the successive structural model described by Hess. The main idea relying on them is to better describe human signal processing by determining feedback paths from the sensory modalities involved in perception and motor control. The human equalization process, namely human's "proprioceptive" feedback, occurs through this simulated feedback path, whose parameters were tuned to match the performance of the quasi-linear model near the crossover region [131,132].

Figure 2.7 shows a block scheme representation of the structural model. Here, the element Y_{d_e} is the transfer function of visual dynamics when perceiving its input signal from a display. Moreover, n_u represents the remnant noise and, as in the quasi-linear model, is considered as an observation noise (and, therefore, put in the human's output), while d is an external disturbance that acts on the controlled element. The parameters K_e and $K_{\dot{e}}$ are the gains of the central processing stage, while τ_0 and τ_1 represent the correspondent time delays. In this model, the pulsing logic $Y_{p_1} = 1$ [133] and element

$$Y_m = \frac{K_m}{(s + 1/T_m)(k - 1)}$$

describes the aforementioned pilot inner-loop feedback. The key aspect is the selection of parameter k, which can be interpreted as the pilot's internal model of the controlled element dynamics and reflects the adaptive characteristics of the human pilot. It will mainly depend upon its transfer function around the crossover frequency.

In the crossover region, it becomes $Y_m \propto sY_c$. Therefore, the following general considerations can be made:

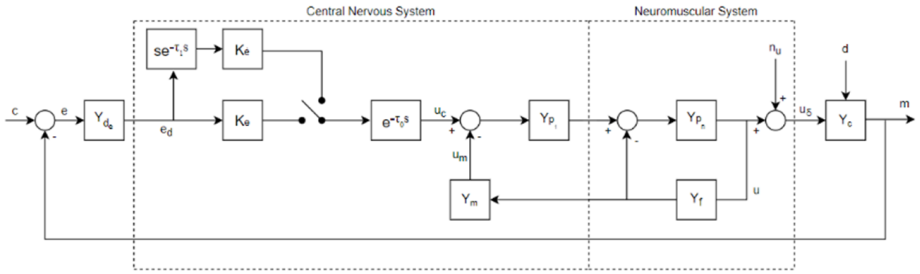

Figure 2.7: Hess structural model of an adaptive human pilot

- $k = 0$: the controlled element is a constant
- $k = 1$: the controlled element is an integrator
- $k = 2$: the controlled element is a square integrator

The representation of the pilot neuromuscular system includes both front and feedback channels. The describing function

$$Y_{p_n} = \frac{\omega_n^2}{s^2 + 2\xi_n\omega_n + \omega_n^2}$$

represents the open-loop dynamics of the limb which is driving the manipulator, while $Y_f = \frac{K_f}{s+1/T_f}$ represents the muscle spindles. After its early definition, the structural model was modified, extended, and applied to different scenarios. For instance, the simple application of a structural model in a tracking and regulation task resulted in a motion cue model [134]. Further experimental activities were directed toward the determination of time delay effects in manual control systems dynamics. In the subsequent analytical work, changes in human equalization performance were observed because of such time delay [135].

Following several modifications done to the original version of the structural model, Hess developed his revised model in [136], willing to include the effects of the pilot's neuromuscular system characteristics in the aircraft control process, along with its ability to perceive forces. Further extensions of the structural models are intended to better specify motion and force feedback [137]. Still, in the aeronautic domain, it was developed the Task-Pilot-Vehicle (TPV) model in [138], which is a simple extension of the structural model in tracking and regulating tasks applied to fast system design. These modifications proved to have a good match with the real data of human describing function [139]. Such kinds of modified versions of the

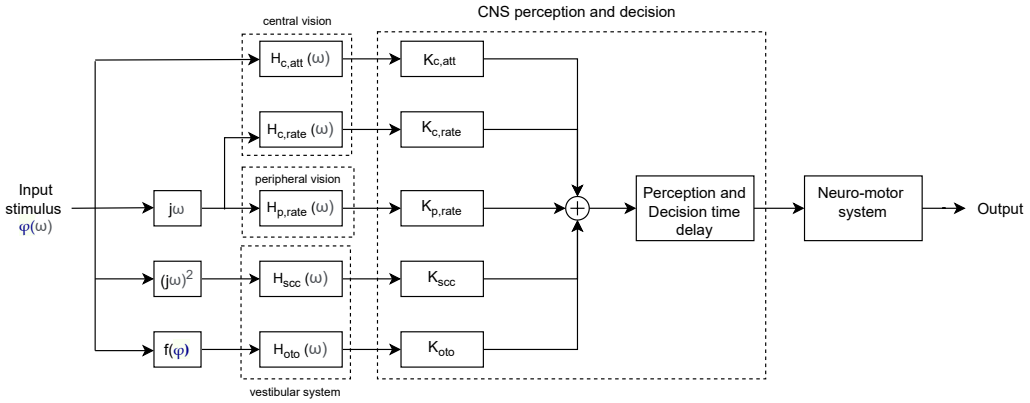

Figure 2.8: Hosman's descriptive model of human control behavior (1996)

model were used in many practical control problems, such as the design of a predictive display that also considers motion cues [139] or the development of an analytical method to assess pilot's fidelity in flight simulators [140], including multi-loop tasks [141, 142]. The procedure which led to the pilot's assessment was performed in [143], where a flight was simulated using a six-degree-of-freedom controller of a rotary wing aircraft, which was executing a vertical maneuver. A structural model of the human was also used to explore the closed-loop nature of a pilot's control behavior when determining a target direction and the analysis of the characteristics of pedal feedback to the pilot [144]. Finally, evaluations of the qualities of aircraft handling were proposed in [145] and [146]. Their prediction, along with the estimation of pilot-induced oscillations, were applied to different controlled elements in the following years [147–149].

2.4.4 Descriptive Model

In Europe during the 1970s, technological development such as the Fly-By-Wire (FBW) aircraft has arisen again research interest in man-machine interaction for aeronautic scientists. Researchers started to consider their human modeling effort as a means to better understand flying handling qualities and performance [150, 151] and to improve the accuracy of flight simulation. For this purpose, better integration of visual and vestibular systems into the control model seemed necessary. Later in the 1990s, Hosman led extensive research efforts with the aim of understanding the influence of the visual and vestibular systems on human perception and, consequently, on its control behavior [95, 152]. This investigation resulted in the definition of the descriptive model, to do so, Hosman presented different experimental works

in which the case study used was a pilot's landing maneuver with an aircraft using a moving-base flight simulator [153]. There, systematic variations of sensory inputs were the base that led to the definition of the descriptive model [154]. Results were applied in closed-loop control tasks where the human was considered as a single-channel information processor with multiple inputs from the sensory systems.

The descriptive model, represented in Figure 2.8, has a multimodality structure, reflecting physiological subsystems that link the states of the controlled element to his perceived states. Here the element of visual perception of displacement is expressed in the time delay $H_{aat}(s) = e^{-\tau_{att}s}$, where the attitude perception delay τ_{att} resulted in being around $50ms$ [89]. The visual perception of a velocity is $H_{rate}(s) = e^{-\tau_{rate}s}$, where the delay parameter varies in the case of central or peripheral vision. In particular, the peripheral system is able to sense only rates, therefore, its dynamic is described by the second equation, but with a shorter time delay ($60ms$) with respect to the one measured in the central vision system ($110ms$) [95]. Such as the delay referred to by McRuer in his crossover model is the sum of the delay associated with the detection of the stimulus in the eye and the one associated with the information processing.

For what concerns the vestibular system, both the semi-circular and otholit canals are modeled respectively as an over-damped torsion pendulum and an accelerometer with over-damped mass-spring-damper characteristics. They both can be represented by second-order differential equations, having the following transfer functions:

$$\begin{aligned} H_{scc}(s) &= \frac{(1+\tau_L s)}{(1+\tau_1 s)(1+\tau_2 s)} \\ H_{oto}(s) &= \frac{(1+\tau_n s)}{(1+\tau_a s)(1+\tau_b s)} \end{aligned} \tag{2.16}$$

In his model, Hosman assumed that tactile and proprioceptive senses were implicitly considered within the vestibular dynamics model. Moreover, the descriptive model assumes that processing in the perception and decision stages by the Central Nervous System and neuromuscular dynamics can be combined and represented by a unique "information processing" transfer function:

$$H_{ip}(s) = K_{ip} e^{-\tau_{ip} s} \,. \tag{2.17}$$

Here, the CNS contributes both to the gain and delay elements, while the neuromuscular dynamics low-frequency effects are approximated by only a

delay factor; thus, τ_{ip} is the sum of delay contributions of both factors. Function f converts the displacement caused by the input stimulus to a specific force output. The descriptive model has been applied in numerous studies in the transport engineering field, focused on the identification of human pilot's dynamics, such as the implementation of optimal forcing functions for identifying human model parameters [155], the investigation of the use of visual information by the operator while controlling of an aircraft [156], or the study of the influence of translational movements on pilot's performance and perception [157, 158].

2.4.5 Biodynamic Models

The biodynamic models were developed to represent the effects of the body dynamics on the human's desired control input in a situation in which it is subject to an accelerating environment. This way, the effects of this kind of motion on human health, comfort, or performance can be predicted [159]. Human control actions can be divided into two general categories: voluntary and involuntary [160]. The models studied in the previous sections were all part of the first category. All of them focused on translating into mathematical expressions the process which converts an idealized voluntary human action into an actual control action. This process takes into consideration aspects such as bandwidth limitations and the delays in human dynamics, put in relation to rigid-body movements and human-induced oscillations.

An alternative kind of modeling technique aims to describe the involuntary human actions, being the direct consequences of the vibrations coming from the environment, which are filtered by the human's body and become an involuntary input into its control system [161–164].

The modeling of biomechanics can be categorized into three types: continuum, discrete, and lumped parameter models. The main difference between them is the way in which the spine is modeled.

In continuum models, the spine is considered a flexible beam; its responses to vertical accelerations were studied by Griffin et al. [159]. In discrete models, the spine is described as a series of interconnected mass-spring-damper elements. The dynamic response can be studied by determining its equation of motion. With respect to the continuum modeling approach, discrete models succeed in representing the human body as a composite of elements (i.e., organs), each one with its own resonance frequency.

In lumped parameter model, the body itself is modeled as an equivalent mass-spring-damper system. Of course, this approach cause models of this type to have only one or two degrees of freedom. Moreover, the efficacy of its analysis is limited to the response to vertical stimuli [165] and is not

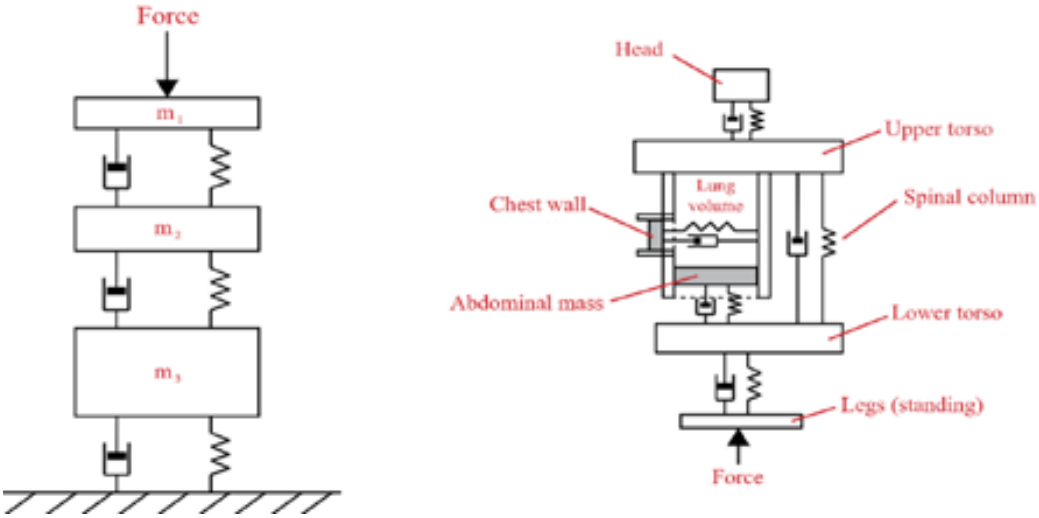

Figure 2.9: Examples of discrete (left) and lumped parameter (right) model structures [65]

able to capture the complex dynamics of the human body, as evidenced by Sirouspour et al. [166] when attempting to model lateral dynamics of a seated subject. This kind of approach was able to avoid instabilities and cancel dynamic feedthrough [167]. Further efforts in biodynamic modeling are the whole-body transmissibility [168, 169], being the ratio between the vibration measured in a certain point of interest and the base vibration (both are functions of frequency).

The area which produced the most research activities in this field was, once again, the aerospace domain. In [170], it was implemented a simulated biodynamic model able to predict both the human dynamic response and tracking performance in vibrating environments, allowing gathering data for whole-body vibration. Based on this model, further experiments were conducted to simulate the transmissibility of vertical base vibrations to lateral and roll accelerations [165, 171, 172]. One of the first important studies on biomechanical effects associated with human-manipulator interaction in high frequencies was carried out by Johnston et al. in 1988 [173].

Modern technological developments of this century, characterized by higher speed of transport systems, motivated further research investigation on the effect of structural vibrations of civil transports [174] and supersonic aircraft [175]. Later, muscular damping and stiffness parameters were studied in relation to the urgency of the performed task [176], suggesting that during tasks that are perceived with a higher urgency level, the body stiffness increase, such as the pilot's grip force. Moreover, in [177], it was defined a

three-dimensional human body model which relied on collected experimental data. While in [178], the error between the intended and actual control action of the human was investigated and put in relation to biomechanical models of the limbs.

2.5 Final considerations

The study of models representing human control behavior when interacting with a controlled machine has played a crucial role in many engineering fields. Emerging technical challenges, such as the development of new robots, aircraft, and vehicles or the spread of advanced simulation frameworks, have motivated through the years the rise of more and more complex mathematical representations. Along with the rise of the application's complexity, the abstraction level of human behavior skill-based description has also increased, making it more difficult for the objective to include accurate functional modeling of the involved physiological structures. For this reason, the parallel research efforts which were performed in motor control theory and sensory feedback description were reviewed in this work. The open discussions in cognitive-science-related research activities were also detailed, for what concerns the presence of internal models of external dynamics with whom a human is interacting in its central nervous system. Correspondent differences in the functional description of the motor apparatus were also identified.

For what concerns the review of human sensory modeling, there were included subjects such as visual perception errors and their modeling, vestibular and proprioceptive sensory dynamics.

Neuromuscular dynamics representations completed the discussion on the control theory representation of involved physiological districts, considering modeling efforts of internal feedback loops provided by tendons and spindles, forward muscular activation dynamics, and their approximation in the frequency range of a manipulative control task.

Passing to a task-based description of the human-machine complex, the aforementioned physiological dynamics were included in more general control structures in which different higher-level human features were also represented. Thus, the human capability to behave in an optimal manner after a certain level of training was represented in the optimal control model, while its adaptability to the machine dynamics is well captured by the classical crossover model or by Hess' structural model.

The degree of integration of underlying physiological processes and mission-based strategies within these models is indeed really variable, being the

advantage of approaches of the structural model and Hosman's descriptive model with respect to previous classical quasi-linear approaches. The ongoing development of the higher-level representation of human control strategies and decision-making, which includes techniques taken from robust control theory, uncertainty propagation, and probabilistic methods, is motivated by the increasing complexity of the application tasks. Therefore, maintaining a bond within the developed models from both a physiological and a control-theory point of view will be increasingly challenging.

Having to get focused on the linear models, in accordance with the relevant research efforts of the last years directed to the description of non-linear dynamics in man-machine interaction, the reader could be prompted to face this topic starting from the simple models overviewed that have the advantages that could be handled by using the classical approach of linear system theory and automatic control methods.

Despite the limitations, these linear models showed good approximation capabilities and easiness of use in practical applications; in the next chapter, we will present a novel linear modeling strategy applied to human-robot interaction.

Chapter 3

Precision Model for control delay identification in robotic manipulation

Human-robot collaboration offers advantages in terms of flexibility in many industrial applications. New generations of intelligent collaborative robots are used without fences, usually in a shared space with human operators, which adds a mutual advantage to classical robotic cells. In complex human-robot collaboration scenarios characterized by continuous physical interaction, analyzing human behavior and control action is crucial to investigate as a base to build any predictive technique. The previous chapter showed how modeling the human control action when interacting with a controlled machine has become an independent research field involving multiple disciplines and approaches over the years. This chapter investigates and applies a linear Precision Model to human-robot interaction, focusing on identifying human reactive delay in a collaborative task.

3.1 Human-in-the-loop control

Several studies regarded human and robot performance evaluation in cooperative work. In [179] human factor was evaluated in virtual scenarios using agent modeling with a discrete transition between blocks. Sadrfaridpour et al. [180] built a trust model in which the performance of the robot and human operator in repetitive collaborative tasks are evaluated, considering the human muscular fatigue and recovery model.

Different modeling approaches have applications in human intention estimation and robot imitation algorithms. For example, Obo et al. [181]

proposed a human-like robot posture generation method based on a steady-state genetic algorithm (SSGA). Huber et al. [182] tried to dynamically understand the joint action of groups of humans working together and transfer such behavioral pattern to human-robot interaction. Erlhagen et al. [183] have developed high-level joint action strategies for human-human interaction. Such approaches either assume perfect rationality or smooth over human idiosyncrasies and noisy observations by providing general accounts and mathematical functions of human performance.

Recently, promising approaches to describe the information transfer relating external dynamics to the human controller were proposed using convolutional neural networks or other machine learning techniques. In [184] a transfer learning approach based on a Convolutional Neural Network (CNN) with raw EMG input data, was used to classify motor control difficulty in a human-robot collaborative scenario. Chen et al. [185] used LSTM networks to learn the characteristics of strongly nonlinear external dynamics of Van der Pol and Lorenz systems. Mu et al. [186] used a reinforcement learning algorithm coupled with two neural networks to implement an event-triggering dynamic strategy for partially unknown systems.

Concerning this kind of black-box approach, other model-based techniques achieved the same goal while developing a better description of the underlying physiological processes which determine the overall human control strategies. The underlying mathematical representation for human control action should be the same used to describe a linear servomechanism [187]. Specifically, a set of linear differential equations with constant coefficients, or equivalently, a transfer function in the frequency domain. In 1965, McRuer et al. in [70] introduced the most famous example that follows such an approach. The model foresaw an integrator and a simple delay element to model the human operator adaptation during the interaction with the machine. The human action was studied with different controlled elements and represented a quasi-linear describing function. In [188] Kleinman et al. developed the "optimal control model" (OCM). Its primary assumption is that a well-trained, well-motivated human behaves optimally while subject to psycho-physical limitations. Unlike the crossover model, the OCM is expressed in state-space variables, facilitating the extension of human-machine analysis to multi-loop control tasks. Here, a Kalman filter represented the human's ability to deduce a system state from perceived information. Concerning pilot aircraft control applications, Hess structural model [189] proposed a detailed description of human perception processes and inner loop feedback. While Hosman's descriptive model [95] studied the interaction between visual and vestibular inputs and their influence on the overall control strategy.

Research in this direction in the robotics domain often investigates the

exploitation of collaborative robot applications using virtual environments. In [190] for example, a neuroadaptive controller is used in a collaborative application with a robotic arm to analyze the human control action. The target point was shown in a virtual environment and randomly changed for each trial. Whereas in [98], a similar virtual setup was combined with a haptic device. The identified human control parameters were the input of a human intention estimator, able to adapt the impedance of the controlled device according to human actions.

However, these approaches do not investigate the effect of the learning process of external dynamics on human control delay. The classical quasi-linear model is the most suitable approach for this while focusing on the description of physiological background processes [98] [191] [133]. The crossover model has often been used in literature for this purpose in the aeronautic domain, characterized by a high-frequency range that facilitates a frequency-domain analysis of the model.

The present work describes and applies such a modeling approach to different human-robot collaboration scenarios using a time-domain approach. The chapter will be structured as follows: in the second section, the model theoretical background will be described in detail; in the third sectionthe proposed application scenario will be presented; in the fourth section, the obtained results will be analyzed and discussed; and in the final section the system identification process implemented in simulation will be illustrated.

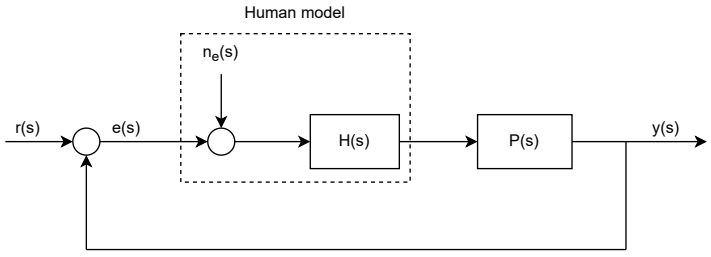

Figure 3.1: Block scheme representing the structure of human-robot control system during a compensatory task, as described by the Crossover Model. Here, $H(s)$ represents the human control dynamics, which is used along with the remnant noise $n_e(s)$ to build the human model. $P(s)$ represents the controlled element's dynamics (in our case, a robot).

3.2 Precision Model of the Human-Robot Complex

Let us recall the McRuer's Crossover (CO) model [70] introduced in the previous chapter. The CO model hints at how humans adapt to different plants to elicit stable and effective control responses. Due to its simplicity, the model proposed aims to avoid common problems related to higher-complexity systems.

It was observed [70] that when an external disturbance is introduced in the system, measured human operator responses were different for different transfer functions of the controlled plant. However, the combined human-machine behavior is approximately the same for all the experiments.

As said in the model introduction, the central theoretic hypothesis relying upon this approach is that the transfer function modulus bode plot has a -20dB per decade slope around the crossover frequency in the frequency domain. The remnant noise n_e (see Figure 3.1) models the non-stationary effects of the pilot behavior. A random process models such a linearly uncorrelated noise with the control input. Usually, the remnant is related to the error signal $e(t)$. It is, therefore, considered as an observation noise.

Given a controlled element, in [27] it was proposed a more detailed Precision model of human control action, which can be described in the Laplace domain by the following equation:

$$H(s) = K_p \frac{\tau_L s + 1}{\tau_I s + 1} \frac{1}{\tau_n s + 1} e^{-s\tau_e} \tag{3.1}$$

Here, we have mainly four factors: a simple static gain element K_p, a lead-lag equalization term $\frac{\tau_L s+1}{\tau_I s+1}$, a time constant relative to the neuromuscular system τ_n and the so-called "effective time delay", being $e^{-s\tau_e}$.

Neuromuscular system dynamics have been extensively discussed in [133], showing additional second-order characteristics typical of spindle and tendon organ ensembles. However, these effects are observable only in very high frequencies. Therefore, they can be neglected for most application scenarios, resulting in the first-order lag term in Equation (3.1).

Moreover, the human operator sets the equalization term to achieve the -20dB decade slope required by the Crossover theory. At the same time, the static gain is used to pilot the crossover frequency value. According to McRuer, the sensitivity of the closed-loop stability on τ_L and τ_I should be very low, leaving the crossover frequency and the effective time delay as the main parameters to consider to ensure stability and minimize the error.

The crossover frequency mainly depends on human adaptation to the

controlled element and, in a minor way, to the input bandwidth ω_i. Therefore, if we try to implement the same general concept expressed by Equation (2.13) by including the controlled element dynamics into the Precision model, we will have that the man-machine complex would be equivalent to

$$H(s)P(s) = K_{pc}\frac{\tau_{LC}s+1}{\tau_{IC}s+1}\frac{1}{\tau_n s+1}e^{-s\tau_e} \tag{3.2}$$

Here, τ_{LC} and τ_{IC} are the lead-lag equalization parameters considered after the initial training phase when the human learned the controlled machine dynamics and adapted its behavior to respect the crossover hypothesis. The gain K_{pc} is now a general expression of the gain of the man-machine transfer function and is equivalent to the crossover frequency.

The effective time delay τ_e results from transport delays of the sensory information to the central nervous system and high-frequency neuromuscular dynamics. In [192], it was given the following empirical relationship:

$$\tau_e = \tau_0 - \Delta\tau(\omega_i) \tag{3.3}$$

Here, the first term τ_0 is the primary time delay when $\omega_i = 0$, depending on the controlled element Y_c. In contrast, the second term $\Delta\tau$ decreases the effective delay with the input bandwidth with a slope entirely independent of the controlled element. Such relation is referred to as the scenario that led McRuer's research activities in the aeronautic domain, where the human controller operates in high-frequency ranges. However, a constant behavior is expected if we focus on the primary delay term dependent on human adaptation to the controlled external dynamics.

Therefore, the reaction time delay should be constant for each human subject, with a small variability attributable to task and environmental variables. In particular, typical values of 0.5s of the primary time delay τ_0 were obtained in [27] for second-order functions of the controlled element.

In this work, the Precision human-machine model has been applied to a human-robot collaboration scenario to understand how to identify better human control characteristics concerning its adaptation to the controlled robot's dynamics. This adaptation process will be translated into properly tuning the model parameters, allowing the embedding of robot and human dynamics into a single transfer function, as done in the general CO model in [70]. Such modeling effort will mainly focus on reactive delay, an easily measurable parameter in which the discussed human behavior is expected to have an effect.

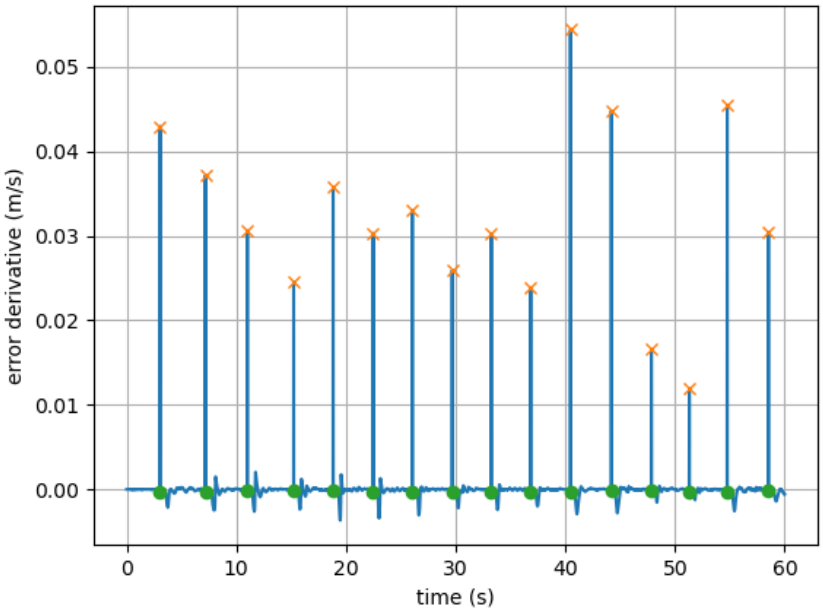

Figure 3.2: Time derivative of the position error signal in a performed experiment. Orange crosses represent local maxima, while green dots the first successive time instant where a sign change is observable.

3.3 Design of Experiment

A simple manual guidance situation was considered, where humans and robots performed a typical point-to-point motion task with continuous physical interaction.

In this scenario, the reactive delay can be derived from the time displacement between the reference position signal and the actual measured position. The point-to-point task is the situation in which this displacement is primarily evident because it is constituted by a sequence of different target points that the human-robot complex has to reach.

Here, the reference signal to consider as the input $r(s)$ in Figure 3.1 is composed of a sum of steps being the series mentioned above of constant reference target points.

Figure 3.2 shows the position error derivative signal $\dot{e}(t)$ during a performed point-to-point task, being $e(t) = r(t) - p(t)$ the position error, $r(t)$ the reference position, and $p(t)$ the actual position. As noticeable, $\dot{e}(t)$ is characterized by a series of local maxima, represented by the orange crosses. Each maximum corresponds to the time frame for the maximum variation in

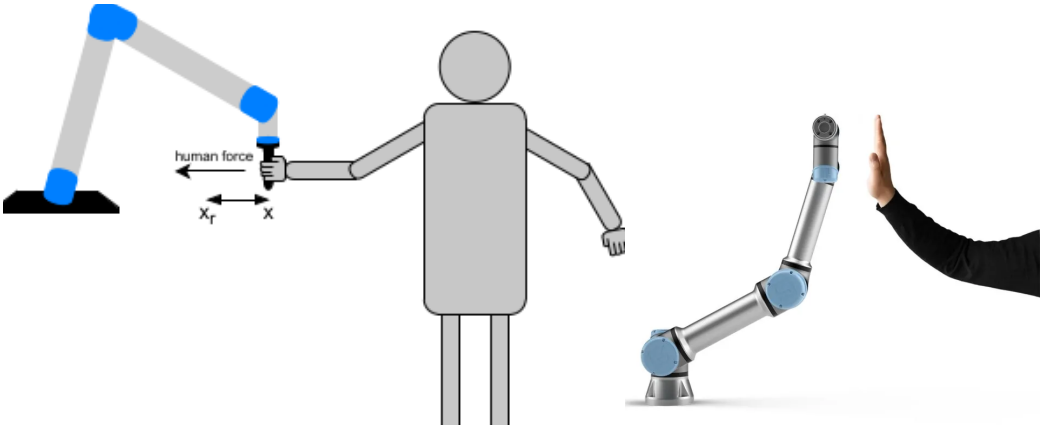

(a) (b)

Figure 3.3: Scheme of the experimental setup (3.3a): The disturbance signal causes a displacement from the initial reference position, and the human reacts by exerting a compensatory force towards the opposite direction.
Picture of the small UR5 robotic arm (3.3b)

Table 3.1: Average delay values for all the human subjects, considering the ten performed experimental trials of each one.

Human subject	1	2	3	4	5	6	7	8	9	10
Average delay	0.6234	0.4075	0.4777	0.4308	0.446	0.626	0.4494	0.5701	0.4086	0.6469
Generated ref points	128	142	130	130	132	132	136	128	151	122

the reference position signal $r(t)$, *i.e.*, corresponding to a target point variation, as will be better detailed in the next section. The green dots represent the following instant in which the error derivative becomes negative, caused by a variation in the actual position $p(t)$ in consequence of the human control action. Therefore, the difference between these two points can be considered a reliable experimental measure of the reactive time delay of the subject.

A cartesian impedance controller was implemented on the robot side, depicted as the controlled element P(s) in Figure 3.1. In the impedance control strategy, a virtual mass-spring-damper element is attached to the robot's end-effector's actual and reference positions. This way, when following a reference trajectory, any interaction with external forces causing deviations from the current path is managed by the system in a compliant way, depending on the parameters set on the virtual mass, spring, and damper.

To reproduce the best conditions to identify the human reactive delay, a simple compensation task was executed following the scheme depicted in Figure 3.3. The human operator had a continuous physical interaction with the robot. A constant low stiffness was set in the Cartesian impedance controller

to ensure a compliant behavior of the robot.

In particular, the proposed experimental setup consisted of a UR5 robotic arm with a gripper in the end-effector, which the operator must hold. A virtual robot arm model was shown to the human operator on a screen using the Rviz software tool [193]. The reference target area, represented by a red square of 2cm in such a virtual environment, was shown. Its position was randomly changed in the x-y plane (in the robot's base frame). The human operator was asked to: reach the target point by manually guiding the robot gripper, holding it for $\Delta t = 3s$, and bringing the robot back to the initial position. If the subject could not hold the robot end-effector within the reference target area for 3s, the counter was reset, and the following virtual reference was not generated until the condition mentioned above was respected.

This operation was continuously repeated with different target points for 60 seconds. Each experiment was performed ten times by ten human subjects with the same random target values. Before recording the experiments, a training phase was performed by executing the described operations until a high level of comfort with the environment was reached and confirmed by the subject.

3.4 Experimental Results

The recorded signals included many step motions since the human subject's reaction in both directions was considered when reaching the random target reference and returning to the initial position. The number of generated references depends on the subject's reaction delay and the precision when holding the robot into the target area. The total number of generated virtual references for each subject is indicated in the second row of Table 3.1, ranging from a minimum of 122 to a maximum of 151, considering all the ten performed experimental trials.

To measure the reaction time delay, it was considered the displacement between each step of the reference position signal and the subsequent change of the actual position. This interval corresponds, in other words, to the difference between the time frame in which the system generates a new virtual reference point, and the time frame in which the human subject starts to move the robot's end-effector.

Figure 3.4 shows a box and whiskers plot representing the range of variation of the measured reaction time delay for each human subject. Here, the vertical axis represents seconds. The mean value for each experiment of 60 seconds was computed to have a robust measure of such value. Then the

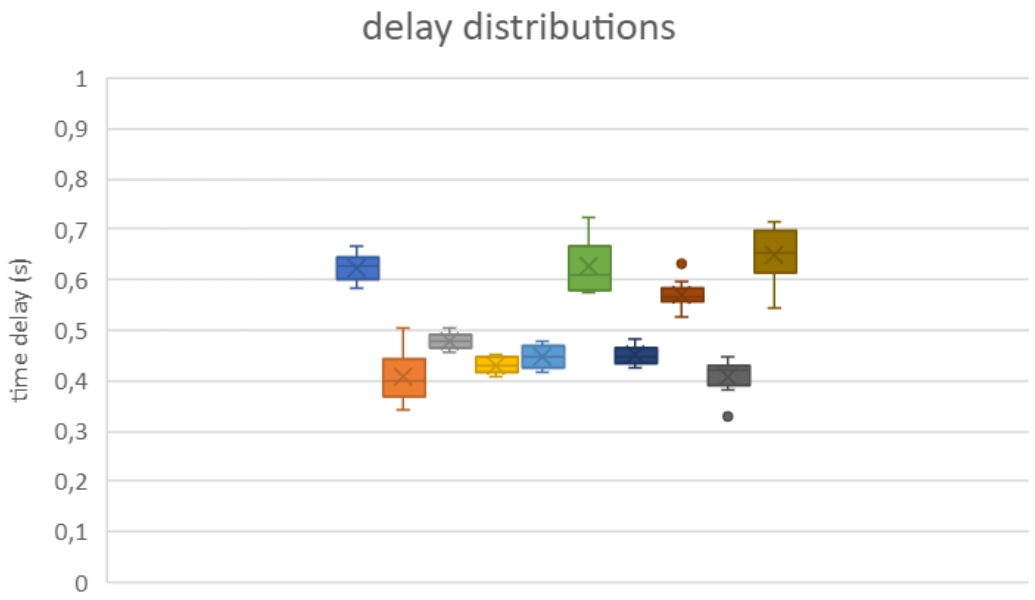

Figure 3.4: Ranges of variation of mean reaction delay values considering the 10 performed experimental trials, for each human subject

series of 10 mean values per subject were considered, and the resulting mean delays are summarized in Table 3.1.

As noticeable, only two outliers are present in all the measured values. Instead, most subjects display a narrow range distributed around the mean values, describing a constant delay around all the experiments. Moreover, such constant mean values significantly differ between one subject and another, confirming what was expected from the theoretical models.

In three cases, the ranges of values presented more consistent variations to the majority done by the other subjects. However, rather than being dependent on environmental or task variables, such behavior can be explained as an effect of the subject training and better adaptation to the external dynamics. This consideration is confirmed if looking at the values in detail.

Figure 3.5 for example, shows the series of measured data for subject 1 (Figure 3.5a) and subject 2 (Figure 3.5b), corresponding to the blue and orange boxes in Figure 3.4. Here, the data trend confirms the above consideration, represented in its linear approximation by the dotted blue line. A narrow range corresponds to the expected constant behavior in the first case. At the same time, the wider range of the orange box in Figure 3.4 is caused by the descending trend observable in Figure 3.5b, which testifies the effect of the learning process of the external dynamics done the subject.

The range of variation of the measured delays is between 0.4 and 0.6 s,

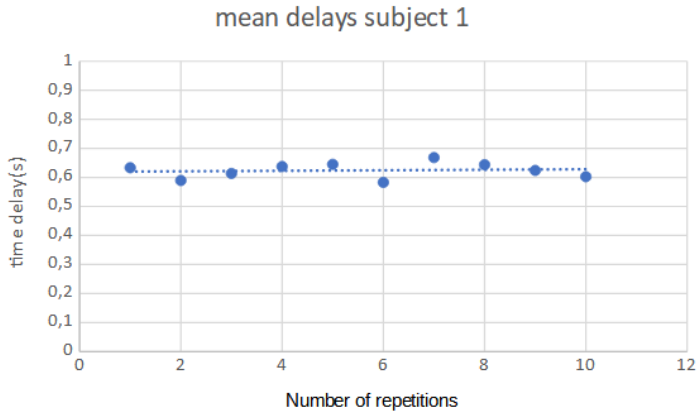

(a)

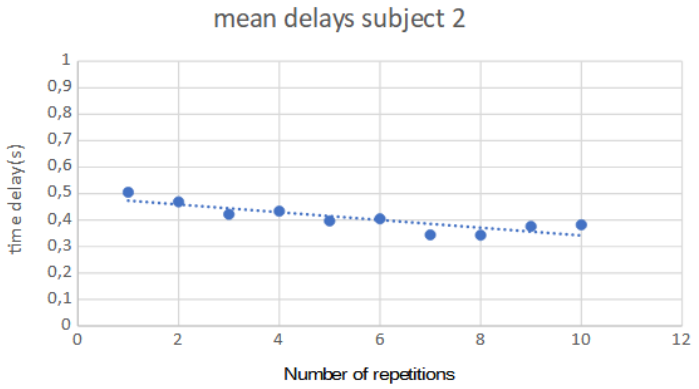

(b)

Figure 3.5: Detail of the measured delays for the first two subjects, boxes in blue and orange in Figure 3.4. The blue dots represent the mean value for each experimental trial, while the dotted line is the best linear approximation of the data trend.

which is compatible with the values obtained by the model. Further details will be given in the following section.

3.5 System Identification

All subjects' experimental data were compared with the simulated Man-Machine Precision Model results, as expressed in Equation (3.2). The considered human model is constituted by five parameters: the gain element K_{pc}, time constants τ_{LC}, τ_{IC} and τ_n, the effective time delay τ_e; each one having a different influence on the model simulated output. The static gain

Table 3.2: Parameters of the human control model defined in Equation (3.2) resulted in optimizing the Prediction Performance Index in the performed simulations. All the values are expressed as an average between the ten performed experiments for all the human subjects. The last raw reports the experimentally obtained effective delay τ_e to be compared with the simulated ones.

Human Subject	1	2	3	4	5	6	7	8	9	10
Crossover Frequency	2.13	2.367	2.249	2.452	2.245	2.037	2.45	2.134	2.519	1.914
τ_n	1.46	1.34	1.384	1.151	1.427	1.594	1.29	1.548	1.252	1.905
τ_{LC}	0.86	0.912	0.865	0.908	0.877	0.871	0.89	0.818	0.947	0.741
τ_{IC}	0.996	0.994	0.991	0.991	0.991	0.996	0.99	0.995	0.996	1
Simulated delay τ_e	0.511	0.351	0.417	0.331	0.415	0.541	0.366	0.53	0.32	0.7
Measured delay τ_e	0.6234	0.4075	0.4777	0.4308	0.446	0.626	0.4494	0.5701	0.4086	0.6469

is responsible for the crossover frequency value, and the time constants give the model response the typical second-order characteristics. In contrast, the effective time delay is the actual output parameter of interest to be compared with the measured values to check the model precision.

The same reference position signal, recorded from the performed experimental trials, was used as input of the simulated system, whose transfer function was implemented using the python control system library. Being $\hat{p}(t)$ the simulated time forced response of the model, we will have a prediction error:

$$\hat{e}(t) = p(t) - \hat{p}(t) \tag{3.4}$$

Where $p(t)$ is the actual position recorded from the experiments, representing the ground truth in this case. For each simulated response, the following Prediction Performance Index (PPI) was defined:

$$PPI = \int_0^{t_s} |\hat{e}(t)| \tag{3.5}$$

Here, the integral of the error modulus was computed within the time window between 0 and t_s, corresponding to the maximum simulated time frame.

The five parameters were varied within reasonable intervals. Specifically, we used 0-10 Hz for the crossover frequency, 0-2 seconds for the three-time constants, and 0-1 second for the effective time delay τ_e. The simulation was run for each value of the five parameters, each run with one variable parameter and the other four fixed until the minimum prediction performance index was reached.

The results are summarized in Table 3.2, where the average values of the ten experimental trials for each subject are reported for all the considered

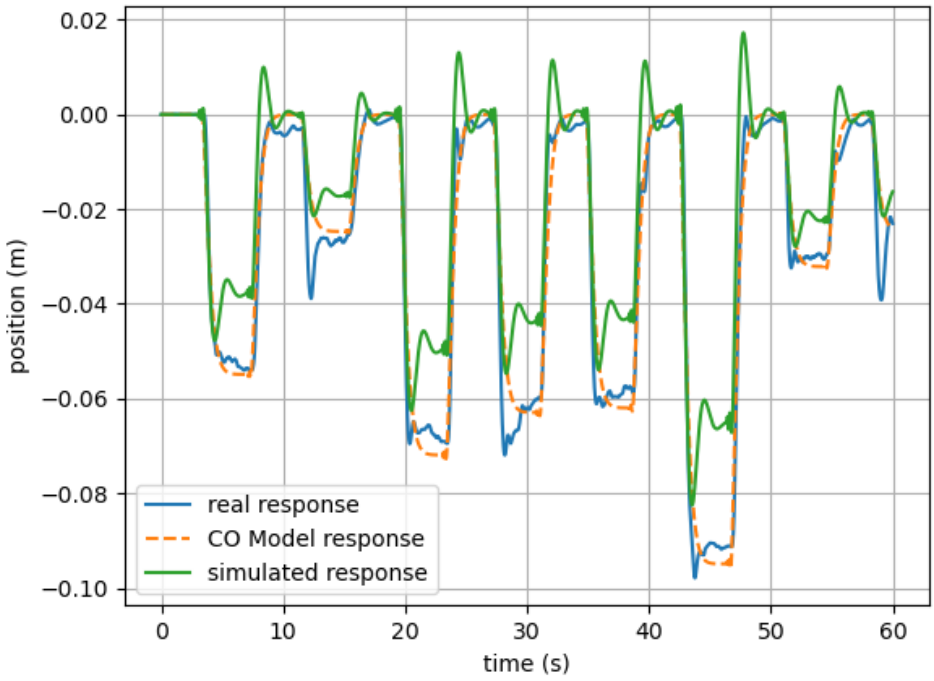

Figure 3.6: Simulated position outputs considering: the identified Precision model (in green), standard CO Model (dashed orange line), and measured position output (in blue). Despite the error in this example seems to be averagely greater in the Precision model, it is also evident how it succeeds in simulating more accurately the first-peak responses that the human generates after each step of the forcing function, which is the most important feature that is necessary for obtaining the human reaction delay.

parameters. The crossover frequency of the model is generally set around 2-2.5 Hz, confirming the low-frequency operational range of the model. The measured reaction delays obtained from the experiments are reported in the last row of the table. Comparing these values with the simulated reaction delays reported in the previous raw, we can observe an error below $0.1s$. This result confirms the match between the identified model and the data.

Another reliable indicator of the model accuracy is the comparison between the measured and simulated outputs, in our case, the actual position of the robot end-effector. Figure 3.6 compares the responses of the identified model (in green) and standard CO model (in orange), overlapped to the measured ground truth (in blue) recorded from the experiment, always considering the simulated parameters when the optimal PPI value has been reached. It is noticeable that, despite the good performance, CO model first-order characteristics fail to represent the first peak observable at each step of the real system response well.

On the other hand, the identified model response presents these second-order characteristics observable in the experimental data due to its lead-lag equalization term. Moreover, model response is completely overlapped with the measured one in the transient phase of each step, which is crucial for obtaining precise esteem of human reaction delay.

3.6 Final considerations

The linear approach of the proposed Precision model was able to accurately describe human-robot physical interaction during a compensatory control task composed of different point-to-point motions to be performed under manual guidance by the human subject. Experimental trials involving ten healthy subjects of different ages were conducted to characterize human control delay according to the studied modeling approach.

The human effective reaction delay parameter was esteemed and extracted from raw post-process data to be reliable and invariant with task variables not dependent on the considered subject. The obtained results were within the expected values of 0.4 to 0.6 seconds, confirming the model's validity. Moreover, the system was identified by simulating a human-robot control model using the recorded experimental data. The model parameters were iteratively updated for each simulation to minimize a performance index defined for this purpose. The simulated results corresponded with the experimental data for the computed effective delay and the raw position output.

Despite the encouraging results, some aspects must be further investigated. For instance, for better practical applicability of this approach, the

human control model should be improved for an online human intention estimation to allow the controlled robot to update its control behavior accordingly during the task. This last consideration was taken into account for the second nonlinear model, which will be proposed later in this work.

Chapter 4

Nonlinear Models

Until now, we have investigated and applied linear modeling techniques for characterizing human behavior when interacting with a controlled machine (in our case, a robot). Such techniques have proved to be useful in accurately representing the various physiological districts involved in the perception, interaction, and control processes. Moreover, in the previous chapter, we have shown how such a model can accurately simulate human response and experimentally identify the reaction delay when an external forcing function is applied to the system. However, linear models are not able to describe all the high-level processes that are involved in complex scenarios. To describe, in a deeper way, human adaptation to the plant when the complexity level of the task increases and to model also higher-level processes, such as decision-making, which are not correlated to traditional physiological subsystems, nonlinear models have to be necessarily investigated.

The investigations of human nonlinear dynamics when controlling a machine are so diversified that finding a common point between them is difficult.

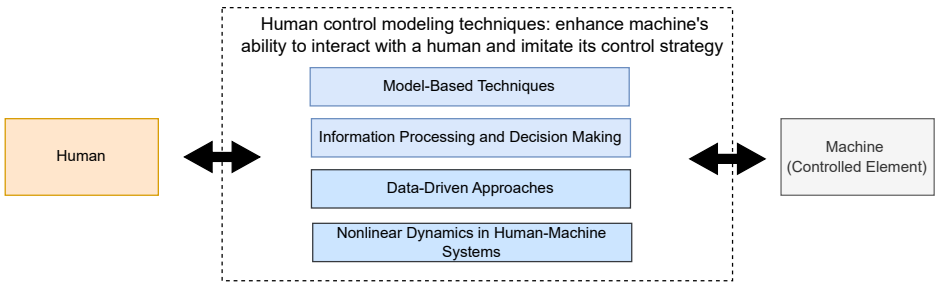

Figure 4.1: Graphical abstract representing the structure of this chapter: how the study of nonlinear dynamics, with different approaches and from different perspective, can be used to represent human behavior and increase the adaptability between human subject and controlled machine

This chapter aims to give a structured overview of the existing techniques, focusing on the underlying physical and physiological human processes.

In this chapter, a human-centered review of the existing efforts will highlight the strengths and limitations of the presented techniques in their effort to model the intrinsic nonlinear dynamics in the human-machine system. Such nonlinearities will be referred to as spatial and temporal variables of functionals which are identifiable within the human physiological control districts involved in sensing and information processing, but also deriving from the interaction with controlled element dynamics and/or the external environment [194]. With respect to the existing review works relative to each research field, this effort will help find a guiding line between more traditional control modeling techniques and modern learning algorithms.

The chapter is structured as follows, in Section 4.1 discusses the Dual loop control model, giving an overview of the human controller when interacting with a controlled machine. Section 4.2 investigates the nonlinear muscular dynamics models. Then in Section 4.3, the focus will be directed toward modeling techniques particularly useful for representing human information processing stages. Then machine learning efforts to model the human decision-making process are investigated in Section 4.4. Lastly, in Section 4.5, practical examples of human-machine schemes in which the described techniques are applied to model complex nonlinear dynamics are considered.

4.1 Dual Loop Control

In the last decades of the last century, Hess investigated human control strategies when interacting with a machine, resulting in his first "structural model" [189]. After the first linear version, Hess noted that often human operators' control strategies resulted in pulsive behavior, which was not linked to any feature of classical linear models. In [129], the pulsive behavior was linked to McRuer's quasi-linear model hypothesis in the frequency-domain context. The assumption was that when faced with a demanding task combined with the controlled element's high-order dynamics, the human operator avoids the computational effort and reduces the number of parameters by using a less computationally-demanding nonlinear strategy rather than a linear one.

The above assumption was applied to the early version of the Hess model, resulting in the Dual Model depicted in Figure 4.2. Such a model resulted from an effort to link the hypothesis behind the crossover theory with the optimal control approach.

The described nonlinear factor results in the various switching elements

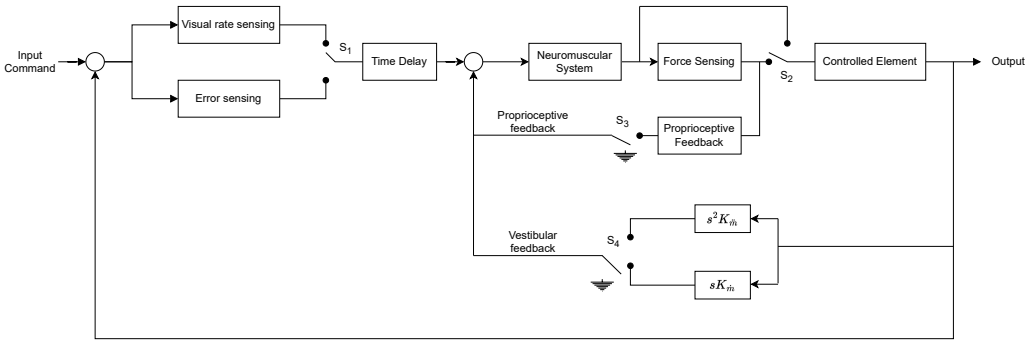

Figure 4.2: Dual model of the human operator in a compensatory task

in Figure 4.2. The first one (S1) allows selecting error or error rate tracking and is supposed to operate in unison with S2, which enables or disables the proprioceptive feedback loop. The physiological reason behind this is that after a triggering event, the pilot control strategy regresses to simple tracking behavior, where the error rate is controlled without the help of proprioceptive feedback. Right after the two described sensing channels, there is a time delay element due to the information processing occurring in the central nervous system, present right before the neuromuscular actuation and internal feedback stages.

Moreover, switch S3 allows modeling both displacement and force sensing inceptors. Ultimately, S4 allows using vestibular rate or acceleration inputs for control, with gain elements dependent on the perceived velocity $K_{\dot{m}}$ or acceleration $K_{\ddot{m}}$ [95]. Ultimately, only neuromuscular and proprioceptive elements need parametrization, lowering the model complexity level. The neuromuscular block is often represented using second-order dynamics [195].

The neuromuscular force output is sensed and transformed into an estimation of the output rate of the controlled element using an internal model of its dynamics. This process is done by the proprioceptive system, which can be described in the Laplace domain using the following equation:

$$H_{\mathrm{ps}}(s) = \begin{cases} K_{\mathrm{ps}}(s+a) \\ K_{\mathrm{ps}} \\ \frac{K_{\mathrm{ps}}}{(s+a)} \end{cases}, \tag{4.1}$$

where s is the Laplace variable in the complex plane, and $a \in \mathbb{R}$. In other words, the proprioceptive system transfer function H_{ps} can be defined, depending on the controlled element dynamics, as a derivative term multiplied by a gain element K_{ps} (first case), through a simple proportional relationship (second case); or as integration (third case). If we indicate the controlled el-

ement transfer function as H_C, the proprioceptive system's dynamics would be chosen in order to satisfy the following relationship around the crossover frequency:

$$H_{\mathrm{ps}}(s) \propto sH_C(s)\,. \tag{4.2}$$

This concept well represents the operator's adaptability to external dynamics. This human's internal representation of machine dynamics expresses the hypothesis behind the crossover model and is equivalent to the Kalman estimator in the optimal control model [101].

The last case of Equation (4.1), in which the inner loop feedback signal is generated by integrating the force applied to the controlled element, is the one in which the effect of the pulsive control behavior on the time integrability of the human is more evident. In fact, the integration of a pulsive input signal can be approximated by

$$Y_{ps} = \sum_{i=1}^{n} A_i \Delta T_i\,, \tag{4.3}$$

being A_i and ΔT_i the equivalent calculated amplitude and time duration of the ith pulse, and Y_{ps} the resulting proprioceptive output signal. The computational burden of such an operation, if compared to integration over time, is significantly lower. In order to represent the discussed pulsive control effect on the inner loop feedback in the most simple and realistic way, the following logic can be added before the neuromuscular system dynamics:

$$\begin{aligned} \frac{d\hat{q}}{dt} &= 0 \quad \text{if} \quad \left|\frac{dq}{dt}\right| < \alpha \\ \hat{q} &= \beta q \quad \text{if} \quad \left|\frac{dq}{dt}\right| \geq \alpha\,. \end{aligned} \tag{4.4}$$

Where q and $\hat{q}$ represent input and output variables, respectively, α and β are the only parameters that must be tuned to reproduce pulsive behavior. The dependence of the model on just two parameters allows it to avoid its over-parametrization and simplifies its adaptability to experimental data. This nonlinear element's action causes the output $\hat{q}$ to remain constant until a sufficiently rapid change in the input q occurs.

Pulsive control due to the "ease of integrability" principle, as hypothesized by Hess, found a physiological interpretation in [196]. In particular, while proportional and derivative control feedback can be actuated using direct sensing organs, such as muscle spindles and Golgi tendon organs, integral control does not have similar sensing input sources and requires higher-level

cognition in the central nervous system [129]. Consequently, when performing acceleration control, the human operator tends to generate a pulsive force rather than a continuous one to facilitate the integration process, being the computational cost of the latter much higher. Different explanations of the same phenomena are possible, for example, linked to energy saving strategy when the required force peak value is low enough.

4.2 Neuromuscular dynamics

The latter consideration suggests the importance of neuromuscular actuation mechanisms as a source of nonlinearity in the human controller. Several dynamical system modeling approaches of the neuromuscular system have been proposed in the literature, starting from simple state-space descriptions [197]. Neuromuscular dynamics are typically nonlinear; for instance, we consider the model of a human limb, and its characteristics can be described in state-space form as

$$\begin{aligned} \mathbf{x}_{t+1} &= f(\mathbf{x}_t, t, \mathbf{u}) + \omega(t) \\ \mathbf{y}_{t+1} &= h(\mathbf{x}_t, t) + \epsilon(t)\,. \end{aligned} \tag{4.5}$$

Where $\mathbf{x}$ is the state vector representing two angles and two angular velocities, $\mathbf{u}$ is the control input corresponding to the two applied joint torques, ω is the process noise, while ϵ the observation noise. The general solution adopted in this nonlinear problem has been to linearize the nonlinear dynamics around a specific operating point in state space. The resulting linear time-varying dynamics can be used only in a small interval around the operating point; in the case of the above example, neglecting the noise terms would be equivalent to

$$\begin{aligned} \mathbf{x}_{t+1} &= \mathbf{A}_t\mathbf{x}_t + \mathbf{B}_t\mathbf{u}_t \\ \mathbf{y}_{t+1} &= \mathbf{H}_t\mathbf{x}_t\,. \end{aligned} \tag{4.6}$$

Here, A is the state transition matrix and B the control transition matrix, while H represents the output measurement matrix.

Most control-theory-based neuromuscular modeling approaches aim to find the correct series of control inputs $u_1 ... u_T$, corresponding to muscle forces and joint torques, making the system execute the desired trajectory in the time horizon $t = T$. Such a control system is an open loop; thus, if susceptible to disturbances, the controller would fail to reach the desired state, not

sensing any state change. Moreover, the direct measurement of trajectories in state space can be problematic in high-dimensional systems, where part of the state may not be directly observable.

To overcome such shortcomings, optimal control approaches have been proposed [198] [199], where the dynamical system is controlled by optimizing an objective function. According to optimal control theory, the controller can directly access output and state variables or estimate their values to implement an optimal control law to maximize the system's performance. A general mathematical expression of the objective function to optimize to achieve this goal is

$$J(\mathbf{x}) = \min_{\mathbf{u}} \left(\phi(\mathbf{x_{t_N}}) + \int_{t_0}^{t_N} [q(\mathbf{x}) + \frac{1}{2}\mathbf{u}^T\mathbf{R}\mathbf{u}] \quad dt \right) . \tag{4.7}$$

The system variables are u, the control torques, forces, or neural commands, and x, often expressed as joint angles, velocities, or muscle activation. Moreover, ϕ is the cost term dependent on the state, describing how a given target was reached. At the same time, q is a state-dependent cost term considered over the whole time horizon t_N, and $u^T Ru$ is the cost dependent on the control input (also considered over the time horizon t_N). The velocity value and the control effort used to perform a given trajectory can be good examples of the last two mentioned cost terms in a practical application.

Optimal control approaches for adapting classical linear techniques, such as Linear Quadratic Gaussian Regulator (LQG), have been proposed for nonlinear dynamics typical of muscles and multi-body limbs. In [200], an Iterative Linear Quadratic Regulator (ILQR) was introduced based on linearizing nonlinear muscular dynamics. An advantage of this approach is that it does not need any predefined target trajectory in the state space to work. ILQR method was also extended in [201] for nonlinear stochastic systems characterized by state-dependent and control-dependent noise. Here, the ILQR technique permitted the description of the nonlinear relation between muscle force, fiber length, and contraction velocity. Further developments led to the use of Extended Kalman Filters (EKF) in systems with additive noise in sensory feedback loops [202, 203].

4.3 Decision-Making and Information Processing

The discussed models helped describe the human-machine system dynamics in a control-theory fashion. The involved physiological districts, sensing, and

actuation systems were put in relation, considering the human as an element of the control loop, and the nonlinear dynamics present in motion command actuation and feedback were put in evidence. However, to understand how human beings act as a controller when interacting with a controlled machine, a deep focus on the information processing stage is crucial to understand how its central nervous system integrates pieces of information to make decisions, learn, and generate commands.

4.3.1 Fuzzy control models

Processes such as human decision-making, inference, and judgment are challenging to characterize precisely. A modeling technique specifically meant to capture this concept is Fuzzy control modeling. If we represent a human controller as a fuzzy subsystem, the core of its control model would be described by the fuzzy rules it will set. Specifically, fuzzy rules describe the human decision-making process starting from formulating a hypothesis and successively mapping the fuzzy set from an input to an output space [204]. Such a mapping process can be defined as the "fuzzification process," while the reverse transformation will be called the "defuzzification." The physiological equivalent of this process is when the neuromuscular system receives an abstract decision from the central nervous system and consequently emits a force to the controlled device/machine. Fuzzy logic control models have been used to represent various human control activities in many research works, achieving good results in overcoming the limitation of approaches relying on a strict categorical division, especially in classification problems. In [205], fuzzy logic classification was used to represent radiologists' reasoning and decision-making process when recognizing breast cancer types from the analysis of medical images. While in [206], a fuzzy architecture was implemented for malware detection and classification in IoT applications. In the aeronautic domain, fuzzy control is suitable for developing a mental model of the pilot during a flight activity [207, 208], primarily referring to a compensatory type of sub-tasks [137]. The fuzzy logic control model was applied to study changes in simulated activity fidelity in aircraft control and Dynamic Multiattribute Decision Making (DMADM) applications [209]. Additionally, fuzzy control theory was used for the safety evaluation of landing operations considering aircraft [210, 211] and rotorcraft [212]. However, the computational efficiency of fuzzy control systems is limited in cases in which a vast number of rules is present [213]. Moreover, it can be challenging to determine the rules when their number is high, and subjective model tuning will make its validation more challenging.

4.3.2 Artificial Neural Networks

For nonlinear dynamical system modeling, Artificial Neural Networks have grown significantly in many research activities in the last years due to their flexibility and ability to imitate human learning, and decision-making. Moreover, when building a model from unstructured data, ANNs proved to be useful to build a reduced low-order model [214] and for their classification capability [215]. Artificial Neural Networks are composed of a linear combination of fundamental units (i.e., neurons), which can provide a linear transformation from the input data $\mathbf{x}$ to output $\mathbf{y}$ through several intermediate hidden layers. Each ANN scheme can vary significantly if the input vector dimension is known. The user usually chooses the dimensionality of the hidden and output layers. The input-output relationship of a single-layer neural structure with m inputs (being m a positive integer greater than 1) and single output would be, in the linear case:

$$y = \sum_{i=1}^{m} \mathbf{x}_i \mathbf{w}_i + q\,. \tag{4.8}$$

Where variable $\mathbf{x}_i (i \in (1, 2, \ldots, m))$ represents the input signal of the model, y represents the output signal, $\mathbf{w}_i (i \in (1, 2, \ldots, m))$ is the weight of each input signal and q is the threshold of the activation function f. Nonlinear activation functions can be used to represent a wider range of dynamics. The more general definition of an ANN constituted by M layers, providing a nonlinear mapping between input and output data, would be:

$$\mathbf{y} = f_M(\mathbf{A_M}, \ldots, f_2(\mathbf{A_2}, f_1(\mathbf{A_1}, \mathbf{x}))\ldots)\,. \tag{4.9}$$

Here, the A_M to A_1 matrices contain the weight coefficients w_i that map each variable from one layer to the next. The weights are chosen to fit the function:

$$\text{argmin}_{\mathbf{A_j}}(f_n(\mathbf{A_n}, \ldots f_2(\mathbf{A_2}, f_1(\mathbf{A_1}, \mathbf{x}))) + \lambda g(\mathbf{A_j}))\,. \tag{4.10}$$

Human behavior and information processing representation are based on the weights of neural networks. Such modeling technique is advantageous in aeronautical applications, for example, when mapping pilot control in research works where extensive data to process are available [216]. In [217], ANN and quasi-linear approaches are confronted in a two-axis tracking task, verifying neural network accuracy in describing nonlinear pilot behavior in aircraft control. In [218], an adaptive neural network controller is used by combining the trained network and a proportional-integral controller in an attempt to find a model-based method for control determination of unknown dynamics.

4.3.3 Neuro-fuzzy systems

Generally, neuro-fuzzy systems can be defined as all the modeling techniques involving artificial neural networks and fuzzy logic. These techniques can be categorized into three classes, depending on the combination of the two elements [219]:

- Cooperative neuro-fuzzy systems
- Concurrent neuro-fuzzy systems
- Hybrid neuro-fuzzy systems

In a cooperative system, the neural component is only present in an initial phase and determines the blocks composing the subsequent fuzzy system using training data. After this stage, only the fuzzy system will be executed.

In concurrent systems, on the other hand, the neural and the fuzzy components work simultaneously. This means that the information is pre-processed by one of the two components and then given in input to the other.

The most promising and utilized models belong to the hybrid systems category. A hybrid neuro-fuzzy system can be imagined as a fuzzy system in which parameters, such as fuzzy sets and fuzzy rules, are determined using a learning algorithm inspired by the neural network theory. Such a neuro-fuzzy system can be entirely created starting from measured input-output data without the *a-priori* knowledge needed to develop fuzzy rules with the traditional approach.

An example of a commonly used model of this type is the Adaptive-Network-Based Fuzzy Inference System (ANFIS), which was proposed for the first time in 1993 [220]. Its structure is composed of five layers. The first hidden layer maps the input variable relative to each membership function. The output layer calculates the global output as the summation of all the signals coming in the input. In particular, input membership function parameters are determined using back-propagation learning algorithms, and the least mean square method is used to determine the consequent parameters. The first advantage is to show both characteristics of neural networks and fuzzy logic, comprising if-then statements more suitable for human-like decision-making logic. In addition, its structure is not a black box, as in the case of neural networks, and therefore can be more easily debugged and improved. Moreover, it has smaller parameters to be determined to provide faster training without loss of generality [221]. Such model recently found diverse domains of application aside from human-machine interaction, such as electric distribution systems [222, 223], speech recognition [224], and economics [225]. In [226], the ANFIS model was used for human fall detection

in comparison with other neuro-fuzzy techniques, such as the Local Linear Model Trees (LOLIMOT) model [227].

In LOLIMOT models, each neuron is a local linear model (LLM) and an associated validity function determines the region of validity of the LLM. The normalized validity functions form a partition of unity for any model input z are:

$$\sum_{i=1}^{M} \phi_i(\mathbf{z}) = 1\,. \tag{4.11}$$

While the output of each LLM is calculated as follows:

$$\hat{\mathbf{y}} = \sum_{i=1}^{M} (\omega_{i,0} + \omega_{i,1} x_1 + ... + \omega_{i,nx} x_{nx}) \phi_i(\mathbf{z})\,, \tag{4.12}$$

where $\mathbf{x} = [x_1, x_2, ..., x_{nx}]^T$. Here, the local linear models depend on $\mathbf{x}$, while the validity functions depend on $\mathbf{z}$ and are typically chosen as normalized Gaussian. The overall LOLIMOT network output is computed as a weighted sum of the LLMs outputs, where the $\phi_i(0)$ can be interpreted as the operating point-dependent weighting factors. The network interpolation between different LLMs is performed with the validity functions, where weights $w_{i,j}$ are linear network parameters. Again, LOLIMOT models were used in various domains of application, such as transportation [228], medicine [229], complex systems [230] and identification of time-variant nonlinear dynamics [231].

A dual fuzzy neural networks (DFNNs) model constituted by two equal neural networks has been used to simulate the physical nervous system in [232]. The advantage of dual fuzzy neural networks (DFNNs) is related to their close similitude to functioning and flexibility typical of humans. As in the case of ANNs, DFNNs can choose a suitable nonlinear mapping of input/output features through an iterative learning phase, in which neuron weights are updated. Such a model was implemented to simulate the relationship between the control signal and human perceived input [233]. Its performance were evaluated to provide insight into the pilot's decision-making process [234]. Moreover, [235] proposed a risk evaluation procedure founded on ANNs with the fuzzy control approach.

Even though in the Neuro-fuzzy model, neural networks and fuzzy logic are integrated, its drawback is to increase the computation and tuning time potentially. Besides, the experimental validation of the obtained model parameters may be tricky.

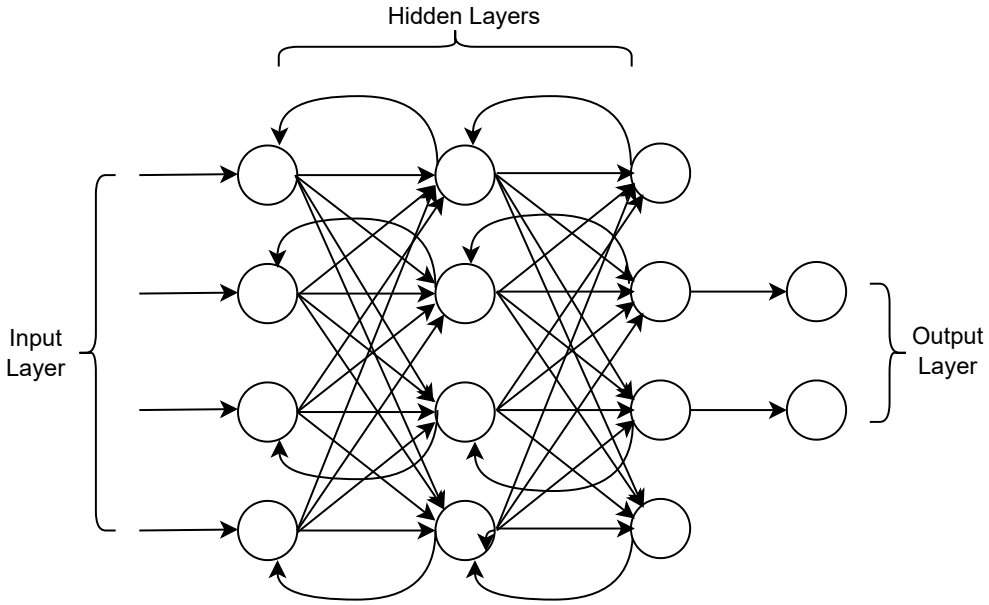

Figure 4.3: General structure of a Recurrent Neural Network and its internal feedbacks

4.4 Data-Driven Approaches

Data-driven approaches have attracted more and more attention in recent years in various application scenarios in nonlinear dynamical system modeling and identification [236]. In human-machine interaction, learning processes starting from unstructured data using different types of Artificial neural networks (ANN) have been used for their processing classification by imitating human learning capability and decision-making, often combined with other learning algorithms, as we will discuss later in this section. A widely used type of network is the Convolutional Neural Network (CNN), traditionally used for capturing spatial relations in data, valid for applications with robust image processing, which are very common in human-robot collaboration [237] or autonomous system navigation [238].

However, for the study of nonlinear dynamics introduced by the human into the system during its control activity, aspects such as its temporal delay [239], or temporal relations in general within the given data series, might be more relevant. Recurrent neural networks (RNNs) are the primary ANNs suitable for processing time series and other sequential data types. RNNs can extract a sequence's contextual information by defining the mutual dependencies between various time stamps. As shown from the scheme represented in Figure 4.3, standard RNN is composed of numerous successive recurrent

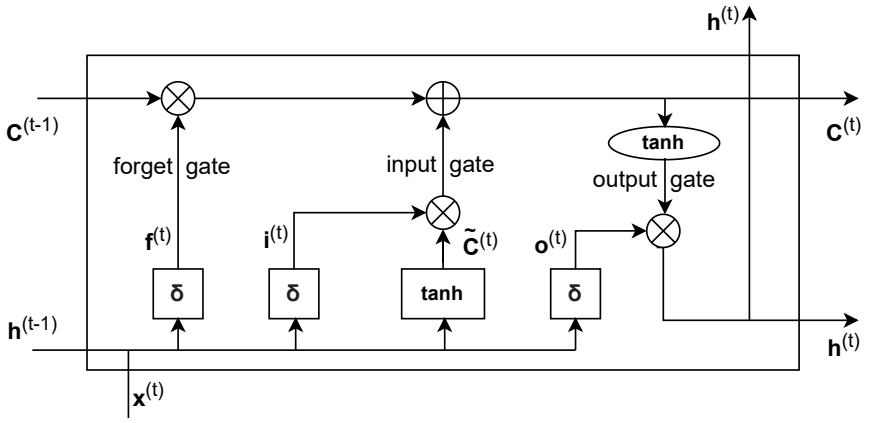

Figure 4.4: Internal structure of an LSTM unit [185]

layers and has a lot of feedforward and feedback connections in the time direction, allowing it to sequentially model its layers to map a sequence with other sequences. This makes it a good choice for dynamic system identification and control.

Concerning its structure, an RNN can be defined as an extension of feedforward ANN with internal loops in hidden layers. The activation of the state of a recurrent hidden layer at each time instant is dependent on that of the previous one. At a given time frame, each non-input unit computes the current activation as the nonlinear function of the weighted sum of all the activations of every connected unit [240]. They have been successfully applied in natural language processing (NLP), image captioning, speech recognition, and other fields. In [241], the authors investigated the approximation capability of continuous-time RNNs to the time-variant dynamical systems. They proved that such network performance for approximating any finite time trajectory of a time-variant system were high. However, despite its suitability to model temporal variations present in the input, depending only on the current information and the previous output, a standard RNN may encounter difficulties when it comes to capturing long-term dependencies of time sequences.

To overcome this limit, a popular type of RNN which was proposed in a lot of research works is the Long Short-Term Memory network (LSTM), An LSTM network is a modified RNN, mainly designed to improve its ability to capture long-term relationships by avoiding premature gradient disappearance in error back-propagation algorithms through time.

LSTM is composed of a combination of units, representing internal structure in Figure 4.4. Each unit simultaneously receives an input vector $\mathbf{x}^{(t)}$

and the state of the hidden layer in the previous time instant $\mathbf{h}^{(t-1)}$ and updates, as output information, the cell state $\mathbf{C}^{(t)}$ and the current state of the hidden layer $\mathbf{h}^{(t)}$. This operation is done through three embedded layers in each LSTM unit: the input, output, and forget gates. The three gates have different roles and work in coordination: the forget gate $\mathbf{f}^{(t)}$ determines the probability that certain information has to be canceled from the cell state vector; the input gate $\mathbf{i}^{(t)}$ identify the new information to be stored, while the output gate $\mathbf{o}^{(t)}$ controls the output of the current hidden state $\mathbf{h}^{(t)}$. Translated into mathematical expressions, LSTM unit operations are the following:

$$\begin{aligned}
\mathbf{f}^{(t)} &= \sigma(\mathbf{W_f}\mathbf{h}^{(t-1)} + \mathbf{U_f}\mathbf{x}^{(t)} + \mathbf{b_f}) \\
\mathbf{i}^{(t)} &= \sigma(\mathbf{W_i}\mathbf{h}^{(t-1)} + \mathbf{U_i}\mathbf{x}^{(t)} + \mathbf{b_i}) \\
\tilde{\mathbf{C}}^{(t)} &= \tanh(\mathbf{W_C}\mathbf{h}^{(t-1)} + \mathbf{U_C}\mathbf{x}^{(t)} + \mathbf{b_C}) \\
\mathbf{C}^{(t)} &= \mathbf{C}^{(t-1)} \odot \mathbf{f}^{(t)} + \mathbf{i}^{(t)} \odot \tilde{\mathbf{C}}^{(t)} \\
\mathbf{o}^{(t)} &= \sigma(\mathbf{W_o}\mathbf{h}^{(t-1)} + \mathbf{U_o}\mathbf{x}^{(t)} + \mathbf{b_o}) \\
\mathbf{h}^{(t)} &= \mathbf{o}^{(t)} \odot \tanh(\mathbf{C}^{(t)}) \,.
\end{aligned} \tag{4.13}$$

Where $\mathbf{W}$, $\mathbf{U}$, and $\mathbf{b}$ represent respectively the recurrent matrix, input weight matrix, and bias vector, σ and *tanh* are sigmoid and hyperbolic tangent functions, and $\odot$ represent the element-wise Hadamard product.

Yeo et al. [242] implemented LSTM networks to build a simulation model of noisy nonlinear dynamical systems using experimental data. Their goal was to identify the best fit of the probability density function of a given stochastic process and to represent the underlying nonlinear dynamics. Chen et al. [185] used LSTM networks to learn the characteristics of strongly nonlinear external dynamics of Van der Pol and Lorenz systems.

As said, neural networks used for unstructured learning have increased their potential by combining them with other learning algorithms. The most promising technology in this sense is Reinforcement Learning.

Unlike supervised and unsupervised learning, reinforcement learning has arisen as the third kind of machine learning paradigm. Using computational Reinforcement Learning algorithms allowed us to quantitatively describe several previously abstract concepts in neuroscience, cognitive, and behavioral science [243].

As detailed in [244], reinforcement learning (RL) can rely on Markov Decision Processes as a learning framework in which a learning agent interacts with an external environment and perceives its state, choose its actions to maximize a numerical reward function. The reward function is a simple

numerical value for each time stamp, which can increase or decrease by one unit in the future due to the agent's actions. Therefore, the goal to maximize the reward function can be translated into maximizing the expected value of the cumulative sum of the scalar reward signal. Being defined from external information acquired from the environment through sensory inputs (in the case of a human operator), the goal to achieve is always defined outside the learning agent. In the case of a human being, that means that the learning agent can be defined as only the subsystem deputed to process the external inputs to define a control strategy (i.e., the central nervous system). The sensory subsystems can be considered part of the environment. In real-world complex situations in which humans are confronted with a challenging task, their duty is to derive efficient representations of the environment from high-dimensional sensory inputs and use them to generalize past experience and be able to use it in new situations [245]. If we consider an episodic task in which the agent-environment interaction can be decomposed into sub-sequences of repeated interactions, there is also a final time step, T. In this case, for a given timestamp t, the reward function to maximize is:

$$G_t = \sum_{k=0}^{T-t-1} \gamma^k R_{t+k+1} \,. \tag{4.14}$$

Where γ, being $0 \leq \gamma \leq 1$, is the discount rate. This parameter determines the present value of future rewards. When γ is close to zero, the weight of immediate rewards is higher and mostly taken into account by the agent; as it approaches 1, the goal takes future reward values more strongly weighted. If we have a continuous interaction in which there are neither definable intermediate steps nor a known final time frame, the above equation can be rewritten with $T = \infty$.

Reinforcement learning algorithms were extensively used in many research works relating to humans interacting with a machine, with many reward functions designed and more suitable for the different application scenarios. In [246], a Deep Deterministic Policy Gradient (DDPG) reinforcement learning algorithm is used to estimate human intentions in a human-robot interaction framework using EMG sensory inputs. At the same time, [247] integrated RL into the robot motion planning in a multi-robot collaborative manufacturing plant to implement human-in-the-loop control in teleoperated robots through augmented reality and digital twin techniques.

In the transport field, [248] adopted microscopic traffic simulation and reinforcement learning to implement the lane-changing strategy in connected and automated vehicles (CAVs). Reinforcement Learning has been successfully used with model-based techniques for systems identification in [249].

This was done to estimate the reward function from online data by acquiring and processing linear and nonlinear external dynamics. Mu et al. [186] used a reinforcement learning algorithm for partially non-modeled nonlinear systems, coupled with two neural networks, to implement an event-triggering dynamic strategy. In robotics, Deep Reinforcement Learning can be used for motion planning in cooperative applications with a human subject, learning how the human interacts with a specific environment and adaptively computing the best way to interact with him [250].

4.5 Nonlinear dynamics in human-machine systems

The discussed modeling techniques and data-driven approaches have been successfully used for describing nonlinear dynamics in many application domains where humans interact with a controlled element.

Transport systems, for example, are a particularly relevant field of application for nonlinear dynamics modeling in human-machine interaction for what concerns the nonlinear dynamics deriving human decision-making, from the nonlinear nature of the controlled element and/or the system, and from human body physical coupling with the controlled system.

For what concerns the first point, connected and automated vehicle (CAVs) development has gained more and more attention from companies and research centers in the last few years. In studies dealing with automated lane changing, machine learning techniques were extensively used for human decision-making modeling and its use in automatic control strategies.

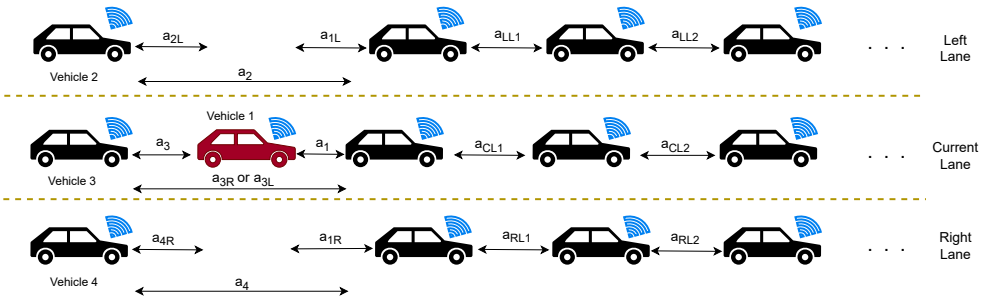

Figure 4.5: Connected Automated Vehicles represented in a lane-change scheme

Let us consider the situation described by Figure 4.5, in which Vehicle 1 (V1) has to choose a lane-change strategy and is followed by vehicles 2,3, and 4. If we discretize the CAV travel as a series of time steps t, and S_t is

the state of the external environment at each step t, we would have that:

$$S_t = \{\tilde{a}_{1L}, \tilde{a}_{1R}, \tilde{a}_{2L}, \tilde{a}_{4R}, \tilde{a}_3, \tilde{\nu}_L, \tilde{\nu}_R, \tilde{\sigma}_L, \tilde{\sigma}_R\}(t)\,. \tag{4.15}$$

Here, $\tilde{a}$ represents the acceleration difference of the considered vehicles (in the subscripts, numbers represent the vehicle and the letter the lane change direction) after V1 lane change; $\tilde{\nu}$ represents the mean acceleration difference between the central and the left or right lanes; $\tilde{\sigma}$ represents the difference between the standard deviations of the acceleration differences. From a learning agent perspective, these acceleration differences represent the gain obtained after a lane change. Therefore, the reward function could be formulated as follows:

$$R_t = a_1^{t+1}\,. \tag{4.16}$$

The subscript number stands for vehicle 1, and $t+1$ represents two consecutive simulation time stamps.

A lot of research efforts on this topic used simulation environments such as Matlab toolboxes [251, 252] to represent vehicles' behavior, or robotic toolkits using partially observable Markov decision processes (POMDPs), such as in [253].

A connected and automated vehicle does not rely on any external supervisor but must autonomously learn with a trial-and-error approach to decide when to make a lane change and how to execute it. One of the most challenging aspects is that the vehicle must evaluate the long-term benefit of such an action and become farsighted in its strategy to maximize the travel's efficiency. For this challenge, reinforcement learning seems to be the preferential approach (as noticeable from its formulation described in the previous section). For instance, in a high-fidelity simulation environment, [254] used a deep reinforcement learning training program for car following. In [248], the authors also used reinforcement learning in a microscopic traffic simulation environment [255] calibrated using actual highway data. Li et al. [256] used an evolutionary learning approach for lane change tested in a highway simulation environment. The optimization problem objective is to maximize the velocity while minimizing the disruption to the following vehicle; if it is impossible to reach this goal in the current lane, a change-lane decision is taken.

In this case, the reward $\mathbf{r_{i,t}}$ depends on the difference between desired velocity $\mathbf{v_d}$ and actual velocity $\mathbf{v_{i,t}}$ of the controlled vehicle and the acceleration of the following one ($\mathbf{a_{k,t}}$):

$$\mathbf{r_{i,t}} = -|\mathbf{v_{i,t}} - \mathbf{v_d}| + \mathbf{a_{k,t}}\,. \tag{4.17}$$

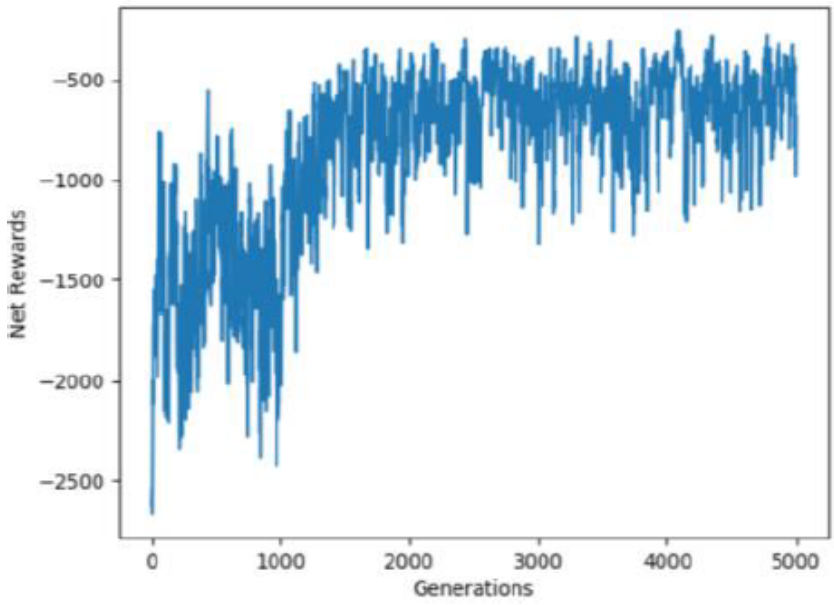

Figure 4.6: Reward values during the system training in evolutionary learning adopted in [256].

If the velocity difference overcomes a certain threshold, the lane is changed. The decision-making process has indeed a purely nonlinear behavior, also reflected by the resulted reward values during the training of the system, shown in Figure 4.6.

However, the lane change has not a time-driven structure but an event-driven one, described as a discrete dynamic process, which can be well represented as a Markov Decision Process. In [257], POMDPs were also used for an automatic lane change in long-distance road experimental trials using automated vehicles. Here, the decision-making process is modeled, referring not only to the controlled vehicle but also to the surrounding environment, inspired by the consideration that human drivers change their behavior when interacting. Reaction modeling is performed by measuring the temporal evolution of the vehicle state, including in it also a reaction and a deviation parameter.

Figure 4.7 represents the differences between the traditional hidden goal method, which applies only to specific regions of interest, and the reactive method, which models the group of vehicles in general and their deviation.

A further aspect of human decision-making in a lane-changing application is related to risk propensity. In [258], the authors proposed a decision model that considered the driver's perception, reasoning, and emotions. Risk propensity considers two mental processes: regret biasing and probability

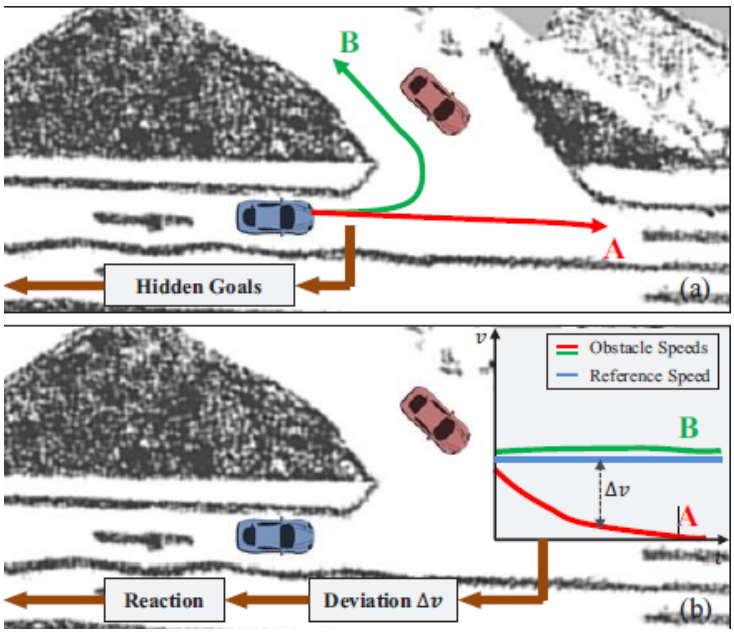

Figure 4.7: Motion intention estimation as explained in [257], using hidden goal (a) and reaction (b) methods.

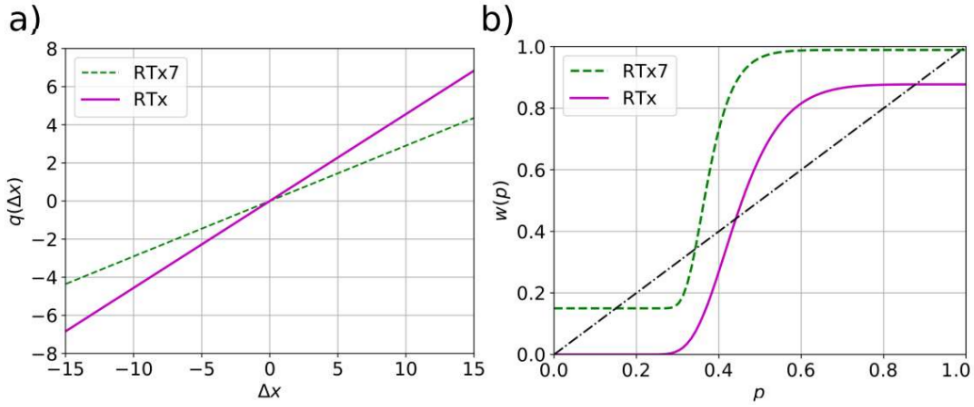

Figure 4.8: Modeling of regret biasing (a) and probability weighting (b) at a cognitive level as studied in [258].

weighting, corresponding to the emotional aspect and cognitive reasoning. Both functions' nonlinearity increases proportionally to the emotional bias and cognitive weighting. The proposed model was tested with a dataset from a naturalistic driving database. Figure 4.8 represents the obtained fitted functions without considering regret biasing and probability weighting (purple line) and with the two terms (green dashed line). Figure 4.8a represents the regret q-functions, which resulted in being linear, indicating the regret influence is not evident in all cases. On the other hand, Figure 4.8b shows a w-function divided into three intervals; in two of them, the function overweights the objective probability (dot-dashed line), indicating a general optimism and bent to take risks.

As said, aside from human decision-making representation, the source of nonlinearity in the human-machine complex may be related to the dynamics of the controlled element. If the human subject continuously controls such devices, this will raise an essential challenge concerning system modeling and control.

In cooperative teleoperated robotic systems, for instance, many nonlinear control approaches have been developed in order to deal with non-passive (and therefore unstable [259]) factors such as the uncertainty of the environment, the presence of variable communication delays, kinematics, and dynamics parametric uncertainty. Such kinds of systems have found vast applications in healthcare [260], space [261], and exploration in dangerous environments [262] and disaster scenarios [263]. Even if Linear control approaches have been successfully developed for robust stability achievement in the presence of uncertain system dynamics, nonlinear controllers proved to guarantee good stability and performance through the exploitation of special properties of nonlinear rigid body dynamics of master and slave manipulators [264].

In [265], nonlinear bilateral control of a teleoperation system with a flexible-link slave manipulator is performed by designing a robust tip position tracking controller for the slave manipulator. The desired trajectory is determined based on the master's position signal, and a force controller for the master robot, which should track the environmental force exerted on the slave manipulator. While [266] proposes a control strategy able to establish position-position kinematic correspondence between master and slave by incorporating in the adaptive controller the models of operators, controlled robots, tools, and environment, as well as their parametric uncertainty. Further approaches, as in [267], enlarged this concept by mapping the human arm stiffness references in a bilateral teleoperation framework, building a "teleimpedance control", later extended with a semi-autonomous contact detection strategy in [268]. Moreover, another challenging aspect of bilateral

teleoperation systems control is related to the presence of communication time delays, which may cause the system to degrade its performance and even result in unstable behavior. The time delays should therefore be considered in the design stage of the controller. In [269], this problem is faced by considering adaptive neural synchronization control of bilateral teleoperation systems with backlash-like hysteresis, one of the most important nonlinearities in robots. While in [270], a finite-time synchronization control method is proposed based on fuzzy approximation of system uncertainties.

Another example of highly nonlinear controlled systems interacting with an unknown external environment consists in multirotor remote control. Multirotor applications were carried out in several research activities, with practical applications like surveillance, photography, video-making, grasp or motion of an object, or military [271]. The equation of motion of a multirotor with a mass m and inertia tensor $\mathbf{J}$ can be written as:

$$\begin{aligned} m\ddot{\mathbf{x}} &= -m\mathbf{g}\mathbf{e_3} + \mathbf{f}\mathbf{R}\mathbf{e_3} \\ \dot{\mathbf{R}} &= \mathbf{R}\hat{\mathbf{\Omega}} \\ \mathbf{J}\dot{\mathbf{\Omega}} &= -\mathbf{\Omega} \times \mathbf{J}\mathbf{\Omega} + \boldsymbol{\tau}\,. \end{aligned} \tag{4.18}$$

Where $\mathbf{f}$ and $\boldsymbol{\tau}$ are the force and torque inputs, $\mathbf{x}$ is the multirotor position with respect to the inertial frame, $\mathbf{\Omega} = [p_B, q_b, r_B]^T$ is the angular velocity vector in the body frame, $\mathbf{g}$ is the gravity force, $\mathbf{e_3} = [0, 0, 1]^T$ and $\mathbf{R}$ is the transformation matrix from the body to an inertial frame.

The hat superscript indicates the transformation map between a vector in $\mathbb{R}^3$ and a 3×3 matrix. The translational dynamics will be:

$$\ddot{\mathbf{x}} = \frac{\mathbf{f}}{m}u_x, \ddot{\mathbf{y}} = \frac{\mathbf{f}}{m}u_y, \ddot{\mathbf{z}} = \frac{\mathbf{f}}{m}u_z - \mathbf{g}\,. \tag{4.19}$$

Where ψ, θ and ϕ are yaw, pitch and roll respectively; and $u_x = (\cos_\psi \sin_\theta \cos_\phi + \sin_\psi \, sin_\phi)$ and $u_y = (\sin_\psi \sin_\theta \cos_\phi - \cos_\psi \sin_\phi)$ and $u_z = (\cos_\theta \cos_\phi)$

If $\boldsymbol{\nu} = [\psi, \theta, \phi]^T$, $\mathbf{T}_\nu$ is the Jacobian to convert $\mathbf{\Omega}$ to $\dot{\boldsymbol{\nu}}$, and $\mathbf{J}_\nu = {\mathbf{T}_\nu}^T \mathbf{J} \mathbf{T}_\nu$ the rotational inertia tensor, the rotational dynamics can be expressed with a Lagrangian formulation as

$$\mathbf{J}_\nu \ddot{\boldsymbol{\nu}} + \mathbf{C}(\boldsymbol{\nu}, \dot{\boldsymbol{\nu}})\dot{\boldsymbol{\nu}} = \boldsymbol{\tau}\,. \tag{4.20}$$

Where C is the Coriolis matrix. If the roll and pitch angles are small, (4.20) can be simplified into

$$\ddot{\phi} = \mathbf{I_{xyz}}\dot{\psi}\dot{\phi} + \frac{\tau_\phi}{\mathbf{I_{xx}}}, \ddot{\theta} = \mathbf{I_{xyz}}\dot{\phi}\dot{\psi} + \frac{\tau_\theta}{\mathbf{I_{yy}}}, \ddot{\psi} = \mathbf{I_{xyz}}\dot{\phi}\dot{\theta} + \frac{\tau_\psi}{\mathbf{I_{zz}}}\,, \tag{4.21}$$

being $\mathbf{I_{xyz}} = \frac{(\mathbf{I_{xx}} - \mathbf{I_{yy}})}{\mathbf{I_{zz}}}$.

Trajectory tracking control for such systems is not accessible due to its nonlinearity, under-actuation, and highly coupled states. Although simple linear controllers such as PID or LQR have been successfully proposed in the past [272–275] for a limited number of non-agile movements, controllers using feedback linearization, backstepping or geometric control techniques are more suitable to handle with the nonlinearity of the system. Various types of Feedback Linearization (FL) techniques were used for multirotor, such as input-output and state-space linearizations [276] have been used for finding the rotor's dynamics linear approximation. For instance, such a linear relationship can be obtained by differentiating (4.19) and ψ in equation (4.21) until the control input terms are explicitly expressed. Controllers designed with this kind of procedure, however, will present high-order derivative terms, which might cause the controller to be less robust for what concerns sensor noise. To derive the input of the position controller, for example, (4.19) is differentiated until the 4th order until the control input term shows up. Attitude controllers in roll, pitch, and yaw angles can be designed similarly. These high-order derivative terms cause performance degradation of the controller as a consequence of disturbances such as the model's uncertainty. Despite this, feedback linearization showed promising results for finding the rotor's dynamics linear approximation. In [277], FL performance were compared with an adaptive sliding mode control technique. While in [278] FL controller was combined with a Luenberger observer.

However, the rotorcraft nonlinearity cannot be eliminated if a modeling error is present in feedback linearization. Thus its stability is not guaranteed. Therefore, backstepping control strategies with sliding mode techniques have been increasingly used to overcome these problems, associated with sliding mode techniques in [279–281]. A backstepping controller with sliding mode techniques is used in [279, 280, 282], based on the nonlinear translational (4.18) and the rotational simplified (4.21). When roll and pitch angles were high, such as in [283, 284], the Lagrangian formulation was preferred, even at a higher computational cost. Xian et al. [285] proposed a different approach in which an energy-based passivity controller controlled a quadrotor with a suspended payload. Also, neural networks were used in multiagent trajectory tracking applications, such as in [286], where an online RNN-based controller enabled the formation of a multiagent system characterized by a leader-follower structure. Such a control strategy allowed each agent to have the same output even with a different number of inputs, facilitating the system task planning.

Extensive research efforts were also directed through modeling unwanted

human control behavior in transport systems, particularly to Rotorcraft-Pilot Coupling (RPC) [287]. For evaluating human-rotorcraft interaction in aspects such as comfort and handling qualities, some performed modeling efforts present in literature were directed towards studying the dynamical behavior of the human body. Understanding such body dynamics, in this case, the upper body is fundamental to identifying potentially dangerous nonlinearities in RPC. These approaches vary significantly and can be classified into two main categories, such as finite element models (FEM); and multibody dynamics (MBD) or lumped parameter models (LPM).

Lumped parameter models are composed of elementary mechanical subsystems, such as lumped masses and viscoelastic elements with linear or nonlinear properties. In the linear case, parameters are relatively easy to identify, with a low associated computational cost and can be easily tuned to fit the biomechanical characteristics of a specific subject. However, in LPM where nonlinear viscoelastic elements are used, the cost of identifying its characteristics may increase, depending on the applied force or displacement. In [288], the authors used a piecewise LPM as an analytical tool to perform a preliminary analysis of vehicle crashworthiness in order to reduce the time required to assemble and tune FEMs and perform a nonlinear finite element analysis in crash testing. In the proposed LPM, the spring and damping coefficients are defined as piecewise linear functions of input displacement and velocity. Lumped parameters nonlinear models are also present in works such as [289], in which a one-degree-of-freedom model was applied for analyzing human body dynamic response during a helicopter landing. In works such as [290, 291], previous state-of-the-art linear models were optimized using a genetic algorithm to capture the nonlinear effects of passengers' dynamic response when subjected to vibrations.

In [292], a multibody model of the upper body was designed by connecting a model of the pilot's arms to a model of the spine. Such a spine model, as well as the scaling procedures, was used for studying seat-to-head transmissibility. This coupled spine-arms model can be used to evaluate the biodynamic response of the human operator in terms of involuntary motion induced on the control inceptors, including the related nonlinearities.

Finite element models have been successfully used in recent research to represent human body behavior during an impact, often in relation to injury risk prediction and vehicle safety. The Total Human Model for Safety (THUMS) is a famous finite element human body model intended for injury analysis [293]; it has been used in association with a model of a vehicle's internal structure, with the purpose of simulating human body kinematics in response to a large impact in a car crash. The geometries of the structurally complex human body parts, including the head, torso, ligaments, joints, and

internal organs, are represented by finite element meshes, and their impact responses have been studied separately. Moreover, in relation to transport safety, within the context of the European project "Human model for safety two" (HUMOS2) [294] human body numerical body models were constructed in order to create a database able to represent the European population with high fidelity. Portions of HUMOS2 models have been used in many research efforts, such as [295] for which thoracic accidents and [296] for head injuries in motorcycle crashes. Another example of FEM used to provide kinematic and kinetic data of the human body in a computationally efficient way has been proposed in [297] by the Global Human Body Models Consortium (GHBMC).

4.6 Final considerations

The presented modeling research efforts of nonlinear dynamics in human-machine interaction successfully captured many aspects of the human learning process, information processing, and control action. From the classical control-theory fashion of dual-loop control to the more recent machine-learning techniques, many advances have been made in identifying the sources of nonlinearity in human control behavior and in implementing models able to transfer such ability to the controlled machines. Modeling and data-driven techniques were presented in a human-centered way in order to show how they succeeded in representing different aspects of the human as a controller. For instance, the decision-making process directed toward achieving an internal goal is well described by reinforcement learning approaches, while optimal control models of the neuromuscular system or biodynamical models are most useful for nonlinear dynamics deriving from human body actuation districts or from its coupling with the controlled element. Moreover, data-driven techniques associated with control systems were analyzed in relation to nonlinearities that derive from the controlled element dynamics and/or the external environment. As proved by the discussed man-machine systems, the discussed algorithms can be combined to increase the level of autonomy and the usability of machines even in complex scenarios such as connected vehicles, automatic lane changes, teleoperation, or remote control of rotorcraft.

This is done while acting in an environment surrounded by humans, with consequent potential issues regarding safety and adding unexpected physical interaction that requires a level of adaptability, which is typical of human beings and constitutes one of the reasons that motivated such modeling efforts. Despite the successes concerning classical control theory models discussed in the first sections, modern machine learning frameworks struggle to capture the physiological context relying upon the human learning process. Neural

networks and algorithms based on reinforcement learning or optimal control paradigm still have almost a black-box approach to what concerns this aspect. Advances in understanding the human brain are still a challenge that motivates many research activities.

However, this way of combining different machine learning and model-based techniques seems to be perfect for our human-robot interaction application scenario. Here, we have partial knowledge of the system and the dynamics involved during a continuous physical interaction. Machine learning frameworks, such as Artificial Neural Networks, can be combined with models characterized by an autoregressive part, a moving average, and exogenous inputs. Their characteristics seem perfect to be used in the presence of noisy and unstructured data. In the next chapter, we will see how the use of ANNs and Narmax models can be used to accurately represent human control behavior when controlling a robot.

Chapter 5

Narmax Model for Human Intention Estimation

5.1 Narmax models

Nonlinear Autoregressive models with Moving Average and Exogenous Input (NARMAX) have been proposed for the first time by Stephen A. Billings [51] Many state-of-the-art research efforts have been widely used to identify nonlinear systems with partially unknown features with good results. As may be deductible from the acronym, NARMAX models derive from the mostly known linear ARMAX models and their variations like AR, ARX, ARMA, and ARIMA.

In [298], Billings considers NARMAX as not only the name of a model but a proper philosophy of nonlinear system identification that consists on five steps:

- Structure detection: Identify the terms present in the model
- Parameter estimation: Estimate its coefficients
- Model validation: Check eventual errors and biases in the model
- Prediction: Forecast model output in several steps in the future
- Analysis: Analyze the dynamical properties of the system

The first step, Structure detection, constitutes the crucial part of Nonlinear model identification. While in the linear case determining model order is relatively easy and is often between the first and third order (making the computations even faster and more efficient), things are far more complicated

and computationally demanding in the nonlinear case, where the number of candidate terms can arise easily if we want, for example, to approximate lag terms with polynomial expansions [299].

Let us consider the experimental setup proposed in Chapter 3, in which our model has to predict the force actuated by a human subject into the robot end-effector when an external reference has been applied to the system. If we indicate the force signal we want to predict as y and the external reference (or exogenous input) as x, the model would be:

$$y(t) = f\Big(y(t-1), \dots, y(t-n_a), x(t-d), \dots, x(t-d-n_b), e(t-1), \dots, e(t-n_c)\Big) \tag{5.1}$$

Where n_a, n_b, and n_c indicate the maximum lag for system output and input and for noise, respectively, and define the order of the model, while d indicates an additional transport delay between input and output.

5.1.1 Polynomial Approximation

The nonlinear function $f(\cdot)$ can be approximated using different strategies, we will focus on them: Polynomial algorithms and Neural Networks. The first one aims to find a piecewise linear equivalent of the nonlinear function. The following equation can describe a polynomial Narmax model with asymptotically stable equilibrium points [300]:

$$\begin{aligned} y_t = \sum_{0} + \sum_{i=1}^{p} \Theta_y^i y_{k-i} + \sum_{j=1}^{q} \Theta_e^j e_{k-j} + \sum_{m=1}^{r} \Theta_x^m x_{k-m} + \sum_{i=1}^{p}\sum_{j=1}^{q} \Theta_{ye}^{ij} y_{k-i} e_{k-j} \\ + \sum_{i=1}^{p}\sum_{m=1}^{r} \Theta_{yx}^{im} y_{k-1} x_{k-m} + \sum_{j=1}^{q}\sum_{m=1}^{r} \Theta_{ex}^{jm} e_{k-j} x_{k-m} \\ + \cdots + \sum_{m_1=1}^{r} \cdots \sum_{m_l=m_{l-1}}^{r} \Theta_{x^l}^{m_1,\dots,m_2} x_{k-m_1} x_{l-m_l} \end{aligned} \tag{5.2}$$

where $\sum_0$ and all the terms with Θ indicate constant parameters, and l is the degree of polynomial nonlinearity. Polynomial algorithms will select a subset of the terms of equation (5.2), also called regressors, which will minimize the error between estimated $\hat{y}(t)$ and real $y(t)$. Examples of these kinds of algorithms are the Forward Regression Least Squares (FROLS) [301], Meta-Model Structure Selection (MetaMSS) [302], Accelerated Orthogonal

Least Squares (AOLS) [303] and Entropic Regression [304, 305]. Most of them use information theory for order selection and select the best regressors and least-squares-based algorithms, in the case of FROLS and AOLS, for parameter estimation. This kind of strategy, as explained in [300], has a critical aspect in required computational time that can become very high due to the fact that the possible model structures to be tested are 2^{n_r}. Here n_r is the number of candidate regressors that depends on the maximum lag $n = n_a + n_b + n_c$ and on the order of the nonlinearity l, that determines the number of polynomial combinations between all input and output terms. In particular:

$$n_r = \frac{(n+l)!}{[n!l!]}.$$

For each model regressor, then, it is still necessary to estimate each single parameter value with the chosen optimization technique. These considerations make it difficult to apply polynomial techniques to the human-robot system, characterized by a high degree of nonlinearity and impulsive force.

5.1.2 Neural-Network Approximation

The second strategy is to approximate the $f(\cdot)$ by using an Artificial Neural Network (ANN). As stated in the universal approximation theorem, "*a neural network with a single hidden layer can accurately approximate any nonlinear continuous functional.*" This consideration makes ANNs the obvious choice for our scope, even if more complex structures rather than the simple single-layer one indicated in the theorem, are used nowadays [306]. In mathematical terms, we have that [307]:

Theorem 1 *Let $\phi(\cdot)$ be an arbitrary activation function. Let $X \subseteq \mathbb{R}$ and X be compact. The space of continuous functions on X is denoted by $C(X)$. Then $\forall f \in C(X)$, $\forall \epsilon > 0$: $\exists n \in \mathbb{N}$, a_{ij}, b_j, $w_i \in \mathbb{R}$, $i \in \{1 \dots n\}$, $j \in \{1 \dots m\}$:*

$$(A_n f)(x_1, \dots, x_m) = \sum_{i=1}^{n} w_i \phi(\sum_{j=1}^{m} a_{ij} x_j + b_j)$$

as an approximation of the function $f(\cdot)$; that is

$$\| f - A_n f \| < \epsilon$$

Therefore, The universality property is independent of the chosen activation function but is a consequence of the multilayer feedforward architecture, as proved by Hornik et al. in [308]. This concept led researchers to

extend such property to different network structures to gain an advantage in modeling different kinds of systems and functionals, as in the case of [309], where the authors starting from the work of Hornik, developed RNNs to map open-loop dynamical system. In [310], the authors derived an approximation error bound with explicit prefactor for Sobolev-regular functions using deep convolutional neural networks (CNNs), while in [311], the approximation performance have been improved by using a multiresolution approach which increases network robustness.

5.1.3 Results

Going back to our setup, the first step to do is the preparation of the dataset in order to correctly feed the network with the correct autoregressive, input, and error elements. The dataset used for training the network is the same used in Chapter 3, previously used for linear model identification. All the signals have been processed considering x and y components and have been normalized between -1 and 1 before being fed to the network. The considered input signal was the randomly generated wave square, which was the reference that human subjects had to follow, while the output signal is, as said, the generated force.

In each time frame t, we ask the network to predict the signal $y(t)$ by finding the optimal internal connections (represented by the network weights values) starting from a window of input data which is composed by:

- $y(t-1), \ldots, y(t-n_a)$ force samples
- $x(t-d), \ldots, x(t-d-n_b)$ reference signal samples
- $e(t-1), \ldots, e(t-n_c)$ noise terms

This window has to change for each sample of the force signal we want to predict and must be built in both the training, validation, and test sets. In our model, $n_a = n_b = n_c = 10$, the window comprises 31 elements.

Noise terms, in particular, have an important role in system modeling. As seen in the linear case in Chapter 2, the human controller itself introduces noise into the system, to which the Crossover model refers as "*remnant noise*." McRuer used to model such noise as a random process linearly uncorrelated with the control input. Physically speaking, such a process is related to the error perceived by the human between the reference signal and perceived feedback and should be treated as an observation noise to add to the system input; the validity of this assumption was experimentally verified in [27]. To stick with this important physical aspect of the human controller

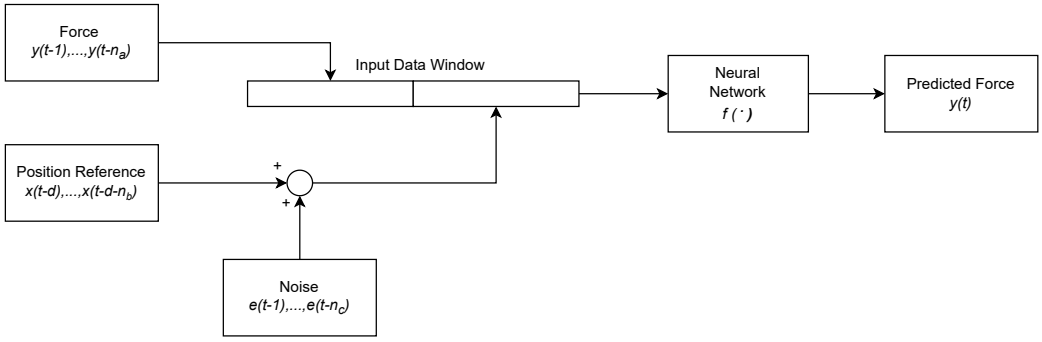

Figure 5.1: Schematic representation of how the proposed Narmax model was constructed by building an input data window at each time t and using an Artificial Neural Network to approximate the nonlinear functional element.

that we want to model, the noise terms $e(t-1)\dots e(t-n_c)$ and reference signal $x(t-d)\dots x(t-d-n_b)$, which is our control input, were added. The resulting terms were used, along with the n_a force samples, as input to the network when building the data window illustrated above.

The final network structure that was chosen is a 4-layer ANN with rectified linear unit (ReLU) activation function, apart from the last layer, which was set as a linear layer as traditionally done not to restrict the output range of variation [311]. The network was trained with a learning rate of 0.001 and mean squared error loss function, which predicted most accurately each time instant of the $y(t)$ signal. The dataset was split into 50% used for training, 25% for validation, and 25% for testing. During the model training phase, the time instant of the force signal whose value has to be predicted has been randomly chosen within the range of indices between $[d+n_b, L_y]$, where L_y indicates the sample size of the signal. This process has to be repeated for each of the three aforementioned subsets, adapting L_y size according to the corresponding indicated percentages.

After the training stage has been completed, to test the model, the force values $y(t) \in [d+n_b, L_y]$, have been forecasted this time following a chronological order, to correctly reconstruct the force signal during the whole duration of the experiment. Figure 5.2 shows the resulting de-normalized predicted force versus the measured one; the brown part represents the portion where the two signals are overlapped. The figure shows a summary of the dataset used for training, constituted of 200 elements, 100 for x and 100 for y components. The chosen experiment was randomly chosen so that there is 1 for each subject for both components, so 1 each decade of the dataset. As evident from the plots, the model is capable of forecasting force samples with an outstanding degree of accuracy, since the overlapped part is almost the

entire amount of the two signals, despite the huge variability between the acquired signals that constitute the dataset in terms of noise and periodicity of the vectors.

To quantitatively evaluate the model's performance, Root Mean Squared Error and R2 score were computed for each predicted signal from the 100 experiments that were used for collecting the dataset. As noticeable, the model's good performance are shown by the very low Root Mean Squared Error, which was preferred to normal Mean Squared Error for its higher interpretability, being of the same unit of measure of input data (in this case Newton).

As noticeable from the data shown in Table 5.1 the RMSE, which as said shows de-normalized data in Newton, is close to 0. The value of the R2 score, which is a numeric value not constituted by a unit of measure and still considers normalized data, is close to its maximum value of 1. It is worthy of a remark on the fact that the R2 score does not have, instead, a lower limit: a model with bad performance could have as low values as possible from its physical characteristics! Both indices testify to the really high performance obtained by the model and its validity.

A concern that may arise from the shown results, is that the model overfits the dataset, being so accurate in the approximation of every generated force in all the noise conditions. If that is true, it would mean that the model is not generally applicable when varying human subjects and the other experimental conditions.

To have an answer to this question, in the next Section, we will test the model generalization capabilities by applying it to a different dataset, with a different forcing function, and with a different robot with respect to what had been used here.

Index	**RMSE x**	**RMSE y**	**R2 score x**	**R2 score y**
1	0.472036235	0.521664149	0.956724633	0.960830384
2	0.489941946	0.642806454	0.960653648	0.949716232
3	0.519541718	0.554902738	0.960189219	0.959170756
4	0.601814676	0.669788111	0.955643017	0.961106611
5	0.574182629	0.658225902	0.96087635	0.96252835
6	0.585448684	0.627132843	0.960482329	0.961794969
7	0.530537037	0.662696702	0.963967534	0.963649709
8	0.617680061	0.724884097	0.964767234	0.962247245
9	0.551281783	0.699222684	0.966718266	0.958319885
10	0.540838129	0.628847549	0.961557462	0.962917097

11	1.001928234	1.632743179	0.960195286	0.946946818
12	0.879766609	1.122209997	0.954856202	0.953832129
13	0.839163153	1.111029515	0.95914142	0.945890859
14	0.773373836	1.203074269	0.955129589	0.951072734
15	0.891532239	1.158637026	0.949615224	0.950984968
16	0.755985785	1.084383216	0.952572305	0.957884578
17	0.685293479	0.921445126	0.953228398	0.954294241
18	0.573845426	0.980308637	0.950972863	0.957289423
19	0.515555599	0.853679632	0.951384536	0.958947792
20	0.732953844	1.276626686	0.941025365	0.937022948
21	0.779908125	1.032217524	0.957220077	0.955973842
22	0.717266276	1.013400762	0.951455669	0.936464505
23	0.659451419	0.813392031	0.968066462	0.960385522
24	0.595282446	0.714604865	0.948058756	0.946671776
25	0.580491582	0.689179515	0.952205569	0.948194036
26	0.637227825	0.80138281	0.96229403	0.963255591
27	0.641417839	0.795405533	0.965880499	0.963530068
28	0.653279451	0.820438478	0.958745918	0.957266842
29	0.696505807	0.931492427	0.954515885	0.97026166
30	0.633404694	0.823071262	0.960112106	0.963946552
31	0.653850802	0.638911347	0.936389479	0.952612566
32	0.527259381	0.633462448	0.941242301	0.946880339
33	0.648364611	0.760147021	0.9448306	0.9525119
34	0.531802732	0.668122088	0.954120572	0.959334652
35	0.496948157	0.959522604	0.955091424	0.937008427
36	0.469225642	0.766567706	0.941583529	0.951641584
37	0.412226024	0.597905458	0.958859779	0.956849482
38	0.513679866	0.541526516	0.951304856	0.957271993
39	0.488406263	0.580186734	0.956285987	0.957061112
40	0.537667398	0.689487665	0.953796888	0.958131693
41	0.810000726	1.001200503	0.959480548	0.967295193
42	0.816242923	1.08466761	0.960760813	0.967652903
43	0.838387612	0.965088842	0.967119422	0.958562475
44	0.756781692	1.113235316	0.961284896	0.958956991
45	0.909424742	1.005840925	0.959332263	0.963989186
46	0.63409503	0.969677432	0.957599245	0.966572981
47	1.057900284	1.351292111	0.961301498	0.956206088
48	0.71832515	0.785362473	0.956490612	0.963244864

49	0.690414144	0.84771881	0.964459701	0.946220406
50	0.613183623	0.764978636	0.969409659	0.966009687
51	0.742447286	0.960810155	0.960201052	0.956050056
52	0.751854625	0.914295651	0.957280078	0.952400024
53	0.811494761	1.238216424	0.942534553	0.954774985
54	0.801926757	1.147018492	0.935714128	0.956892106
55	0.800856941	1.033023894	0.948548094	0.955067056
56	0.858715064	1.075729024	0.939555377	0.967784763
57	0.776043582	1.036302229	0.963472345	0.955151007
58	0.755968542	1.033446737	0.948050068	0.966379937
59	0.949616911	1.375363849	0.933001818	0.962863828
60	1.016029316	1.455973209	0.938462374	0.957735294
61	0.44272718	0.451795379	0.935553434	0.969999585
62	0.502331117	0.493711302	0.936199774	0.958587934
63	0.542155534	0.603473038	0.927183852	0.946375419
64	0.490480574	0.555177238	0.951736575	0.954753754
65	0.466246555	0.54974428	0.945880337	0.956059571
66	0.438220919	0.468733171	0.947413566	0.956953769
67	0.423949319	0.480391149	0.950661121	0.954565105
68	0.48883597	0.535027873	0.931848345	0.956498211
69	0.481457007	0.57267078	0.947277832	0.951858001
70	0.52182963	0.618782586	0.938644815	0.938375534
71	0.491386615	0.607104793	0.937202986	0.945512594
72	0.463411188	0.597224165	0.951821046	0.947026245
73	0.532284003	0.648179002	0.95797053	0.955360121
74	0.53142484	0.649036079	0.954641615	0.958479429
75	0.585957896	0.734377326	0.961540867	0.961957569
76	0.601249499	0.842698817	0.954111628	0.953575918
77	0.619303016	0.637448297	0.966617421	0.934785461
78	0.687656891	0.743184784	0.961381829	0.927876761
79	0.592401816	0.658418071	0.953752515	0.946422712
80	0.628193068	0.664767329	0.942279814	0.936807898
81	0.742072066	1.083717746	0.949598424	0.957108816
82	0.850080368	1.206421153	0.921889782	0.94543225
83	0.922698646	1.220767547	0.918371174	0.952035447
84	0.894367366	1.402564313	0.917593521	0.94120114
85	1.133547374	1.820029435	0.948960106	0.94123321
86	0.938934707	1.359940352	0.917720283	0.934916194

87	1.060884229	1.73831993	0.910323347	0.940331842
88	1.14246511	1.507356616	0.917072358	0.940996278
89	0.90528934	1.223504068	0.92624921	0.946063163
90	0.955415892	1.14667481	0.941171141	0.937761062
91	0.390547613	0.410679524	0.954216646	0.95810864
92	0.415624598	0.427568629	0.956806357	0.948533138
93	0.486593196	0.409988808	0.935246045	0.942162937
94	0.458686577	0.427382061	0.945552973	0.948642137
95	0.440944996	0.411954816	0.940034109	0.951950269
96	0.439976922	0.348811568	0.949425666	0.96367613
97	0.456322357	0.407657337	0.948594671	0.954207793
98	0.429119011	0.34507542	0.949096734	0.9616144
99	0.465654266	0.395928492	0.943786995	0.952985548
100	0.450937512	0.415887569	0.936107923	0.948991599

Table 5.1: Root mean square error (in Newton) and R2 Score considering the predicted versus the measured human force. RMSE index, being expressed with the same unit of measure of input data, considers de-normalized values. R2 score is a numeric value with the upper bound of 1 and still uses normalized values.

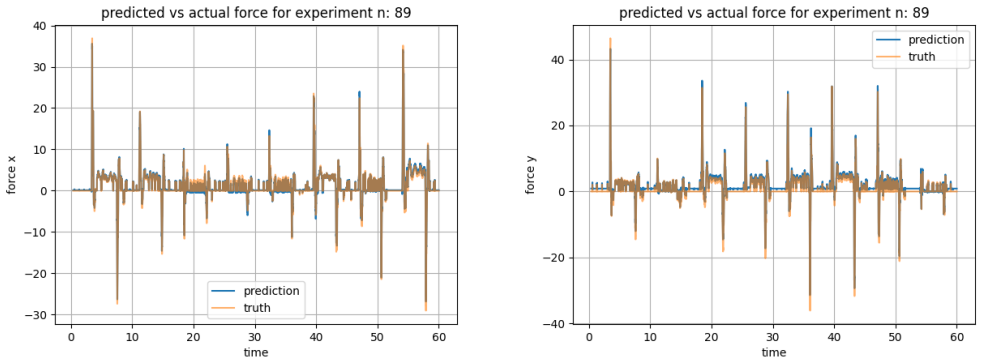

(a) **(b)**

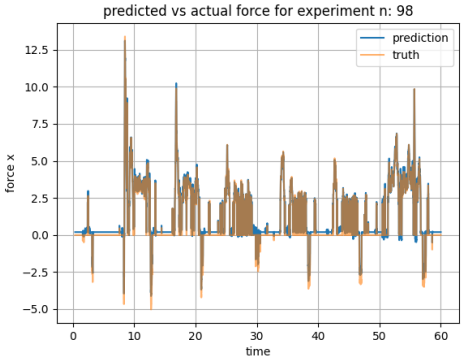
predicted vs actual force for experiment n: 98
prediction
truth
force x
time

(c)

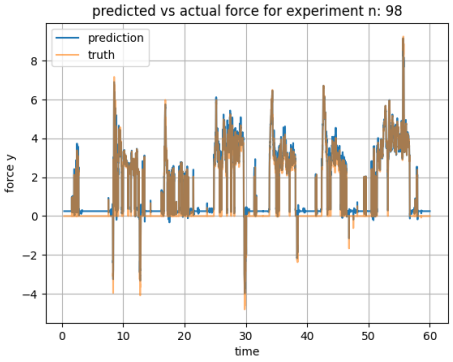
predicted vs actual force for experiment n: 98
prediction
truth
force y
time

(d)

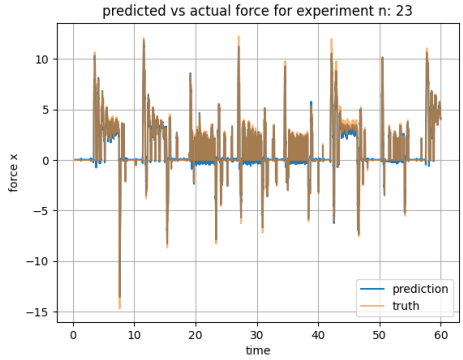
predicted vs actual force for experiment n: 23
prediction
truth
force x
time

(e)

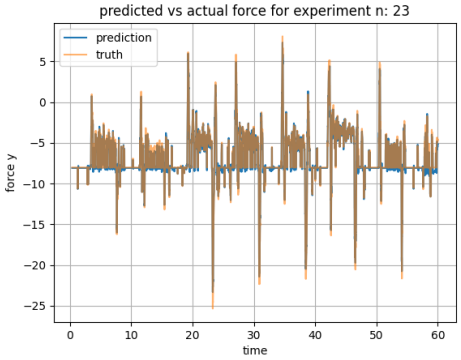
predicted vs actual force for experiment n: 23
prediction
truth
force y
time

(f)

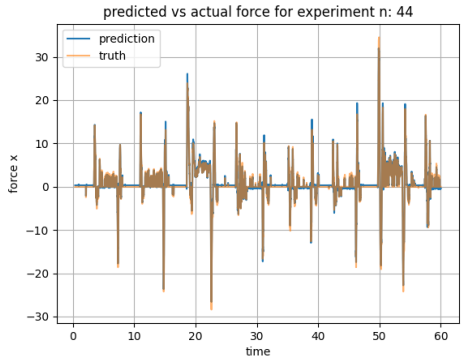
predicted vs actual force for experiment n: 44
prediction
truth
force x
time

(g)

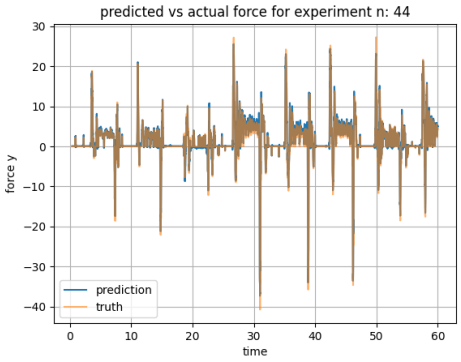
predicted vs actual force for experiment n: 44
prediction
truth
force y
time

(h)

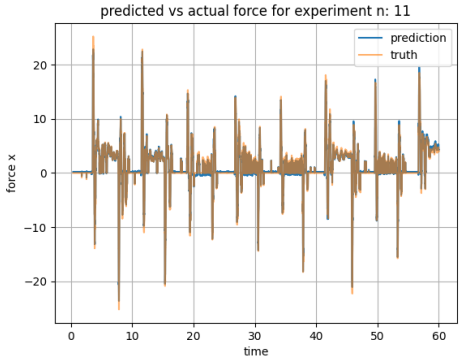
predicted vs actual force for experiment n: 11
prediction
truth
force x
time

(i)

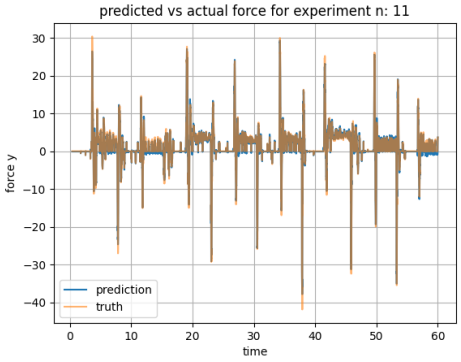
predicted vs actual force for experiment n: 11
prediction
truth
force y
time

(j)

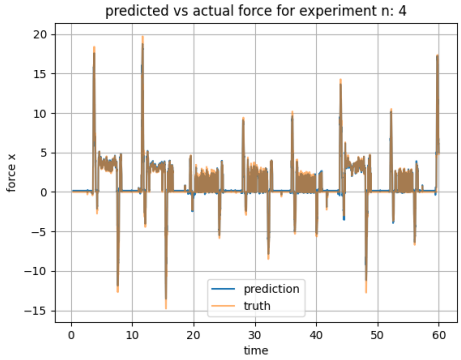
predicted vs actual force for experiment n: 4
prediction
truth
force x
time

(k)

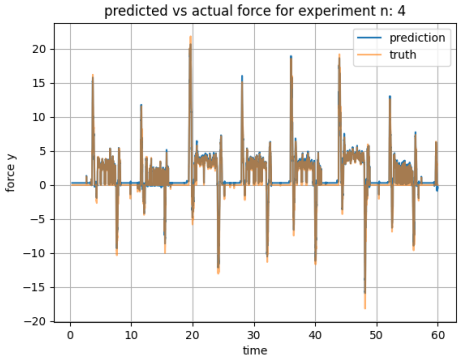
predicted vs actual force for experiment n: 4
prediction
truth
force y
time

(l)

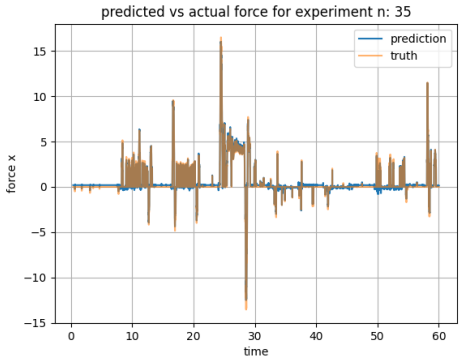
predicted vs actual force for experiment n: 35
prediction
truth
force x
time

(m)

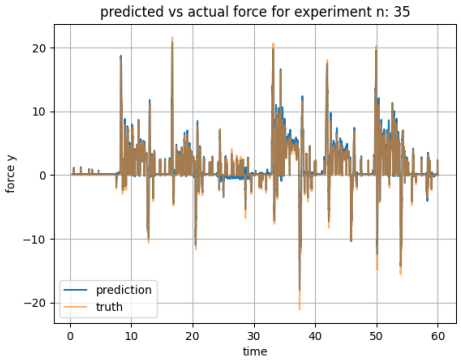
predicted vs actual force for experiment n: 35
prediction
truth
force y
time

(n)

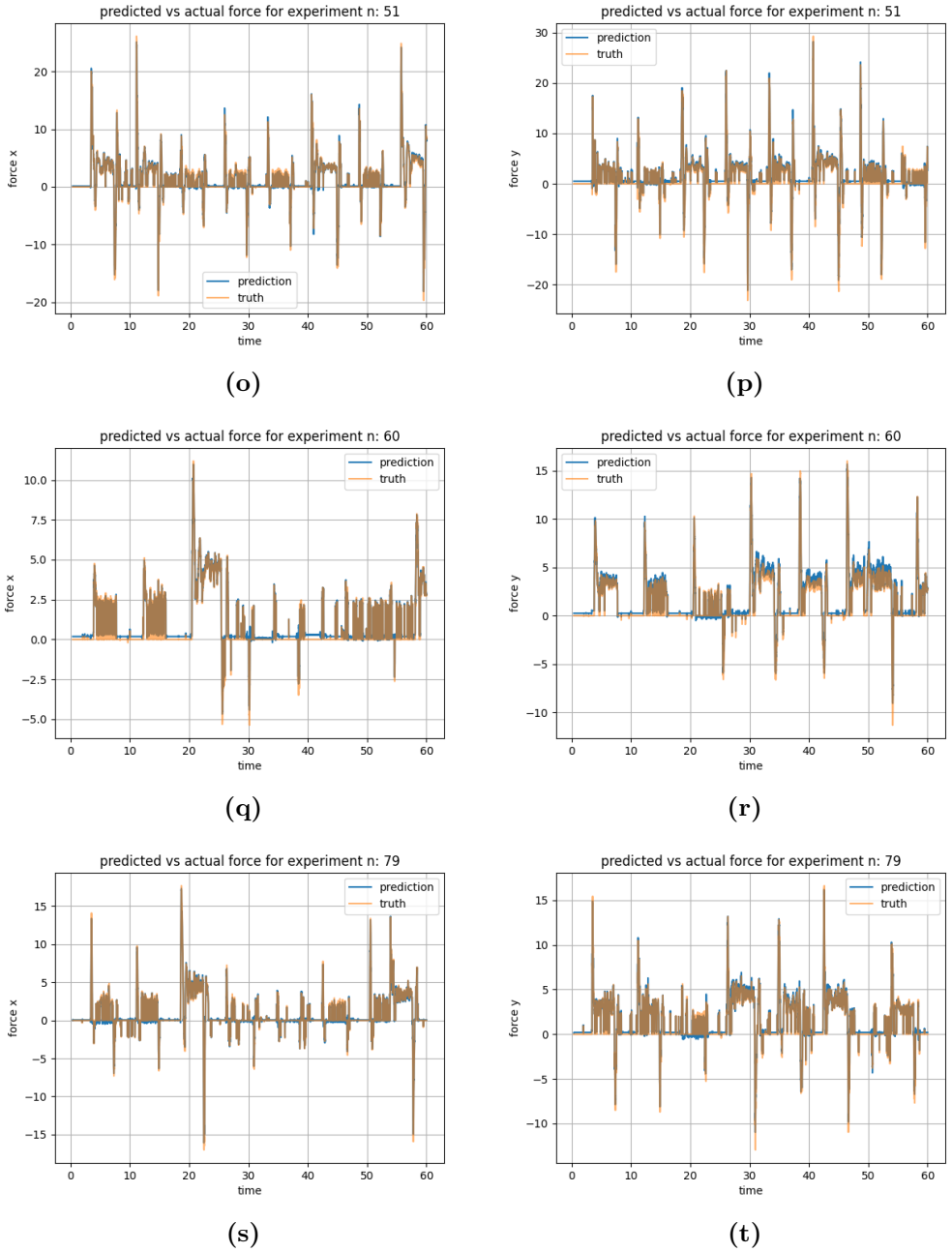

Figure 5.2: Measured vs. predicted force values of both x and y components. Chosen experiments are a summary of 20 experiments extracted (1 every 10) from the original dataset of 100 experiments.

Figure 5.3: Comau NS16 industrial robot

5.2 Human intention estimation

5.2.1 Experimental Setup

The human model described in Section 5.1 was used to estimate human intention in a collaborative manipulation task, whose setup was similar to the one proposed in Chapter 3. The experimental setup has some differences with respect to what was proposed for the first time in the linear case and then used for building the nonlinear model in the previous section, where the model was built offline starting from the collected experimental data.

The model has now been tested online in a similar setup but with a different robot and different randomly generated reference signals.

In particular, a Comau ns16 robotic arm was chosen. This was done for two main reasons; the first is the weight difference: ns16 weighs 335 Kg against the 20 Kg of the UR5 robotic arm previously used. The difference in the mass of the robot is reflected in the inertia that the arm has during a motion; when a human operator is performing a manipulation task manually guiding the ns16 robot, suddenly stopping its movement when the target point is reached requires more effort respect when UR5 is used. This aspect increases the importance of the proposed human intention estimation framework to help the robot anticipate its stop or start movement according to what the operator wants.

The second reason is also related to the added value of the model. Comau robot, unlike the Universal Robot, is not built to be collaborative but is an industrial robotic platform imagined to perform assembly tasks, lifting

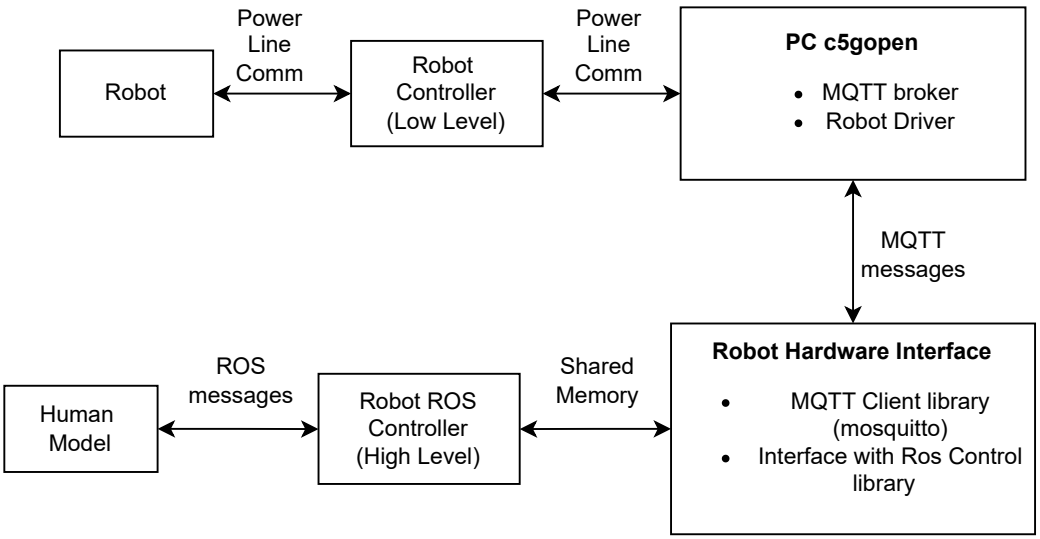

Figure 5.4: Schematic representation of the hardware and software components constituting the robot control logic.

medium-sized payloads (its payload limit is 16 Kg) in an isolated workspace. This means that, since the manufacturer did not give the robot collaborative capabilities in the first place, they can be reached, thanks to the proposed framework, by increasing its intelligence and adaptability.

Figure 5.4 represents the control logic structure of all the robotic platform's components. The robot controller communicates via Power Line with the arm on one side and via MQTT protocol with the PC client on the other. PC client is equipped with ROS Melodic software framework, which proved to be useful for sensor fusion and robot control with high-level architecture in many applications and ROS Control library. In the ROS laptop, two software components were implemented to allow communication with the robot and its control with real-time performance:

- *robot hardware interface* Responsible for managing the communication between the robot and ROS Control.
- *robot ROS controller* where the proper high-level control logic is present.

The robot hardware interface had the duty of managing outbound communication with the robot, implemented in the write method, and inbound communication, which gives robot feedback to the high-level controller, present in the read method. On one side, as said, the robot communicates with the MQTT protocol; on the other, ROS Control frameworks work with shared memory variables. For this reason, within the software component of the

hardware interface, a C++ client MQTT library was implemented for converting the content of memory cells (message payload) into JSON messages, which were sent to the robot through Mosquitto MQTT broker and vice-versa.

The robot controller, similar to what was described in Chapter 3, contained the high-level admittance controller, which decided robot behavior during physical interaction with the human subject. Again, the Robotiq FT300 force-torque sensor was mounted in the robot end-effector to read the external force applied by the human. Once known the force $\mathbf{F}_{ext}$, the position error $\Delta\mathbf{x}$, and cartesian velocity $\dot{\mathbf{x}}$ vectors, the acceleration commanded to the robot by the controller will be:

$$\ddot{\mathbf{x}} = \mathbf{I}_{pinv}(\mathbf{F}_{ext} - \mathbf{K}\Delta\mathbf{x} - \mathbf{D}\dot{\mathbf{x}}) \tag{5.3}$$

Where $\mathbf{I}_{pinv}$ represents the pseudo-inverse of the inertia matrix, while $\mathbf{K}$ and $\mathbf{D}$ are the stiffness and damping matrices, respectively. Since the Comau robot can be controlled in position only, the computed acceleration $\ddot{\mathbf{x}}$ has to be integrated twice, before being sent.

To avoid numerical errors due to the excessive number of computations and numerical approximation of data, before being processed by equation (5.3), a deadband was applied to the external force vector, considering as null all the forces between -2 and 2 Newton. Moreover, for what concerns the velocity $\dot{\mathbf{x}}$, the following exponential filter was applied:

$$\dot{\mathbf{x}}_f = c\dot{\mathbf{x}} + (1 - c)\dot{\mathbf{x}}_f \tag{5.4}$$

Where c is a constant parameter that has been set to 0.8.

However, the admittance controller and the necessary data pre-processing are not the main peculiarities of this work. The main difference with respect to the previously proposed controller consists of an additional software component that communicates with the robot controller: the Python script containing the human model predictor.

The human model described in the first section has been loaded into a ROS node using the Pickle Python library. First, the force and the actual position vectors have been acquired from the FT sensor and the robot, respectively. Both signals have been stored in queues of a fixed size of 50 samples, a trade-off between having queues as short as possible and having a safety margin of at least ten samples in case of failure from one of the two considered sources of information. Secondly, both queues have been normalized between -1 and 1, necessary to be processed by the model, which has been trained with normalized values. Then both queues were used to build

the input data window, as explained in the first section, and the model forecasted the next x and y force components. Finally, the predicted values have been de-normalized and sent to the main admittance controller.

On its side, the controller needs a position value to consider as the next reference position and anticipate human motion. For this reason, before being used, the predicted human force was converted into velocity by multiplying its value by a factor of $\frac{1}{d_v}$, which corresponds to the reciprocal of a virtual damping constant d_v, and then integrated into the final position value.

Even though the application scenario in which this work is focused is the continuous physical interaction and a proper trajectory planner is not needed, a state-machine motion planning stage was necessary to avoid unstable and dangerous behavior:

- State 0: The current reference is the starting position, and the motion is disabled. A new reference is received, and the controller checks if such reference is between an interval comprised between 1 mm and 0.3 m. If such a condition is verified, the motion is enabled.
- State 1: motion is enabled; the robot's goal is to minimize the position error between actual and reference positions with a speed depending on the stiffness value set to the controller.
- State 2: The new goal position has been reached, the current position is set as the new starting position, and motion is disabled.

As said, the experimental setup was similar to the one described in the second Chapter, with a different reference signal for each experiment. Again, the reference signal was generated as a sequence of points randomly chosen with x and y components between $[-0.1, 0.1]$ meters from the starting position, which was set as a reference point in the sequence between every two random points. This way a complete step is performed for every generated point; the resulting forcing reference function is a square wave consisting of a sequence of steps.

Human subjects were asked to manually guide the robot towards the next reference position, displayed as a yellow dot on a screen showing the x-y plane also containing the robot model. The resulting experimental setup is shown in Figure 5.5

The model, as said, was used to forecast the next human force online. For this reason, a fast computational time is required, so both the human estimator node and the ROS robot controller node (using the same nomenclature indicated in Figure 5.4) were synchronized to run with a loop period of $0.00125s$, which corresponds with good approximation to $800Hz$.

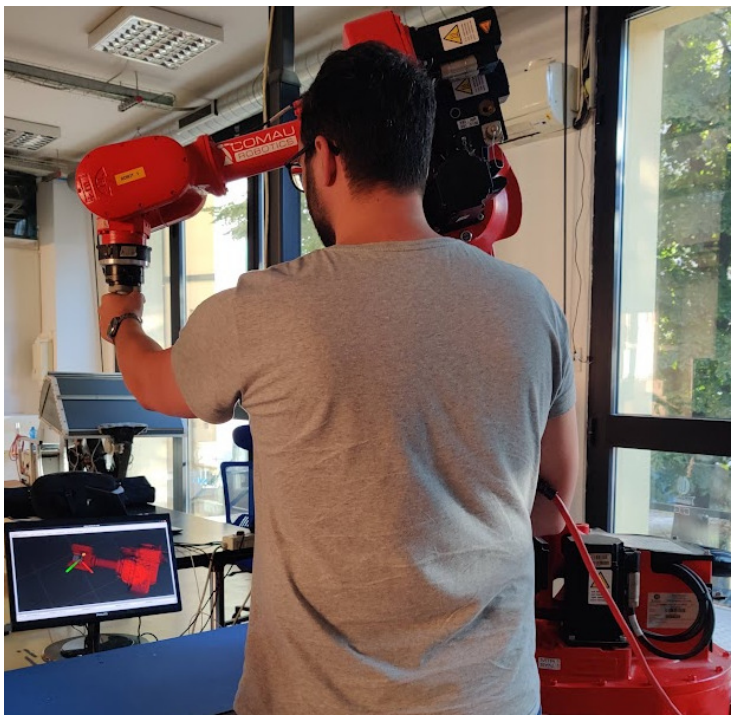

Figure 5.5: Experimental setup with a human subject performing a manual guidance task with the robot, following the virtual reference displayed on a screen.

In some experiments, the state machine, which converted the predicted force to a position reference for the robot, was used; in others, it was not.

5.2.2 Results

The obtained results in the case in which only the admittance controller was used are shown in Figure 5.6, while Figure 5.7 shows the results observed when the forecasted force was converted first to a velocity, and then to a position reference which was sent to the robot using the state-machine approach described above. Below each force plot is also shown the correspondent position tracking error, one for each component.

In all the plots, the first rows, showing two superimposed vectors, represent the force's x and y components, respectively. The blue curve represents the measured force acquired by the FT300 force sensor, while the orange curve is the force forecasted by the model.

The first observable thing is that all the force curves present an initial temporal shift, which in some cases is of $3-5s$. Going on with the experiment, the time delay between the two force signals kept decreasing until it became negligible in the last ten seconds of the experiments. This happens due to the fact that the two queues used as input windows from the model were initialized with null values in all their elements at the beginning of each experiment. This caused a "temporal offset" since the model needed some time to fill its two queues of 50 samples each with the real measured values. This requires $0.0625s$ only to fill the queues and more time to reflect this change in the model output, which is obviously zero at the beginning.

Despite this, the signal produced by the model accurately reflects the measured force even in the first "tuning part" of the experiments where the time delay was considerable and kept being high until the last part, in which the two signals are almost superimposed.

Another consideration is that in the majority of cases, the robot ROS controller failed to distinguish between unwanted external contact, which has to be managed in a compliant way according to the admittance control law of equation (5.3), and force produced by the human subject, which has to be converted to a position reference as quickly as possible. The state-machine algorithm and the model alone appear insufficient to perform such a complex task.

However, when the human reference was correctly recognized, such as in Figure 5.7 $a-d$, and in part of Figure 5.7 $i-l$, the advantages in terms of performance are evident. In fact, the force signals present only the first peak, after which the robot reaches the position desired by the human operator; the successive noisy part of the force signal, which was observable in the

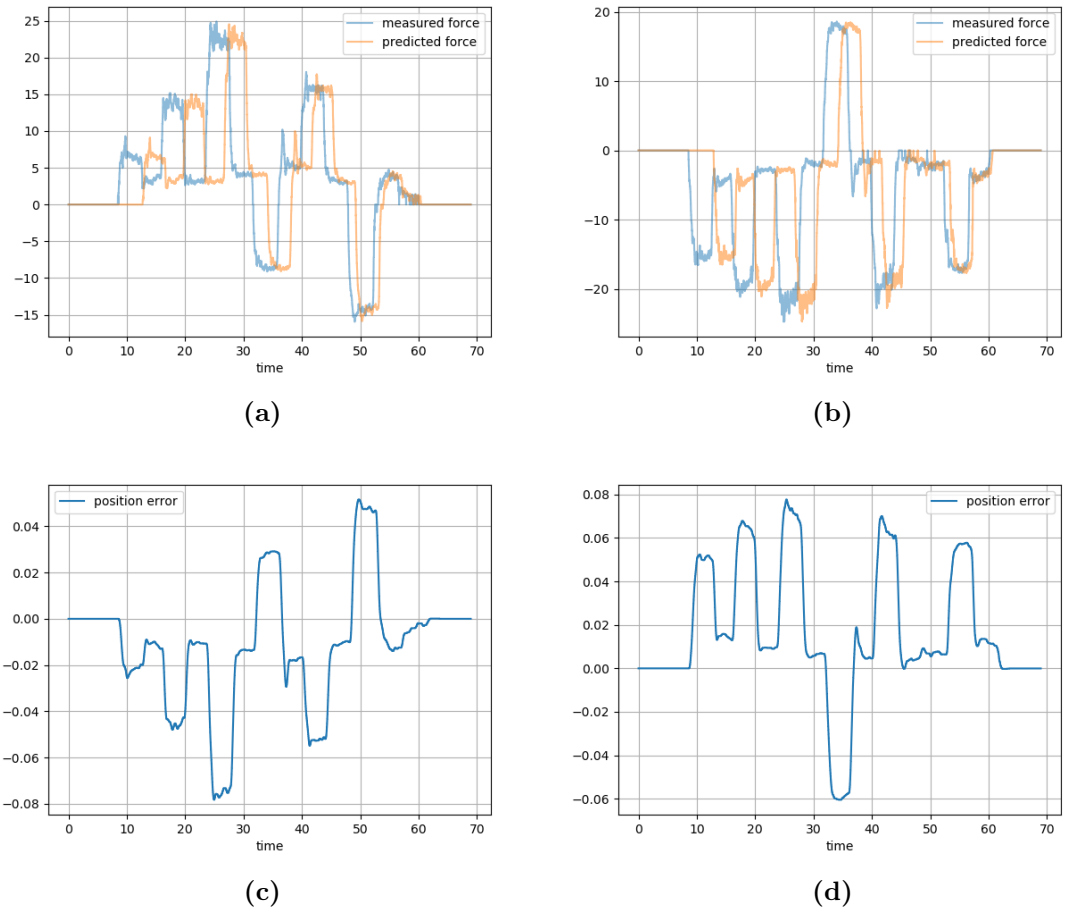

Figure 5.6

previously used data, is not present anymore.

Also the position tracking error indicates a visible improvement, decreasing from over $0.1m$ present in other cases to the maximum of $0.42m$ observable in Figure 5.7 *c* and the $0.29m$ in *d*. Even the central part of Figure 5.7 *k* and *l*, where the characteristic impulsive behavior is noticeable, confirms this consideration.

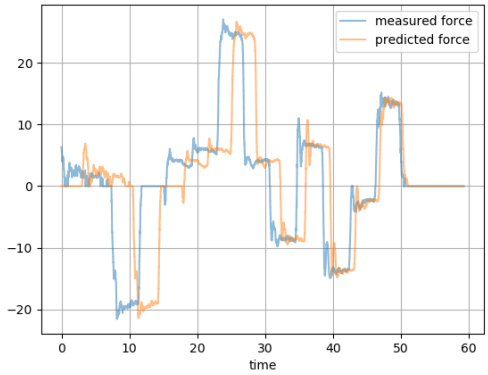

(e)

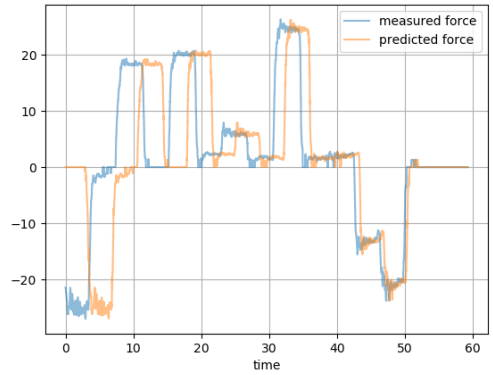

(f)

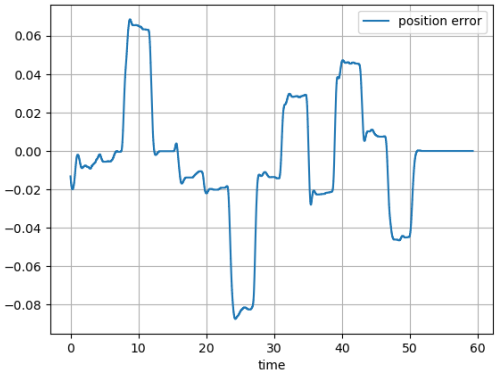

(g)

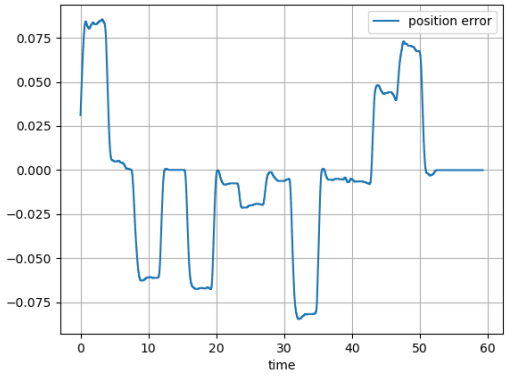

(h)

Figure 5.6

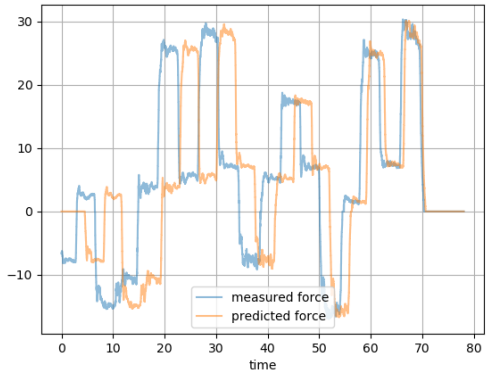

(i)

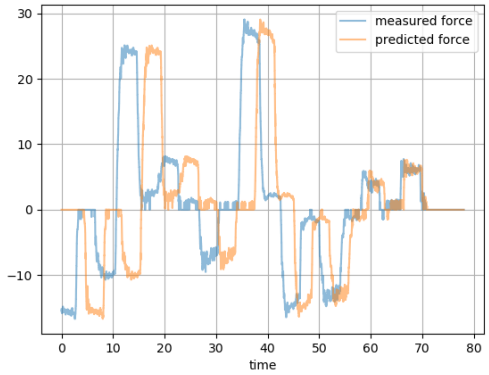

(j)

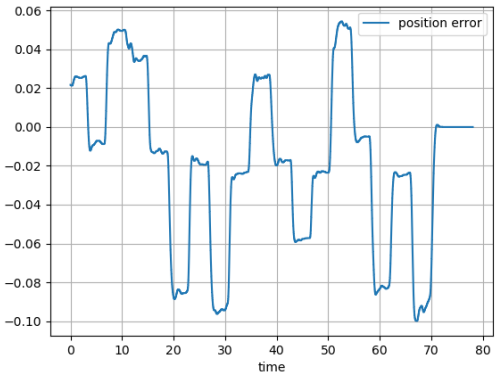

(k)

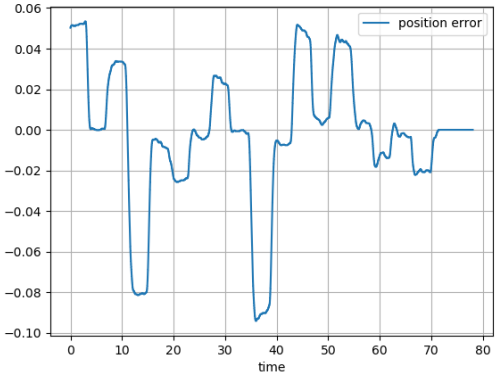

(l)

Figure 5.6

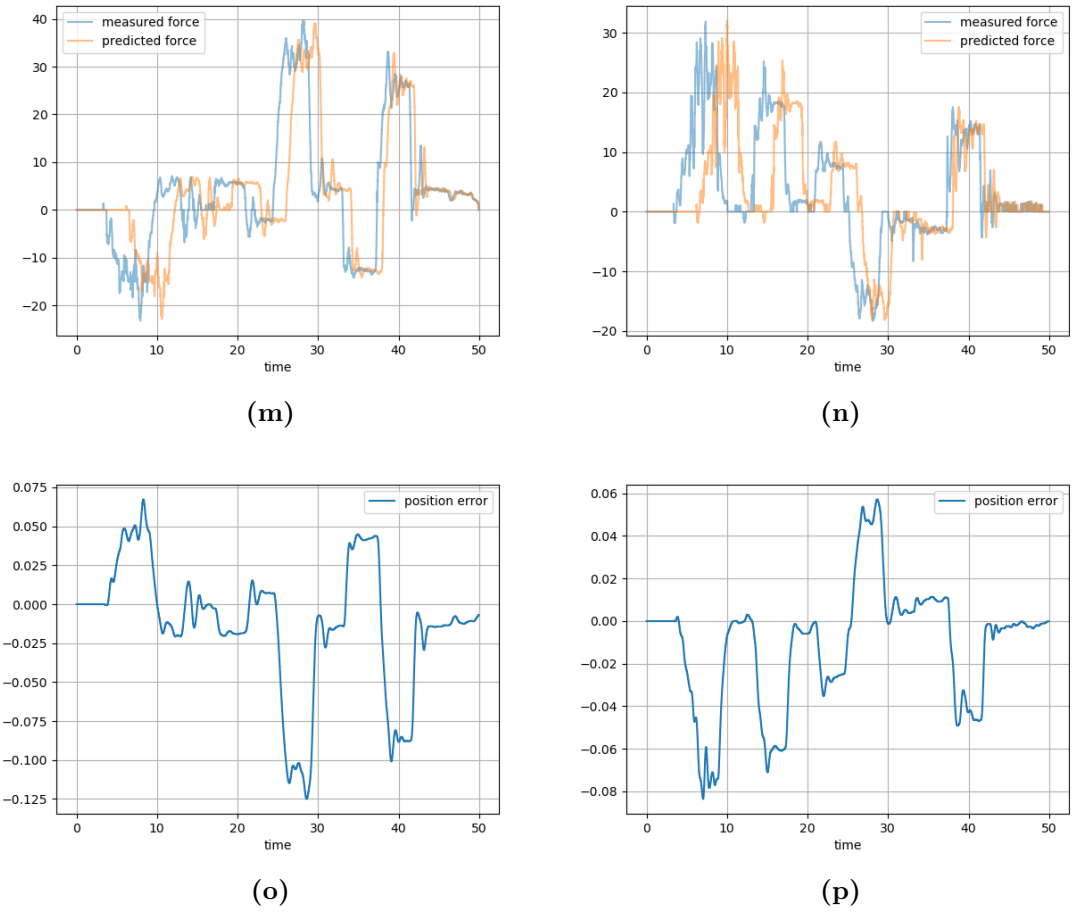

Figure 5.6: Measured vs. predicted force values (first rows) and position tracking error (second rows) of both x (first columns) and y (second columns) components for each experiment. Differently from what was previously done, force value is now forecasted online.

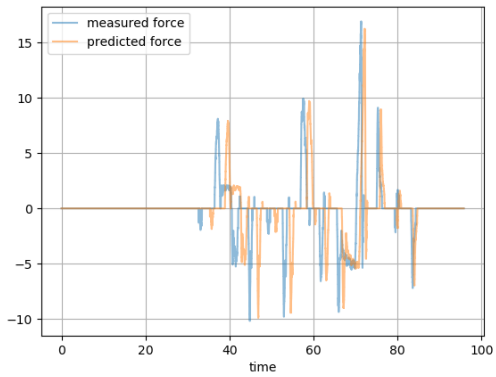

(a)

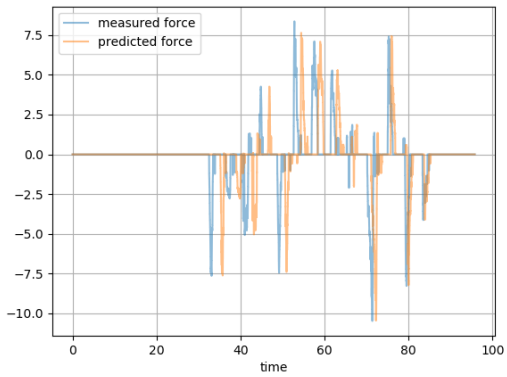

(b)

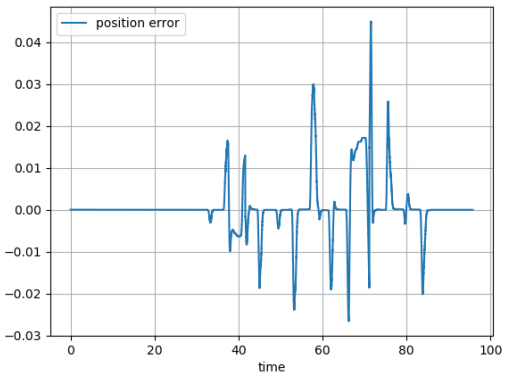

(c)

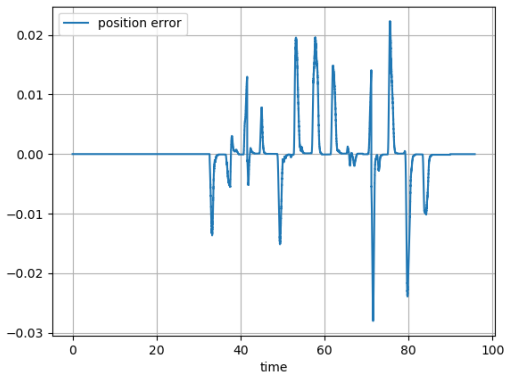

(d)

Figure 5.7

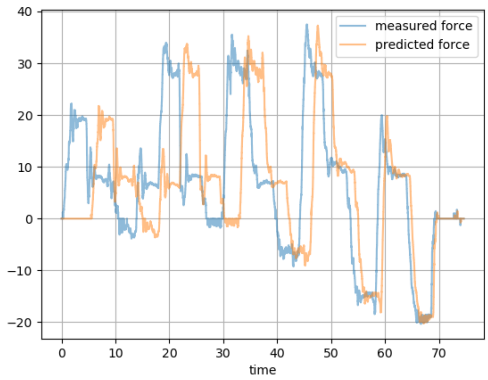

(e)

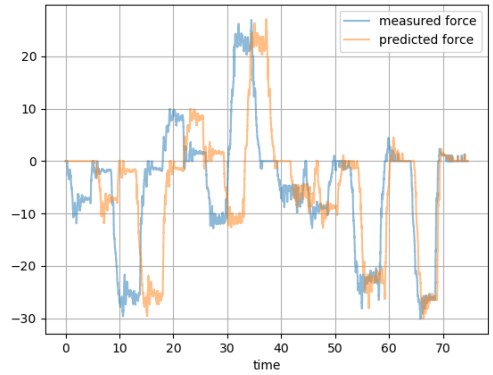

(f)

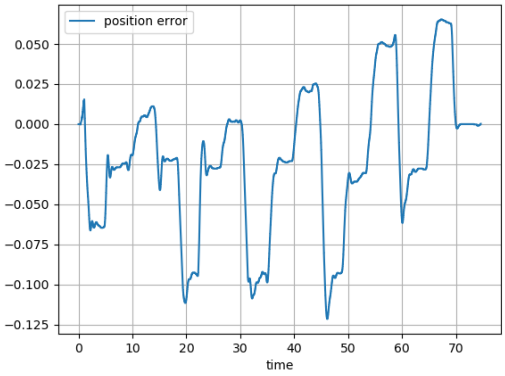

(g)

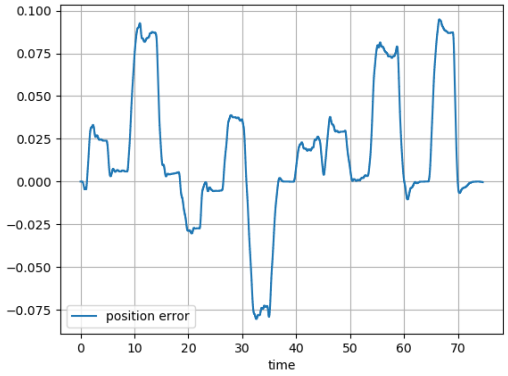

(h)

Figure 5.7

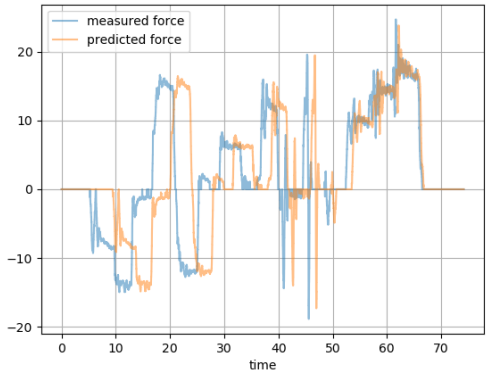

(i)

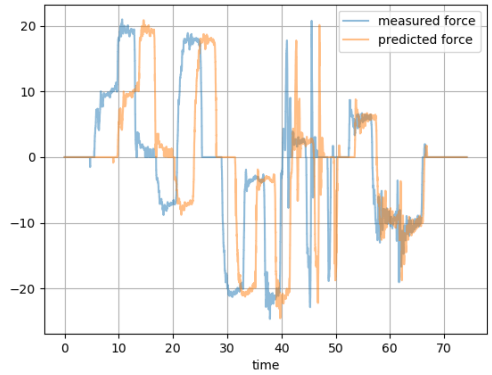

(j)

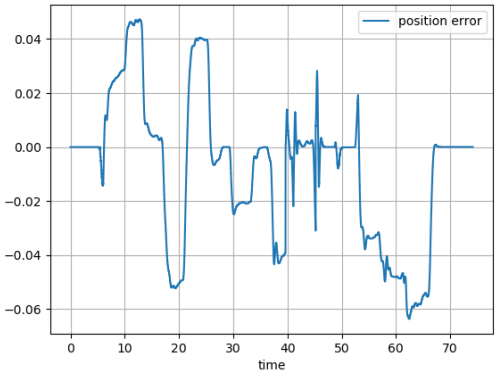

(k)

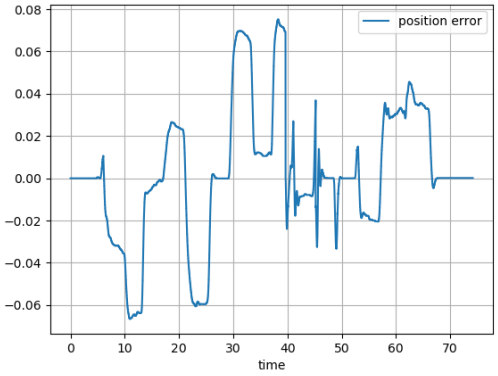

(l)

Figure 5.7

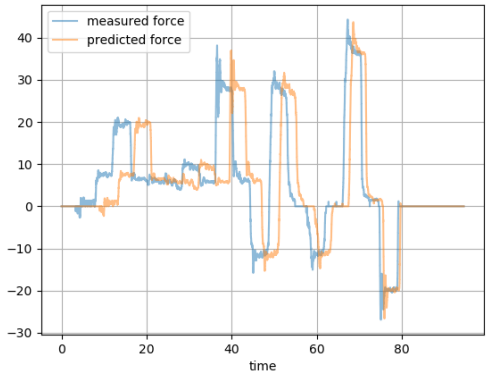

(m)

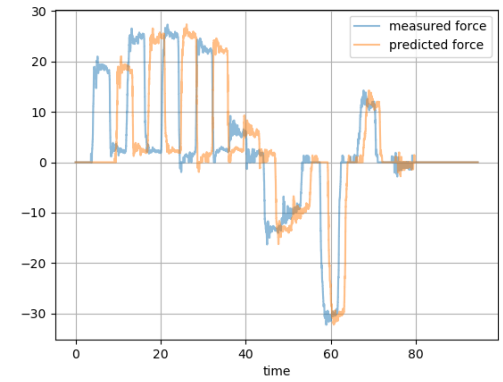

(n)

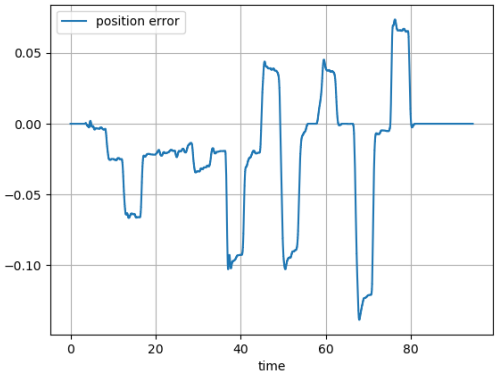

(o)

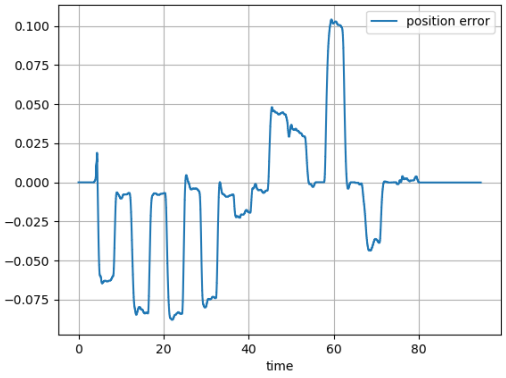

(p)

Figure 5.7

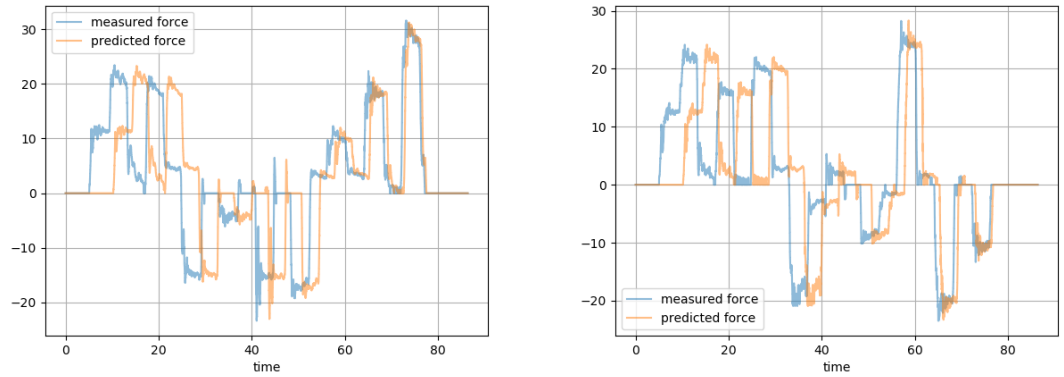

(q)

(r)

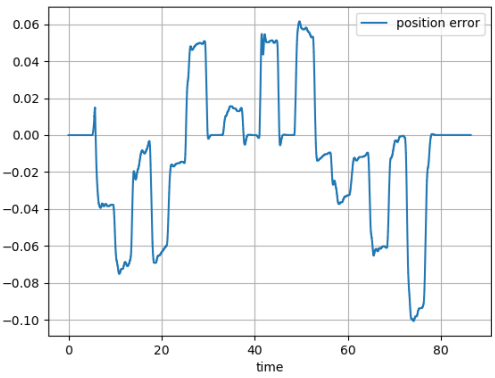

(s)

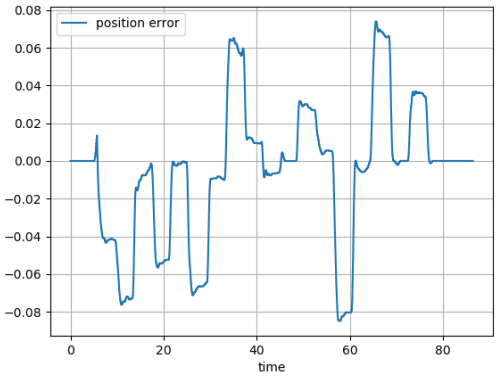

(t)

Figure 5.7: Measured vs. predicted force values (first rows) and position tracking error (second rows) of both x (first columns) and y components (second columns) for each experiment, using the state-machine approach to convert it to a position reference.

Chapter 6

Control Delay Estimation in Human-Robot Interaction

As mentioned in Section 5.1, complex impulsive and highly nonlinear dynamics observable in human-robot interaction struggle to be completely represented in all its aspects by techniques assuming to approximate the system to known simple linear equivalents, such as in the case of the Crossover model experimentally studied in detail in Section 3.2. For this reason, the use of a more complex technique, such as Narmax models, which are able to deal with unknown dynamics, helped to increase the level of the model's accuracy.

However, in cases where the system is partially known, its complexity can be reduced with different strategies. In the next chapter, the use of Peak-to-Peak Dynamics for this scope will be explored, while here we will see how the knowledge of part of the system can help to extract from raw experimental data useful information which instead would require more complicated and time-demanding techniques.

The example will be, once again, the time delay. As we saw in chapter 3, estimating time delay, considering different subjects can require a certain effort. In the proposed modeling technique, in fact, it was necessary to perform preliminary data processing to obtain the derivative of the position error useful to approximate the reaction time heuristically; then the use of identification techniques to optimize the model's parameters so that it would be able to simulate the human-machine system's response.

Now, having a reliable model of the human response only, producing an output force signal, which is the input of the robot control law expressed in equation (5.3), the knowledge of the controlled element's dynamics will allow us to obtain all the system's parameters in a fast and equally reliable way.

In order to better investigate the control delay of the model in the context of human-robot interaction, the transport delay was considered as the time

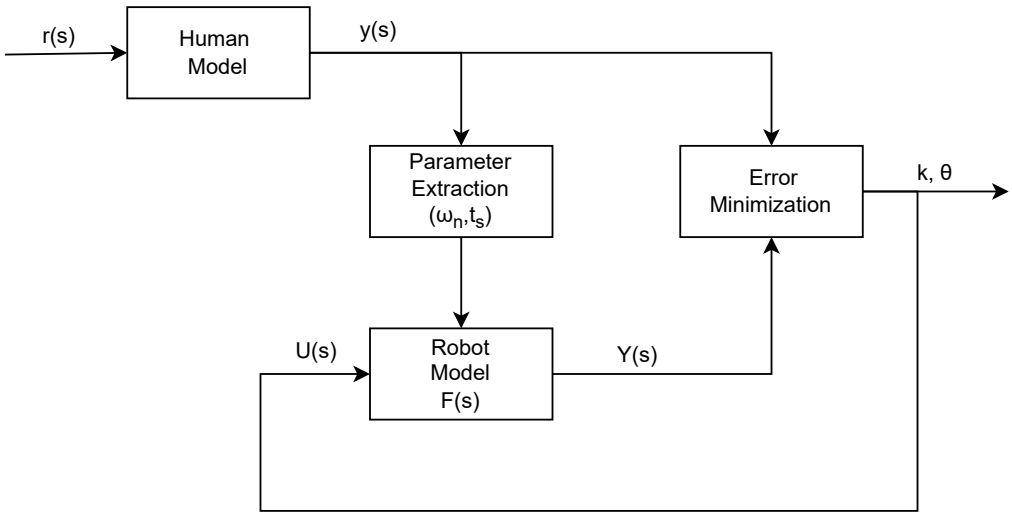

Figure 6.1: Schematic representation of the delay estimation algorithm.

lag between the instant in which the human subject receives the stimulus from the forcing function and generates a force and the instant in which the robot receives such force. So, if we consider a simple block scheme of the system in which human and robot elements are sequentially connected, such as in the case of the linear CO model of Chapter 2, we ideally are now between the two blocks.

First of all, we have to estimate the robot transfer function. In our collaborative manipulation task, robot dynamics can be approximated as a second-order transfer function with a gain k, a natural frequency ω_n, and damping ratio ϵ:

$$F(s) = \frac{k}{s^2 + 2\epsilon\omega_n s + \omega_n^2} \,. \tag{6.1}$$

As shown in Figure 6.1, it is necessary to extract the frequency and damping parameter values from the human output $y(s)$ to build the robot transfer function. To do so, the force signals have been segmented into sections of 5 seconds duration each. For each window of signal, the oscillation period T was identified as the ratio between the window duration and number of oscillations, then

$$\omega_n = 2\frac{\pi}{T} \,.$$

Knowing the natural frequency, the ϵ parameter was derived from the settling time formula:

$$t_s = \frac{3.9}{\epsilon\omega_n} \,;$$

where $\tau = \frac{1}{\epsilon\omega_n}$ in the system time constant and t_s is the settiling time approximated after 3.9τ.

Once the transfer function F(s) of the robot controller is built, its output signal $Y(s)$ can be expressed as $Y(s) = F(s)U(s)$, where the input signal $U(s)$ is:

$$U(s) = \frac{1}{s} - \frac{1}{s}e^{-s\theta} \tag{6.2}$$

Here, θ represents the delay itself. A 4th-order Padé polynomial can well approximate the exponential part of the function. This way, being the input of the robot function directly calculated from the delay θ, and the robot function itself dependent only on the gain k, the optimal k, and θ parameters can be estimated by an iterative algorithm that minimizes the root mean squared error between the simulated $Y(s)$ signal and the output of the human model $y(s)$. This final stage is represented in Figure 6.1 by the error minimization block and the subsequent loop. In other words, this process is equivalent to anticipating the robot model's output until it coincides with an acceptable degree of accuracy with the output of the human model.

The results are shown in Table 6.1. It can be noticed that the oscillations of optimal parameters value between each experiment are almost negligible for the gain k and small for the time delay θ, which is distributed around the value of 0.3 seconds.

Index	**Period**	**Epsilon**	**Omega**	**Gain**	**Delay**	**RMSE**
1	0.1555	0.0193	52.181	2.5	0.298	2.2475
2	0.1296	0.0161	56.634	2.5	0.29	2.4750
3	0.1334	0.0166	53.437	2.5	0.278	2.4905
4	0.1548	0.0192	51.724	2.4	0.296	3.1595
5	0.1517	0.0188	51.953	2.5	0.267	3.0525
6	0.1546	0.0192	50.468	2.5	0.287	2.9547
7	0.1658	0.0206	49.669	2.4	0.286	2.9653
8	0.1636	0.0203	52.866	2.5	0.29	3.3834
9	0.1519	0.0189	51.839	2.4	0.281	3.2193
10	0.1551	0.0193	53.209	2.5	0.283	2.9257
11	0.1450	0.0180	52.181	2.6	0.325	5.3826
12	0.1217	0.0151	57.662	2.5	0.327	4.6006
13	0.1194	0.0148	57.433	2.5	0.334	4.3815
14	0.1155	0.0143	60.402	2.5	0.326	4.5168
15	0.1182	0.0147	58.004	2.5	0.326	4.4452

16	0.1098	0.0136	60.174	2.5	0.326	3.9863
17	0.1268	0.0158	54.921	2.5	0.338	3.5094
18	0.1253	0.0156	54.579	2.5	0.327	3.6054
19	0.1046	0.0130	62.229	2.5	0.306	3.2054
20	0.2161	0.0268	56.977	2.5	0.321	3.8185
21	0.1010	0.0125	66.111	2.7	0.335	3.5022
22	0.1026	0.0127	64.513	2.6	0.326	3.1613
23	0.1028	0.0128	64.513	2.6	0.327	3.4248
24	0.1106	0.0137	61.087	2.5	0.315	2.6977
25	0.1262	0.0157	58.575	2.5	0.321	2.6062
26	0.1054	0.0131	63.599	2.5	0.32	3.4739
27	0.1202	0.0149	59.032	2.5	0.313	3.7603
28	0.1154	0.0143	58.804	2.5	0.299	3.6272
29	0.1129	0.0140	60.174	2.5	0.324	4.1181
30	0.1161	0.0144	58.804	2.5	0.296	3.5908
31	0.1232	0.0153	57.890	2.6	0.315	2.5276
32	0.1428	0.0177	53.780	2.5	0.308	2.2940
33	0.1294	0.0161	57.662	2.5	0.3	2.9136
34	0.1425	0.0177	51.839	2.5	0.321	2.8352
35	0.1504	0.0187	50.240	2.5	0.297	3.0548
36	0.1676	0.0208	53.437	2.5	0.336	2.7918
37	0.1377	0.0171	54.465	2.5	0.311	2.3276
38	0.1938	0.0241	50.925	2.5	0.301	2.1996
39	0.2804	0.0348	52.524	2.5	0.32	2.3290
40	0.1643	0.0204	50.583	2.5	0.296	2.9647
41	0.1232	0.0153	55.378	2.5	0.352	4.2927
42	0.1188	0.0148	56.177	2.5	0.308	4.4177
43	0.1214	0.0151	55.721	2.5	0.332	4.5774
44	0.1270	0.0158	56.063	2.5	0.314	4.5013
45	0.1338	0.0166	51.153	2.5	0.306	4.8120
46	0.1249	0.0155	55.607	2.6	0.311	3.9243
47	0.1307	0.0162	53.551	2.5	0.321	5.8130
48	0.1181	0.0147	57.548	2.5	0.312	3.2490
49	0.1455	0.0181	49.441	2.5	0.329	3.8370
50	0.1197	0.0149	57.433	2.5	0.305	3.5187
51	0.1177	0.0146	59.375	2.5	0.309	3.8801
52	0.1200	0.0149	57.890	2.5	0.314	3.6323
53	0.1228	0.0153	55.721	2.5	0.311	4.4842

54	0.1213	0.0151	58.918	2.5	0.313	4.2957
55	0.3149	0.0391	49.212	2.4	0.338	4.2891
56	0.1286	0.0160	54.807	2.5	0.32	4.5250
57	0.1211	0.0150	57.890	2.5	0.312	4.1196
58	0.1240	0.0154	53.894	2.5	0.323	4.0612
59	0.1312	0.0163	53.437	2.5	0.313	5.2791
60	0.1283	0.0159	58.918	2.5	0.311	5.4367
61	0.1356	0.0168	55.264	2.6	0.307	1.8006
62	0.1333	0.0166	56.292	2.7	0.309	1.7296
63	0.1204	0.0150	59.603	2.6	0.312	1.9298
64	0.1324	0.0165	55.264	2.6	0.298	2.0855
65	0.1266	0.0157	54.465	2.6	0.316	1.9340
66	0.1326	0.0165	56.063	2.6	0.314	1.7050
67	0.1574	0.0195	49.212	2.6	0.304	1.8004
68	0.1215	0.0151	57.890	2.6	0.31	1.9447
69	0.1150	0.0143	62.115	2.6	0.31	1.9713
70	0.1224	0.0152	56.977	2.6	0.304	1.9737
71	0.1295	0.0161	54.465	2.6	0.317	2.1282
72	0.1371	0.0170	52.980	2.6	0.323	2.0923
73	0.1326	0.0165	55.264	2.5	0.321	2.5884
74	0.1397	0.0174	53.894	2.5	0.311	2.6593
75	0.1443	0.0179	52.295	2.5	0.307	3.2107
76	0.1227	0.0152	56.748	2.5	0.295	3.3325
77	0.1312	0.0163	52.866	2.5	0.324	2.8992
78	0.1250	0.0155	56.977	2.5	0.322	2.9160
79	0.1382	0.0172	50.240	2.5	0.308	2.7119
80	0.1271	0.0158	55.835	2.5	0.312	2.4921
81	0.3345	0.0415	52.752	2.4	0.29	4.1356
82	0.1163	0.0144	59.831	2.4	0.293	4.1216
83	0.1165	0.0145	59.260	2.4	0.292	4.4143
84	0.1121	0.0139	61.430	2.4	0.29	4.4727
85	0.1109	0.0138	62.115	2.5	0.282	5.8097
86	0.1116	0.0139	58.918	2.4	0.296	4.3111
87	0.1170	0.0145	58.233	2.3	0.275	5.9275
88	0.1149	0.0143	62.914	2.4	0.267	5.3416
89	0.1123	0.0140	61.658	2.4	0.281	4.5463
90	0.1169	0.0145	60.288	2.4	0.282	4.4289
91	0.1315	0.0163	58.918	2.7	0.33	1.4029

92	0.1324	0.0164	56.177	2.7	0.33	1.5262
93	0.1239	0.0154	58.119	2.7	0.341	1.3392
94	0.1267	0.0157	54.807	2.7	0.32	1.4988
95	0.1134	0.0141	60.060	2.7	0.328	1.3432
96	0.1333	0.0166	55.721	2.7	0.327	1.3807
97	0.1380	0.0171	51.839	2.7	0.329	1.4723
98	0.1595	0.0198	49.327	2.7	0.326	1.3727
99	0.1752	0.0218	48.756	2.7	0.315	1.4545
100	0.1438	0.0179	50.925	2.7	0.322	1.4086

Table 6.1: Identified parameters for the controlled element's transfer function and delay estimation.

Chapter 7

Peak-to-Peak Dynamics

7.1 Peak dynamics in complex systems

A continuous system is said to have Peak-to-peak dynamics (PPD) if we can determine the value of its next peak starting from the values of the past m peaks, where m is a finite number called "memory." In the presence of peak-to-peak dynamics, the system can be described by reduced order models, gaining an advantage in computational time.

PPD property was pointed out for the first time by Lorenz in his famous model of forced dissipative nonperiodic flow [312]. Lorenz discovered that, given a chaotic system producing an output $y(t)$, it will exist a set:

$$S_{PPP} = (y_k, y_{k-1}) \tag{7.1}$$

called "Peak-to-Peak-Plot" (PPP), which maps the pairs of consecutive peaks in the feature space. Moreover, Lorenz discovered that the blob of points of these peak pairs in the feature space can be approximated with a high degree of accuracy by one or more curves in the relevant plane. This property is strictly related to the geometrical characteristics of the chaotic attractor of the system, which has to be nearly two-dimensional [313].

Since Lorenz's first description of this property, systems with PPD have been studied in many fields and formalized more in detail. As explained by Candaten et al. in [52], a system is said to present PPD when:

$$y_{i+1} = Y(y_i, \ldots, y_{i-m+1}) \tag{7.2}$$

Where m is the "memory" number defined above. When the memory factor is 1, PPD is said to be "simple"; in all other cases it is "complex."

This means that when PPD is present, the occurrence of the next peak of a system, which may be potentially constituted by a considerable number of

differential equations, can now be obtained by usually at most two previous peaks, obtaining a reduced-order model.

When PPD is complex, the prediction of the next peak can't be obtained only from the last peak; in this case, extra information is needed. To answer this question, Candaten et al. introduced the concept of "pointer" $x_i \in 1, 2, \ldots, k$, which indicates the input states x_i that can influence y_{i+1} value. If we add this new consideration to the previous PPD definition, we obtain the so-called "peak-to-peak canonical form":

$$\begin{aligned} y_{i+1} &= Y^*(y_i, x_i) \\ x_{i+1} &= A^*(y_i, x_i) \end{aligned} \tag{7.3}$$

Where A^* is a function which is piecewise constant with respect to y_i.

The canonical form equation of PPD tells us that the system describing the dynamics of the peaks is only slightly more complex than a first-order discrete-time system but definitely less complex than a second-order one. On the other hand, it is known that in a generic single-output nth-order system, n samples of the output variable are equivalent to a single sample of the n-dimensional state vector [314]. The implication of this is that as said, the knowledge of a single peak y_i can't be considered, generally speaking, sufficient to forecast the peak y_{i+1}. To do so, it is needed at least the knowledge of (y_{i-1}, y_i) ($m = 2$ in the first equation). Such consideration is restricted to the dynamics within the system's attractor, i.e., involving the peaks y_{i-1}, y_i, y_{i+1}.

PPD has been successfully applied to state space models with piecewise linearized functional [315], Rosenzweig-MacArthur prey-predator model [52] and prey-predator model applied to dynastic cycles [316, 317].

In [318], a parameter estimation method for chaotic systems based on PPD is proposed. The method consists on finding the best match between the aprioristic continuous-time model, the 1-D map generated with a parameter-dependency, and the 1-D map derived from the data.

This shows how studying the presence of PPD in a system can be useful for deriving methods and modeling techniques to estimate parameters from data or constructing control methods, even in complex scenarios characterized by chaotic oscillations [319].

7.2 Peak forecasting in Narmax models

In order to verify the presence of PPD in our system, the model was re-trained to predict the output signal only in correspondence with its peaks.

First, the dataset was analyzed to find automatically only the highest peak, both positive and negative: each force signal was rectified, and the peaks were identified with a simple iterative algorithm able to find local maxima.

First of all, for the sake of simplicity, the dataset was slightly modified to let the model work with one signal each time. To do so, a new "flattened" dataset was created by listing the x and y components of the original dataset used previously.

The new dataset, which now has 200 elements, was iteratively processed to find peak values and their indices. Two thresholds have been set to exclude lower local peaks: the first to put a lower limit on the sample distance between peaks and the second for setting their minimum amplitude to 10 Newton.

Due to the system's complexity, simple PPD is not expected; it is therefore necessary to consider the aforementioned vector of input states, which helps the system forecast the next peak. The starting structure we are considering is the Narmax model defined in chapter 5, which already considers input states x for its own structure.

Therefore, with reference to the Narmax model scheme depicted in Figure 5.1, the input data window to use for the model to forecast the y_i peak is now constituted of

$$(y_{i-1}, \ldots, y_{i-n_a}, x_{i-d} + e_{i-1}, \ldots, x_{i-d-n_b} + e_{i-n_c}) .$$

Here, the inputs $x_{i-d} \ldots x_{i-d-n_b}$ are summed to the noise elements before being fed to the model, as explained in Chapter 5, while $y_{i-1}, \ldots y_{i-n_a}$ are the corresponding model's outputs. As expected, the model order was reduced from 10 to 5, and the computational time required for processing each epoch during the training phase has been reduced.

The obtained results are shown in Figure 7.1, which similarly to what was done in chapter 5 is a summary of 1 element extracted from each 10 (so that all the participating subjects are represented at least once). The predicted peak value is marked with a cross, while ground truth is depicted with a circle.

It is noticeable that, despite the reduced model's order, which now uses only five samples to forecast the next peak, the accuracy of the model's predictions is still high, as testified numerically in Table 7.1, which shows RMSE and R2 scores for all the dataset elements. Again, RMSE values are de-normalized raw data in Newton, while the R2 score is a pure number without a unit of measure, which considers normalized data and has a maximum value of 1 but no minimum value. The model accuracy is not the same as the one obtained by the complete order model; this is evident by looking at both indices, but the difference is not significant in most cases if we consider that the model order has been halved.

Index	RMSE	R2 score
1	0.788339991	0.984102289
2	0.725375491	0.993396867
3	1.079683635	0.986859713
4	1.609704872	0.982254959
5	1.08281791	0.991408623
6	1.008284119	0.988558621
7	0.931611907	0.99322937
8	1.728268578	0.985502424
9	1.018048423	0.994210846
10	1.003195685	0.990444132
11	1.459309264	0.985108439
12	2.363259029	0.972155156
13	1.508443645	0.989092005
14	1.494334458	0.982399077
15	2.064005666	0.9764583
16	1.447664974	0.981804595
17	1.535668639	0.983054394
18	1.33286821	0.977115116
19	1.178677982	0.980116781
20	2.201940923	0.972528222
21	1.562160761	0.979179375
22	1.082219691	0.984050921
23	0.984120028	0.990432938
24	1.232267544	0.95421644
25	0.900772997	0.98501785
26	1.623998854	0.979499231
27	1.715041214	0.983190894
28	1.465886765	0.978817114
29	1.788331704	0.983938895
30	1.67177289	0.976332122
31	0.837577763	0.989210803
32	0.74601141	0.986216124
33	1.186428466	0.981827996
34	1.237821331	0.972808293
35	1.355472768	0.975913031
36	1.297130116	0.967902326
37	1.522094272	0.975370036

38	1.383624688	0.972180932
39	1.010817197	0.988343303
40	1.00870708	0.988077678
41	1.659605218	0.979847703
42	1.520351736	0.988210014
43	1.529860854	0.990129081
44	1.841965508	0.986852834
45	2.689196992	0.981592561
46	1.679639479	0.980152297
47	2.975631008	0.986071534
48	1.504156687	0.852564616
49	1.381148568	0.983825904
50	1.58623922	0.985105352
51	2.157918914	0.9754759
52	2.61490871	0.971331842
53	2.836532672	0.96159056
54	1.937992672	0.960898201
55	1.533815737	0.987320403
56	2.53052834	0.967247676
57	1.415935605	0.983044513
58	1.829277589	0.967035857
59	2.341216934	0.966440844
60	2.460776101	0.977637881
61	0.757814533	0.985042217
62	1.091056101	0.973323797
63	1.14141269	0.948349373
64	0.974553309	0.986800137
65	1.253143445	0.96020847
66	0.929401379	0.978523722
67	0.862626962	0.983112412
68	1.049272752	0.954620193
69	1.08079809	0.97823663
70	0.968355499	0.964750538
71	0.718978771	0.987028876
72	0.710409281	0.990405616
73	1.450555337	0.973428614
74	1.120832433	0.986586709
75	1.452150649	0.988459512

76	1.296102417	0.986753456
77	1.471494369	0.987067883
78	1.464810797	0.988061197
79	1.351577868	0.986105979
80	1.528646248	0.966779776
81	2.285519768	0.978410232
82	2.03922869	0.979159903
83	2.545457207	0.969702104
84	1.95652686	0.966975999
85	2.744755774	0.969720866
86	3.303986123	0.948482713
87	3.439728692	0.939132387
88	4.151723825	0.966321736
89	2.258075221	0.973300637
90	2.255182412	0.989172831
91	0.971004542	0.960111735
92	0.862135661	0.979907123
93	0.816984419	0.962556275
94	0.837133309	0.977655702
95	0.752242931	0.97321827
96	1.112011206	0.919645687
97	0.921000959	0.957066871
98	0.921810967	0.956699177
99	0.737493315	0.98718053
100	1.06874344	0.948608385
101	1.13996848	0.974152566
102	1.641845252	0.977262103
103	1.135011829	0.990018743
104	1.620401248	0.987409852
105	1.753576499	0.98268228
106	1.647318109	0.983117082
107	1.50197268	0.989466314
108	1.459769153	0.991593147
109	1.806381987	0.98759626
110	2.01952643	0.955048411
111	4.815407612	0.973012232
112	2.340010225	0.983713935
113	3.092741323	0.96563548

114	2.692527757	0.986940272
115	2.238865373	0.979425785
116	1.874865709	0.987931003
117	2.418547449	0.969258482
118	2.071027145	0.984671081
119	1.774527604	0.98353061
120	3.841984175	0.979696259
121	1.915991022	0.935322235
122	1.863168099	0.982459119
123	1.222474116	0.988615719
124	1.417796029	0.972952924
125	1.19244136	0.980851094
126	1.810652062	0.976067762
127	1.364983567	0.990800968
128	1.949633316	0.979571538
129	2.069876918	0.983577529
130	1.592419362	0.987348357
131	1.146598459	0.951497941
132	1.414019224	0.969827181
133	1.247394212	0.991370042
134	1.241090754	0.988778735
135	2.24550043	0.980680135
136	1.444770464	0.98218391
137	1.428562051	0.979813778
138	1.370777508	0.982038859
139	1.035363207	0.992980075
140	1.222805204	0.990162584
141	2.224625371	0.968883479
142	2.054135658	0.987936138
143	1.96443072	0.986842866
144	2.54560456	0.988778346
145	2.298085647	0.978966382
146	1.911381202	0.982550392
147	3.289867689	0.990561465
148	1.754870473	0.973634474
149	1.584504532	0.982275816
150	1.764032442	0.987473683
151	2.795055958	0.960781695

152	1.971200564	0.989225206
153	2.711882133	0.987154963
154	2.456913946	0.984797367
155	2.195676238	0.985811117
156	2.292469824	0.983266292
157	2.850358671	0.982820434
158	1.978433391	0.984263818
159	3.023687404	0.984168236
160	3.98407289	0.985796984
161	1.353618974	0.978789886
162	0.64816183	0.990290071
163	1.266052149	0.977586218
164	1.059784346	0.985009721
165	1.9077246	0.951594648
166	0.761334038	0.984881957
167	1.168835592	0.98107986
168	0.971689551	0.989914382
169	0.998288251	0.983312646
170	1.383867045	0.977346606
171	1.010725284	0.990169455
172	1.176041741	0.98549683
173	1.428250885	0.986669631
174	1.220689798	0.978542547
175	1.492783939	0.985418007
176	1.801209095	0.980552903
177	1.47687845	0.972900573
178	1.711189456	0.979119171
179	1.999302332	0.970044578
180	1.723981168	0.964440686
181	2.400796282	0.98665399
182	3.114271727	0.985664649
183	2.631438752	0.991785954
184	2.760578719	0.984032109
185	4.200163696	0.985407384
186	3.081537786	0.986950575
187	4.937921452	0.986064218
188	3.321557961	0.991983014
189	2.388344044	0.986569583

190	2.413074624	0.991536574
191	0.747572904	0.961423518
192	0.57412443	0.970306154
193	0.971716943	0.870003885
194	0.977127922	0.951678867
195	0.756831961	0.968787903
196	0.445994275	0.976850096
197	0.485708516	0.982915193
198	0.608354906	0.980008811
199	0.9440247	0.964636603
200	0.663964704	0.961805728

Table 7.1: Results of peak forecasting of the proposed Narmax model for all the listed elements of the dataset. Root mean square error is expressed in Newton and is calculated by de-normalizing data, while the R2 Score considers normalized data.

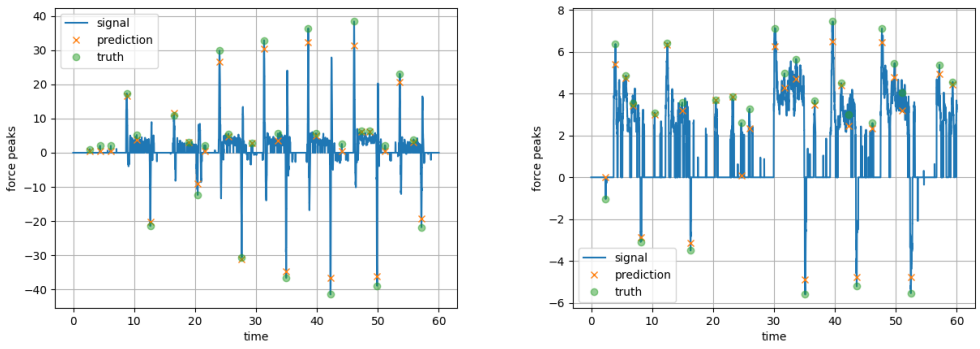

(a) **(b)**

Figure 7.1

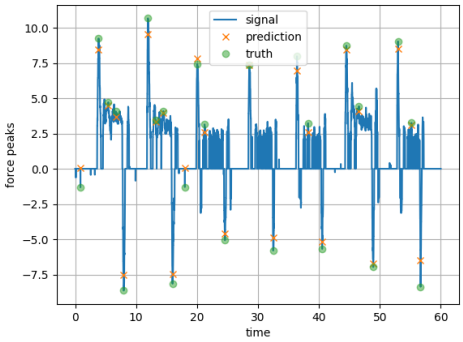

(c)

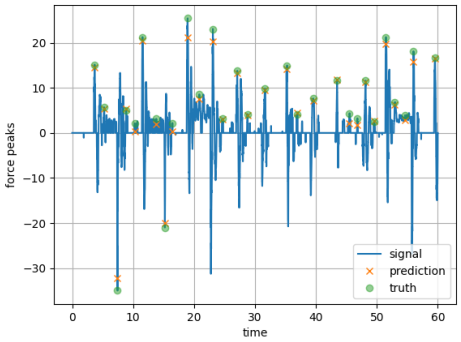

(d)

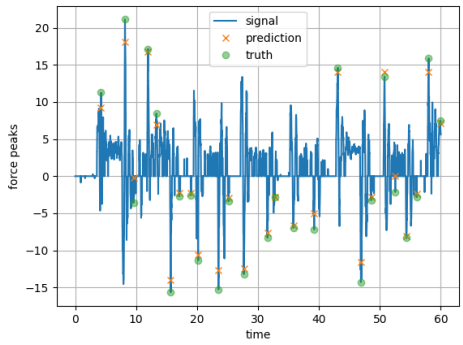

(e)

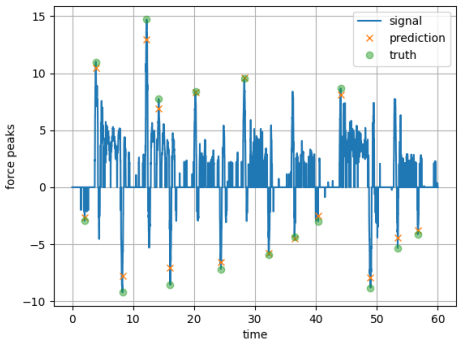

(f)

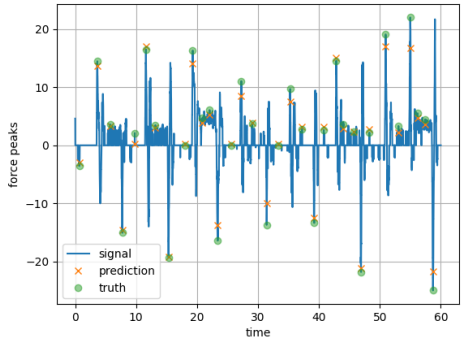

(g)

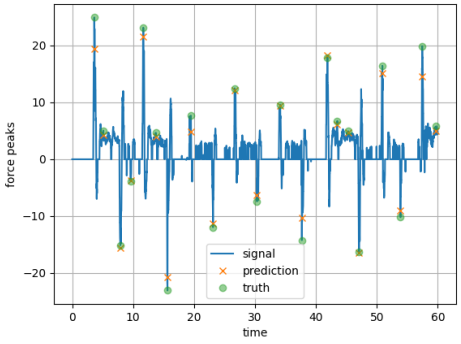

(h)

Figure 7.1

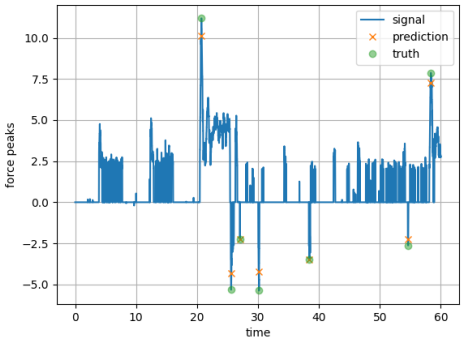

(i)

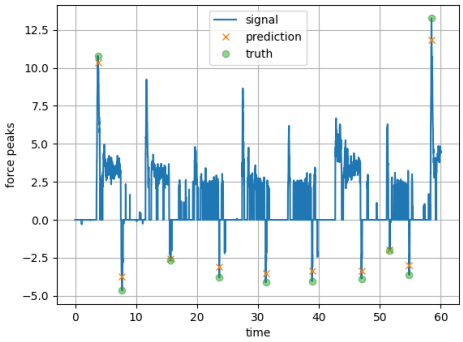

(j)

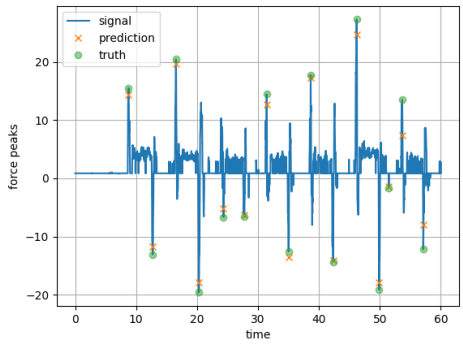

(k)

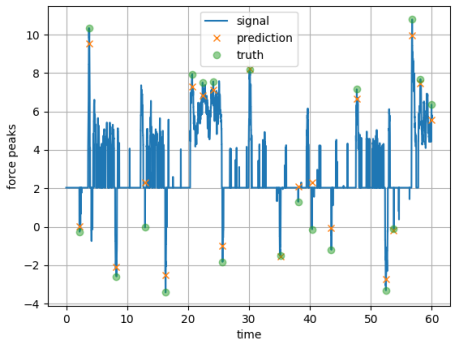

(l)

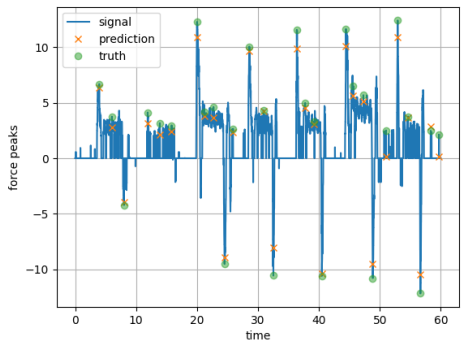

(m)

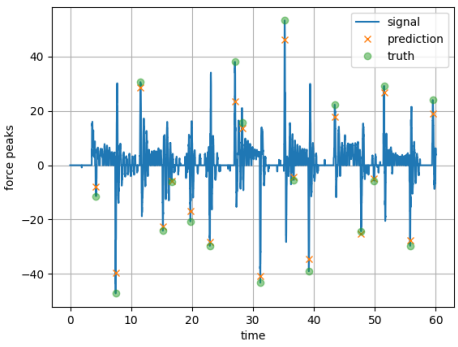

(n)

Figure 7.1

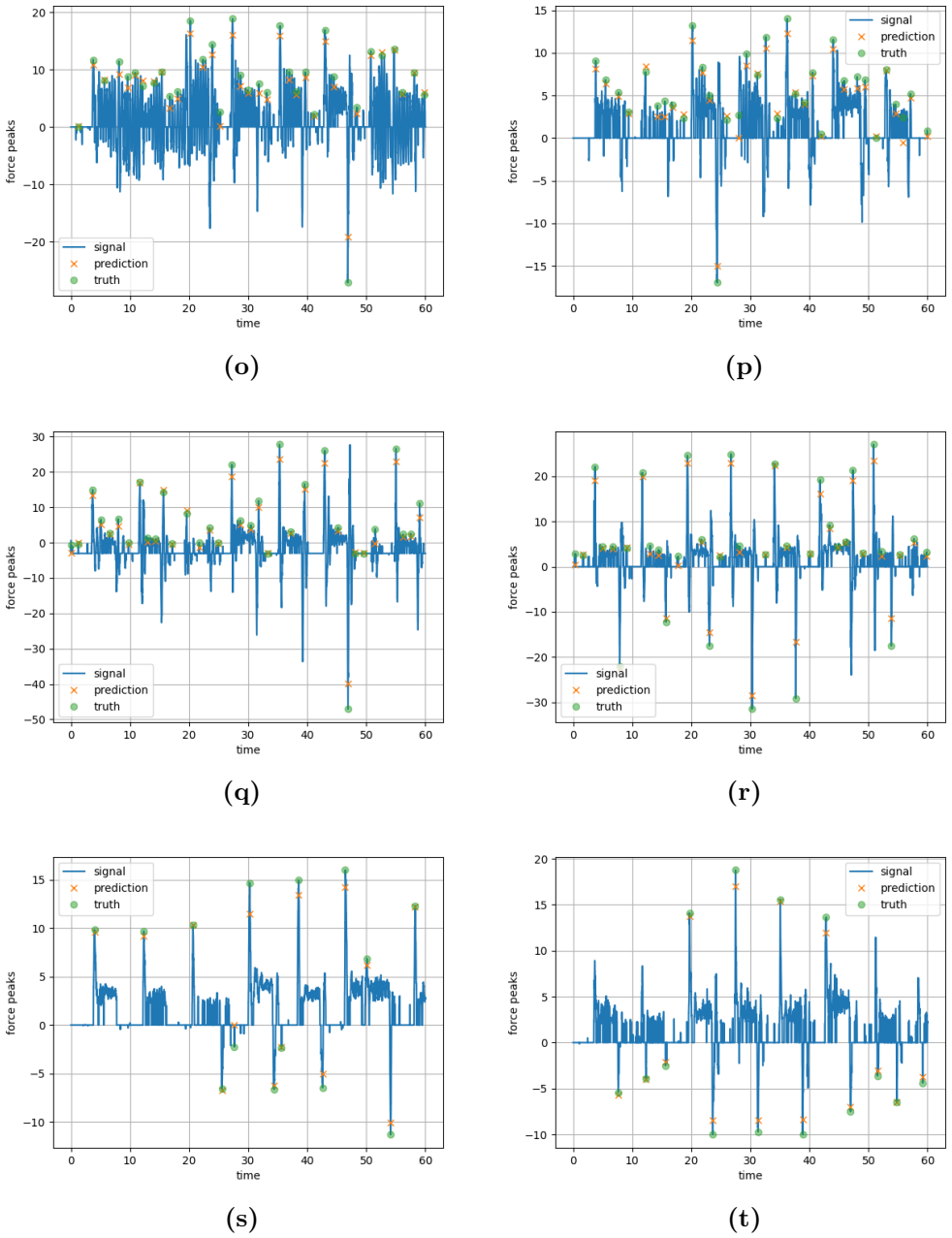

Figure 7.1: Measured vs. predicted peak values (respectively indicated as dots and crosses) displayed in a summary of 20 experiments extracted (1 every 10) from the original dataset of 200 listed elements (100 for x and 100 for y signal components).

Conclusion

In this thesis a vast variety of human models aiming to represent its control behavior when interacting with a controlled machine were investigated and, most importantly, used to create custom modeling approaches inspired by such vast state-of-the-art techniques that were applied in the context of human-robot interaction.

In the first part of this work, the linear modeling techniques were investigated. Such approaches proved to be able to represent well human physiological control districts, which are involved in the perception, control, and actuation processes. Moreover, we saw how such physiological representations can be linked to higher-level control-theory fashioned models like the Crossover Model, Structural Model, Optimal Control Model, etc.

The aforementioned linear approaches, with particular reference to the Crossover Model, were used to propose a *Precision Model of the human-robot complex* when performing a cooperative manipulation task with a collaborative robot, which in the first proposed experimental study was the Universal Robot's UR5 manipulator. The proposed model proved to be able to accurately represent human reaction when an external forcing function is applied to the system. This consideration was verified from two perspectives: the experimental identification of human reaction delay time with particular attention to intra-subject constancy and inter-subject variability and the model's capability to simulate well the position vector of the human-robot complex offline after the experiment.

In the work's second part, we focused on nonlinear dynamics and modeling efforts directed towards their representation. Nonlinear models proved to be able to represent complex processes involved in the human control strategy such as decision-making, the creation of a long-term strategy able to overcome short-term goals, and the ability of humans to transform their behavior from a linear one to a nonlinear impulsive one when the complexity level of the demanded task increases.

Such techniques were studied in the first place in a different application scenario: the transport systems. Such a field, in fact, is one of the

first in which artificial intelligence frameworks were successfully applied to represent human decision-making and its ability to deal with complex problems. This led to the development of systems able to perform automatic lane-changing, as said finding a long-term strategy based on reinforcement learning framework, and the control of quadrotors facing highly nonlinear external dynamics.

In the study of nonlinear state-of-the-art models, a focal point of our study was how data-driven and model-based techniques can be combined to represent partially unknown dynamics. Such consideration led us to the definition of a nonlinear Narmax model, able to describe human response with a precision level that would not be possible with any linear technique.

The proposed Narmax model was able to simulate and forecast human control behavior and estimate its intention during an interaction task with a compliant collaborative robot. The model was trained and tested in the first place with the same experimental data acquired and used in the previously proposed linear model. This time, the model was used to represent human force output, which, from a control block scheme point of view, is the robot's input. Highly impulsive components characterize such force signal, it is noisy, and present high variability between each experiment and each subject.

Despite this, both the RMSE and the R2 score value testify to the outstanding model performance when forecasting x and y force components at each instant. The plots also testify to this consideration, where the ground truth and the prediction signals are superimposed almost entirely.

To verify model generalization capabilities, it was tested with new data produced by a different experimental setup and using a different robot, the Comau NS16. This time, a further step was performed: to let the robot know the human intention nearly in real-time, the model was used to forecast human-generated force online. Position and force signals were acquired in order to let the model forecast the x and y components of the force reference that the human will generate after the next 12 milliseconds, which is the time required by the model to compute a new prediction.

With respect to state-of-the-art approaches like [190] and [98], the proposed modeling and control techniques proved to be able, despite the simplicity of their structure, to replicate and forecast highly nonlinear and impulsive output dynamics of the human control behavior during a continuous interaction.

This consideration is confirmed by the generated force plots, where the predicted force samples reproduce the ground truth vector with high fidelity at each instant. The "real-time" performance of the proposed framework proved to have a slow initial tuning phase and a reliable and fast second phase, where the time delay became almost negligible.

The robot high-level controller showed some difficulties in distinguishing human-generated reference force, which had to be converted to a position reference to let the robot anticipate human motion from unwanted external contacts. The state-machine approach alone has some limitations in performing such a complex duty, which will have to be performed by another dedicated framework. Despite this, in the few cases in which the human reference was recognized, the advantages seemed to be important by looking at both force outputs and the position tracking error.

Aside from the human model, the robotic platform's model can also be approximated. In this case, the admittance controller and its virtual mass-spring-damper system can be modeled as a second-order transfer function. The knowledge of both the system's main components allowed us to extract the information about control delay from empirical data, obtaining a mean delay value of 0.3 seconds. The optimization and identification techniques were relatively simple if compared to more complex approaches which have been proposed [320, 321] when less information on the system dynamics was available.

The optimal model used to obtain predictions at every time frame in which the human interacted with the robot was a narmax model of the 10th order. However, as known, several interesting techniques have been proposed in the past to lower model order and complexity. In particular, Peak-to-Peak Dynamics (PPD) have been successfully studied and applied in the past for complex systems characterized by chaotic behavior. To exploit their applicability in our model, the latter was re-trained to forecast only the peak values of the system's output, but reducing its order as much as possible, without excessively affecting its accuracy. The results showed prediction performance comparable to the ones obtained with the complete order model, but the order was reduced from 10 to 5, further reducing model complexity and required computational time. To the best of our knowledge, this was the first attempt to study PPD in Narmax models.

Bibliography

[1] Laura M Hiatt, Cody Narber, Esube Bekele, Sangeet S Khemlani, and J Gregory Trafton. Human modeling for human-robot collaboration. *The International Journal of Robotics Research*, 36(5-7):580–596, 2017.

[2] Bin He, Han Yuan, Jianjun Meng, and Shangkai Gao. Brain–computer interfaces. *Neural engineering*, pages 131–183, 2020.

[3] Jerry Bergman. Connectome: How the brain's wiring makes us who we are. *Journal of Interdisciplinary Studies*, 28(1–2):192–194, 2016.

[4] Henry Markram. The human brain project. *Scientific American*, 306(6):50–55, 2012.

[5] Mitsuo Kawato, Kazunori Furukawa, and Ryoji Suzuki. A hierarchical neural–network model for control and learning of voluntary movement. *Biological cybernetics*, 57:169–185, 1987.

[6] Masao Ito. Mechanisms of motor learning in the cerebellum. *Brain research*, 886(1–2):237–245, 2000.

[7] Michael I Jordan and David E Rumelhart. Forward models: Supervised learning with a distal teacher. In *Backpropagation*, pages 189–236. Psychology Press, 2013.

[8] Anatol G Feldman and Mindy F Levin. The equilibrium–point hypothesis–past, present and future. *Progress in motor control: A multidisciplinary perspective*, pages 699–726, 2009.

[9] Antoine Falisse, Lorenzo Pitto, Hans Kainz, Hoa Hoang, Mariska Wesseling, Sam Van Rossom, Eirini Papageorgiou, Lynn BarOn, Ann Hallemans, Kaat Desloovere, et al. Physics–based simulations to predict the differential effects of motor control and musculoskeletal deficits on gait dysfunction in cerebral palsy: a retrospective case study. *Frontiers in human neuroscience*, 14:40, 2020.

[10] Friedl De Groote and Antoine Falisse. Rapid predictive simulations to study the interaction between motor control and musculoskeletal dynamics in healthy and pathological human movement. In *Converging Clinical and Engineering Research on Neurorehabilitation IV: Proceedings of the 5th International Conference on Neurorehabilitation (ICNR2020), October 13–16, 2020*, pages 327–331. Springer, 2022.

[11] Huaiwu Zou, Haoran Tao, Zhou Zhou, and Bingshan Hu. Identification of mechanical impedance parameters of human upper limbs using mechanical perturbation method. In *Man–Machine–Environment System Engineering: Proceedings of the 21st International Conference on MMESE: Commemorative Conference for the 110th Anniversary of Xuesen Qian's Birth and the 40th Anniversary of Founding of Man–Machine–Environment System Engineering 21*, pages 141–147. Springer, 2022.

[12] Uğur Demir, Sıtkı Kocaoğlu, and Erhan Akdoğan. Human impedance parameter estimation using artificial neural network for modelling physiotherapist motion. *Biocybernetics and Biomedical Engineering*, 36(2):318–326, 2016.

[13] Arnold Tustin. The nature of the operator's response in manual control, and its implications for controller design. *Journal of the Institution of Electrical Engineers–Part IIA: Automatic Regulators and Servo Mechanisms*, 94(2):190–206, 1947.

[14] RA Hess. Human–in–the–loop control. In *Control System Applications*, pages 327–334. CRC Press, 2018.

[15] Kunfu Wang, Jian Su, Peng Zhang, Baiqiao Huang, and Wei Feng. Interaction design of display and control equipment based on man–machine–environment system engineering. In *International Conference on Man–Machine–Environment System Engineering*, pages 869–877. Springer, 2021.

[16] Guangjiang Wu, Yiqian Wu, Xi Lu, Shenghang Xu, and Chuan Wang. Human–machine interface optimization design based on ecological interface design (eid) theory. In *Man–Machine–Environment System Engineering: Proceedings of the 20th International Conference on MMESE*, pages 715–723. Springer, 2020.

[17] Ha Quang Thinh Ngo, Anh Son Tran, Van Keo Dong, and Jiwang Yan. Implementation of the mathematical model for service robot to

avoid obstacles and human. In *Proceedings of the Future Technologies Conference (FTC) 2021, Volume 2*, pages 513–525. Springer, 2022.

[18] Ha Quang Thinh Ngo, Van Nghia Le, Vu Dao Nguyen Thien, Thanh Phuong Nguyen, and Hung Nguyen. Develop the socially human–aware navigation system using dynamic window approach and optimize cost function for autonomous medical robot. *Advances in Mechanical Engineering*, 12(12):1687814020979430, 2020.

[19] Mahdi Khoramshahi and Aude Billard. A dynamical system approach to task–adaptation in physical human–robot interaction. *Autonomous Robots*, 43:927–946, 2019.

[20] Pedro Neto, Miguel Simão, Nuno Mendes, and Mohammad Safeea. Gesture–based human–robot interaction for human assistance in manufacturing. *The International Journal of Advanced Manufacturing Technology*, 101:119–135, 2019.

[21] Daniel Ullrich, Andreas Butz, and Sarah Diefenbach. The development of overtrust: An empirical simulation and psychological analysis in the context of human-robot interaction. *Frontiers in Robotics and AI*, 8:554578, 2021.

[22] Lorenzo Desideri, Cristina Ottaviani, Massimiliano Malavasi, Roberto di Marzio, and Paola Bonifacci. Emotional processes in human-robot interaction during brief cognitive testing. *Computers in Human Behavior*, 90:331–342, 2019.

[23] Juan Pablo Vasconez, Diego Carvajal, and Fernando Auat Cheein. On the design of a human-robot interaction strategy for commercial vehicle driving based on human cognitive parameters. *Advances in Mechanical Engineering*, 11(7):1687814019862715, 2019.

[24] Jingyao Wang, Manas Ranjan Pradhan, and Nallappan Gunasekaran. Machine learning–based human-robot interaction in its. *Information Processing & Management*, 59(1):102750, 2022.

[25] Jens Rasmussen. Skills, rules, and knowledge; signals, signs, and symbols, and other distinctions in human performance models. *IEEE transactions on systems, man, and cybernetics*, (3):257–266, 1983.

[26] Shuting Xu, Wenqian Tan, Alexander V Efremov, Liguo Sun, and Xiangju Qu. Review of control models for human pilot behavior. *Annual Reviews in Control*, 44:274–291, 2017.

[27] Duane T McRuer and Ezra S Krendel. Mathematical models of human pilot behavior. *AGARDograph AGARD-AG-188*, pages 1–83, 1974.

[28] Maide Bucolo, Arturo Buscarino, Luigi Fortuna, and Salvina Gagliano. Bifurcation scenarios for pilot induced oscillations. *Aerospace Science and Technology*, 106:106194–106199, 2020.

[29] Mudassir Lone and Alastair Cooke. Review of pilot models used in aircraft flight dynamics. *Aerospace Science and Technology*, 34:55–74, 2014.

[30] Shuting Xu and Yu Wu. Modeling multi-loop intelligent pilot control behavior for aircraft-pilot couplings analysis. *Aerospace Science and Technology*, 112:106651–106663, 2021.

[31] Sheng Han, Hong Zhu, Qishui Zhong, Kaibo Shi, and Oh-Min Kwon. Adaptive event-triggered fuzzy positioning control for unmanned marine vehicles with actuator saturation and hybrid attacks. *IEEE Transactions on Fuzzy Systems*, pages 1–13, 2023. doi:10.1109/TFUZZ.2023.3243066.

[32] Madhumita Ray, Nabanita Mahata, and Jamuna Kanta Sing. Uncertainty parameter weighted entropy-based fuzzy c-means algorithm using complemented membership functions for noisy volumetric brain mr image segmentation. *Biomedical Signal Processing and Control*, 85:104925–104937, 2023.

[33] T Miyoshi, S Tano, Y Kato, and Thierry Arnould. Operator tuning in fuzzy production rules using neural networks. *[Proceedings 1993] Second IEEE International Conference on Fuzzy Systems*, pages 641–646, 1993.

[34] Suman Dey, Narath Moni Reang, Arindam Majumder, Madhujit Deb, and Pankaj Kumar Das. A hybrid ann-fuzzy approach for optimization of engine operating parameters of a ci engine fueled with diesel-palm biodiesel-ethanol blend. *Energy*, 202:117813–117830, 2020.

[35] Wanxin Shi, Zheng Huang, Honghao Huang, Chengyang Hu, Minghua Chen, Sigang Yang, and Hongwei Chen. Loen: Lensless optoelectronic neural network empowered machine vision. *Light: Science & Applications*, 11(1):1–12, 2022.

[36] Tao Huang and Rui Fu. Prediction of the driver's focus of attention based on feature visualization of a deep autonomous driving model. *Knowledge-Based Systems*, 251:109006–109016, 2022.

[37] Olaide N Oyelade, Absalom E Ezugwu, Mubarak S Almutairi, Apu Kumar Saha, Laith Abualigah, and Haruna Chiroma. A generative adversarial network for synthetization of regions of interest based on digital mammograms. *Scientific Reports*, 12(1):1–30, 2022.

[38] Maxwell A Konnaris, Matthew Brendel, Mark Alan Fontana, Miguel Otero, Lionel B Ivashkiv, Fei Wang, and Richard D Bell. Computational pathology for musculoskeletal conditions using machine learning: advances, trends, and challenges. *Arthritis Research & Therapy*, 24(1):1–15, 2022.

[39] Zhaoyi Zhang, Songyang Cheng, and Claudia Solis-Lemus. Towards a robust out-of-the-box neural network model for genomic data. *BMC Bioinformatics*, 23(1):1–29, 2022.

[40] Matan Rusanovsky, Ofer Beeri, and Gal Oren. An end-to-end computer vision methodology for quantitative metallography. *Scientific Reports*, 12(1):1–27, 2022.

[41] Roushanak Haji Hassani, Mathias Bannwart, Marc Bolliger, Thomas Seel, Reinald Brunner, and Georg Rauter. Real-time motion onset recognition for robot-assisted gait rehabilitation. *Journal of Neuro-Engineering and Rehabilitation*, 19(1):1–14, 2022.

[42] Weifeng Ma, Haojie Xue, Xiaoyong Sun, Sijia Mao, Liudi Wang, Yang Liu, Yuchen Wang, and Xuefen Lin. A novel multi-branch hybrid neural network for motor imagery eeg signal classification. *Biomedical Signal Processing and Control*, 77:103718–103735, 2022.

[43] Vincent M D'Anniballe, Fakrul Islam Tushar, Khrystyna Faryna, Songyue Han, Maciej A Mazurowski, Geoffrey D Rubin, and Joseph Y Lo. Multi-label annotation of text reports from computed tomography of the chest, abdomen, and pelvis using deep learning. *BMC Medical Informatics and Decision Making*, 22(1):1–12, 2022.

[44] Wiebke Bartolomaeus, Youness Boutaib, Sandra Nestler, and Holger Rauhut. Path classification by stochastic linear recurrent neural networks. *Advances in Continuous and Discrete Models*, (13), 2022. doi:10.1186/s13662-022-03686-9.

[45] Shuhuan Wen, Tao Wang, and Sheng Tao. Hybrid cnn-lstm architecture for lidar point clouds semantic segmentation. *IEEE Robotics and Automation Letters*, 7(3):5811–5818, 2022.

[46] Yuxin Dai, Qimei Chen, Jun Zhang, Xiaohui Wang, Yilin Chen, Tianlu Gao, Peidong Xu, Siyuan Chen, Siyang Liao, Huaiguang Jiang, et al. Enhanced oblique decision tree enabled policy extraction for deep reinforcement learning in power system emergency control. *Electric Power Systems Research*, 209:107932–107943, 2022.

[47] Mohammed H Alabdullah and Mohammad A Abido. Microgrid energy management using deep q-network reinforcement learning. *Alexandria Engineering Journal*, 61(11):9069–9078, 2022.

[48] Kai Zhong, Zhibang Yang, Guoqing Xiao, Xingpei Li, Wangdong Yang, and Kenli Li. An efficient parallel reinforcement learning approach to cross-layer defense mechanism in industrial control systems. *IEEE Transactions on Parallel and Distributed Systems*, 33(11):2979–2990, 2021.

[49] Charley M Wu, Eric Schulz, Timothy J Pleskac, and Maarten Speekenbrink. Time pressure changes how people explore and respond to uncertainty. *Scientific Reports*, 12(1):1–14, 2022.

[50] Tor A Johansen and Bjarne Foss. Constructing narmax models using armax models. *International journal of control*, 58(5):1125–1153, 1993.

[51] Sheng Chen and Steve A Billings. Representations of non-linear systems: the narmax model. *International journal of control*, 49(3):1013–1032, 1989.

[52] Matteo Candaten and Sergio Rinaldi. Peak-to-peak dynamics: A critical survey. *International Journal of Bifurcation and Chaos*, 10(08):1805–1819, 2000.

[53] R. C. Miall, D. J. Weir, D. M. Wolpert, and J. F. Stein. Is the cerebellum a smith predictor? *Journal of motor behavior*, 25(3):203–216, 1993.

[54] D. M. Wolpert, Z. Ghahramani, and M. I. Jordan. An internal model for sensorimotor integration. *Science*, 269(5232):1880–1882, 1995.

[55] M. Kawato. Internal models for motor control and trajectory planning. *Current opinion in neurobiology*, 9(6):718–727, 1999.

[56] A. G. Feldman, V. Goussev, A. Sangole, and M. F. Levin. Threshold position control and the principle of minimal interaction in motor actions. *Prog Brain Res*, 165:267–281, 2007.

[57] Daniel M Dubois. Theory of computing anticipatory systems based on differential delayed-advanced difference equations. In *AIP Conference Proceedings*, volume 627, pages 3–16. American Institute of Physics, 2002.

[58] E. Burdet, K. P. Tee, I. Mareels, T. E. Milner, C. M. Chew, D. W Franklin, and M. Kawato. Stability and motor adaptation in human arm movements. *Biological cybernetics*, 94(1):20–32, 2006.

[59] A. G. Feldman. Functional tuning of nervous system with control of movement or maintenance of a steady posture. 2. controllable parameters of the muscles. *Biophysics*, 11:565–578, 1966.

[60] E. Bizzi, N. Accornero, W. Chapple, and N. Hogan. Posture control and trajectory formation during arm movement. *J Neurosci*, 4:2738–2744, 1984.

[61] T. Flash. The control of hand equilibrium trajectories in multi-joint arm movements. *Biol Cybern*, 57:257–274, 1987.

[62] Kawato M. Gomi H. Equilibrium-point control hypothesis examined by measured arm-stiffness during multi-joint movement. *Science*, 272:117–120, 1996.

[63] M. L. Latash and G. L. Gottlieb. Reconstruction of shifting elbow joint compliant characteristics during fast and slow movements. *Neuroscience*, 43:697–712, 1991.

[64] Kawato M. Katayama M. Virtual trajectory and stiffness ellipse during multijoint arm movement predicted by neural inverse models. *Biol Cybern*, 69:353–362, 1993.

[65] P. L. Gribble and D. J. Ostry. Compensation for interaction torques during Â· single and multi-joint limb movement. *J Neurophysiol*, 82:2310–2326, 1999.

[66] P. G. Morasso and M. Schieppati. Can muscle stiffness alone stabilize upright standing. *J. Neurophysiology*, 82:1622–1626, 1999.

[67] T. E. Milner and C. Cloutier. Compensation for mechanically unstable loading in voluntary wrist movement. *Exp Brain Res*, 94:522–532, 1993.

[68] T. D. Sanger. Neural network learning control of robot manipulators using gradually increasing task difficulty. *IEEE Trans Robotics Automat*, 10:323–333, 1994.

[69] M. Katayama, S. Inoue, and M. Kawato. A strategy of motor learning using adjustable parameters for arm movement. In IEEE, editor, *Proceedings of the 20th Annual International Conference of the IEEE Engineering in Medicine and Biology Society*, pages 2370–2373, Hong Kong, 1998.

[70] Duane T McRuer. Human pilot dynamics in compensatory systems. Technical report, System technology Inc. Hawthorne Ca., 1965.

[71] M. M. Van Paasen, Van Der Vaart, J. C., and J. A. Mulder. Model of the neuromuscular dynamics of the human pilot's arm. *Journal of aircraft*, 41(6):1482–1490, 2004.

[72] S. A. Fayazi, N. Wan, S. Lucich, A. Vahidi, and G. Mocko. Optimal pacing in a cycling time-trial considering cyclist's fatigue dynamics. *American Control Conference*, pages 6442–6447, 2013.

[73] L. Ma, D. Chablat, F. Bennis, and W. Zhang. A new simple dynamic muscle fatigue model and its validation. *International journal of industrial ergonomics*, 39(1):211–220, 2009.

[74] J. Z. Liu, R. W. Brown, and G. H. Yue. A dynamical model of muscle activation, fatigue, and recovery. *Biophysical journal*, 82(5):2344–2359, 2002.

[75] S. K. Uppal and A. Vaz. Motion control of a phalange using tendon-based actuation system: A bond graph approach. pages 1479–1486. Springer, Singapore, 2022.

[76] N. Mishra and A. Vaz. Bond graph modeling of a 3-joint string-tube actuated finger prosthesis. *Mechanism and Machine Theory*, 117:1–20, 2017.

[77] A. Vaz, K. Singh, and G. Dauphin-Tanguy. Bond graph model of extensor mechanism of finger based on hook-string mechanism. *Mechanism and Machine Theory*, 91:187–208, 2015.

[78] P. S. Tsang and M Vidulich. Principles and practice of aviation psychology. In *A*. CRC Press, 2002.

[79] R. Curry, L. Young, W. Hoffman, and D. Kugel. *A pilot model with visual and motion cues.* In Proceedings of the AIAA visual and motion simulation conference, 1976.

[80] F. H. Previc and W. R. (Eds.) Ercoline. *Spatial disorientation in aviation (Vol. 203).* Aiaa, 2004.

[81] D. K. Schmidt and B. J. Bacon. An optimal control approach to pilot/vehicle analysis and the neal-smith criteria. *Journal of Guidance, Control, and Dynamics*, 6(5):339–347, 1983.

[82] Ads-33e-prf-aeronautical design standard, performance specification, handling qualities requirements for military rotorcraft. Technical report, 2000.

[83] A. H. Nguyen, L. Mai, and H. N. Do. Visual object tracking method of spatio-temporal context learning with scale variation. In *In International Conference on the Development of Biomedical Engineering in Vietnam.*, pages 733–742. Springer, Cham., July 2020.

[84] J. Henriques, R. Caseiro, P. Martins, and J. Batista. High-speed tracking with kernelized correlation filters. *IEEE Trans Pattern Anal Mach Intell*, 37:583–596, 2015.

[85] F. Chen, W. Xie, and T. Xia. Target tracking algorithm based on kernel correlation filter with anti-occlusion mechanisms. In *In15th IEEE International Conference on Signal Processing (ICSP)*, volume 1, pages 220–225. IEEE, 2020.

[86] W. Luo, J. Xing, A. Milan, X. Zhang, W. Liu, and T. K. Kim. Multiple object tracking: A literature review. *Artificial Intelligence*, 293(10344):8, 2021.

[87] A. Kumar and I. Ghosh. Non-compliance behavior of pedestrians and the associated conflicts at signalized intersections in india. *Safety Science*, 147(10560):4, 2022.

[88] A. Roy, M. Hossain, and Y. Muromachi. A deep reinforcement learning-based intelligent intervention framework for real-time proactive road safety management. *Accident Analysis and Prevention*, 165:106512, 2022.

[89] H. Heerspink, W. Berkouwer, O. Stroosma, R. van Paassen, M. Mulder, and B. Mulder. Evaluation of vestibular thresholds for motion detection

in the simona research simulator. page 6502. In Aiaa modeling and simulation technologies conference and exhibit, August 2005.

[90] P. W. Halligan, A. Zeman, and A. Berger. *Phantoms in the brain*. 1999.

[91] D. Purves and R. B. Lotto. *Why we see what we do redux: A wholly empirical theory of vision*. Sinauer Associates, 2011.

[92] R. Telban, F. Cardullo, and L. Guo. Investigation of mathematical models of otolith organs for human centered motion cueing algorithms. *In Modeling and Simulation Technologies Conference*, 4291, 2000.

[93] A. Berthoz, B. Pavard, and L. R. Young. Perception of linear horizontal self-motion induced by peripheral vision (line-arvection) basic characteristics and visual-vestibular interactions. *Experimental brain research*, 23(5):471–489, 1975.

[94] C. Fernandez and J. M. Goldberg. Physiology of peripheral neurons innervating semicircular canals of the squirrel monkey. ii. response to sinusoidal stimulation and dynamics of peripheral vestibular system. *Journal of neurophysiology*, 34(4):661–675, 1971.

[95] Ruud Hosman and Henk Stassen. Pilot's perception in the control of aircraft motions. *Control Engineering Practice*.

[96] A. Phatak, H. Weinert, I. Segall, and C. N. Day. Identification of a modified optimal control model for the human operator. *Automatica*, 12(1):31–41, 1976.

[97] J. R. Ragazzini. Engineering aspects of the human being as a servomechanism. in Proceedings of the Meeting of the American Psychological Association, 1948.

[98] Satoshi Suzuki and Katsuhisa Furuta. Adaptive impedance control to enhance human skill on a haptic interface system. *Journal of Control Science and Engineering*, 2012, 2012.

[99] M. MartÃnez-GarcÃa, T. Gordon, and L. Shu. Extended crossover model for human-control of fractional order plants. *IEEE Access*, 5:27622–27635, 2017.

[100] A. Takacs, L. Kovacs, I. Rudas, R. E. Precup, and T. Haidegger. Models for force control in telesurgical robot systems. *Acta PolytechnicaHungarica*, 12(8):95–114, 2005.

[101] Sheldon Baron, DL Kleinman, and WH Levison. An optimal control model of human response part ii: prediction of human performance in a complex task. *Automatica*, 6(3):371–383, 1970.

[102] David L Kleinman, S Baron, and WH Levison. An optimal control model of human response part i: Theory and validation. *Automatica*, 6(3):357–369, 1970.

[103] R. D. Wierenga. An evaluation of a pilot model based on kalman filtering and optimal control. *IEEE Transactions on Man-Machine Systems*, 10(4):108–117, 1969.

[104] D. K. Schmidt. Pilot modeling and closed-loop analysis of flexible aircraft in the pitch tracking task. *Journal of Guidance, Control, and Dynamics*, 8(1):56–61, 1985.

[105] M. Innocenti. *The Optimal Control Pilot Model and Applications*. ADVISORY GROUP FOR AEROSPACE RESEARCH AND DEVELOPMENT NEUILLY-SUR-SEINE (FRANCE), 1988.

[106] D. Doman. Optimal control pilot modeling for resolving cooper-harper rating discrepancies. In *In Aiaa atmospheric flight mechanics conference and exhibit*, pages 176–186, Portland, OR, August 1999. AIAA-1999-4091.

[107] D. B. Doman and M. R. Anderson. A fixed–order optimal control model of human operator response. *Automatica*, 36(3):409–418, 2000.

[108] S. Baron and D. L. Kleinman. The human as an optimal controller and information processor. *IEEE Transactions on Man-Machine Systems*, 10(1):9–17, 1969.

[109] C. Wang et al. A revised optimal control pilot model for computer simulation. In *2nd International conference on bio-informatics and biomedical engineering*. IEEE, 2008.

[110] E. G. Gai and R. E. Curry. A model of the human observer in failure detection tasks. *IEEE Transactions on Systems, Man, and Cybernetics, SMC*, 6(2):85–94, 1976.

[111] D. L. Kleinman and W. R. Killingsworth. A predictive pilot model for stol aircraft landing. *NASA CR–2374*, 1974.

[112] R. A. Hess. Obtaining multi-loop pursuit-control pilot models from computer simulation. In *Proceedings of the Institution of Mechanical Engineers*, pages 189–199, Part G, 2008. Journal of Aerospace Engineering.

[113] R. A. Hess. Multi–axis pilot modelling: Models and methods for wake vortex encounter simulations. *In Presentation to WakeNet–Europe Safety Workshop*, 3, June 2010.

[114] A. V. Efremov, A. V. Ogloblin, and A. V. Koshelenko. Evaluation and prediction of aircraft handling qualities. *23rd atmospheric flight mechanics conference*, (AIAA-98-4145), 1998.

[115] C. R. Edkins. *The prediction of pilot opinion ratings using optimal and suboptimal pilot models*, volume AD-278 679. Wright-Patterson Air Force Base, OH,, 1994.

[116] R. A. Hess. Prediction of pilot opinion ratings using an optimal pilot model. *Human Factors: The Journal of the Human Factors and Ergonomics Society*, 19(5):459–475, 1977.

[117] A. SchÃ¶nfeld. Modified optimal control model and wake vortex encounter. *Presentation at the WakeNet-Europe specific workshop: Models and Methods for WVE Simulations*, 3, June 2010.

[118] M. M. Lone. *Pilot modeling for airframe loads analysis*. PhD thesis, University of Cranfield, 2013.

[119] M. M. Lone and A. K. Cooke. Pilot-model-in-the-loop simulation environment to study large aircraft dynamics. *Proceedings of the Institution of Mechanical Engineers, Part G: Journal of Aerospace Engineering*, 227(3):555–568, 2012.

[120] R. A. Hess. Optimal control approximations for time delay systems. *AIAA Journal*, 10(11):1536–1538, 1972.

[121] W. H. Levison. Alternative treatments of attention-sharing within the optimal control model. In *In Systems, man and cybernetics conference proceedings*, pages 744–749. IEEE, 1989.

[122] P. Gawthrop, I. Loram, M. Lakie, and H. Gollee. Intermittent control: A computational theory of human control. *Biological Cybernetics*, 104(1):31–51.

[123] G. Johannsen and W. B. Rouse. Mathematical concepts for modeling human behavior in complex man-machine systems. *Human Factors*, 21(6):733–747, 1979.

[124] K. R. Pattipati, D. L. Kleinman, and A. R. Ephrath. A dynamic decision model of human task selection performance. *IEEE Transactions on Systems, Man, and Cybernetics*, 13(2):145–166, 1983.

[125] M. Menner, P. Worsnop, and M. N. Zeilinger. Constrained inverse optimal control with application to a human manipulation task. In *IEEE Transactions on Control Systems Technology*. IEEE, 2019.

[126] J. Mainprice, R. Hayne, and D. Berenson. Predicting human reaching motion in collaborative tasks using inverse optimal control and iterative replanning. In *IEEE International Conference on Robotics and Automation (ICRA)*, pages 885–892. IEEE, May 2015.

[127] I. G. Jin and G. Orosz. Connected cruise control among human-driven vehicles: Experiment–based parameter estimation and optimal control design. *Transportation research part C: emerging technologies*, 95:445–459, 2018.

[128] R. A. Hess. Structural model of the adaptive human pilot. *Journal of Guidance, Control, and Dynamics*, 3(5):416–423, 1979.

[129] Hess, Ronald A. A rationale for human operator pulsive control behavior. *Journal of Guidance and Control*, 2(3):221–227, 1979.

[130] R. H. Smith. A theory for handling qualities with applications to milf-8785b. Technical report AFFDL-TR-75-119, WPAFB, OH: Air Force Flight Dynamics Lab, 1975.

[131] R. A. Hess. A pilot modeling technique for handling-qualities research. *6th Atmospheric Flight Mechanics Conference*, January 1980.

[132] R. A. Hess. Analyzing manipulator and feel system effects in aircraft flight control. *IEEE Transactions on Systems, Man, and Cybernetics*, 20(4):923–931, 1990.

[133] Raymond E Magdaleno and Duane T Mc Ruer. Experimental validation and analytical elaboration for models of the pilot's neuromuscular subsystem in tracking tasks. Technical report, NASA, 1971.

[134] R. A. Hess. Model for human use of motion cues in vehicular control. *Journal of Guidance, Control, and Dynamics*, 13(3):476–482, 1990.

[135] R. A. Hess. Effects of time delays on systems subject to manual control. *Journal of Guidance, Control, and Dynamics*, 7(4):416–421, 1984.

[136] R. A. Hess. Unified theory for aircraft handling qualities and adverse aircraft–pilot coupling. *Journal of Guidance, Control, and Dynamics*, 20(6):1141–1148, 1997.

[137] Gary R George. *New methods of mathematical modeling of human behavior in the manual tracking task*. State University of New York at Binghamton, 2008.

[138] R. Heffley. Use of a task-pilot-vehicle (tpv) model as a tool for flight simulator math model development. In *AIAA guidance navigation, and control conference*, Toronto, ON, Canada, August 2010. AIAA.

[139] A. V. Efremov and M. S. Tjaglik. The development of perspective displays for highly precise tracking tasks. *In Advances in aerospace guidance, navigation and control*, 163–174, 2011.

[140] R. A. Hess and T. Malsbury. Closed-loop assessment of flight simulator fidelity. *Journal of Guidance, Control, and Dynamics*, 14(1):191–197, 1991.

[141] R. A. Hess, T. Malsbury, A. Atencio, Jr., and Atencio Jr. Flight simulator fidelity assessment in a rotorcraft lateral translation maneuver. *Journal of guidance, control, and dynamics*, 16(1):79–85, 1993.

[142] R. A. Hess and W. Siwakosit. Assessment of flight simulator fidelity in multiaxis tasks including visual cue quality. *Journal of Aircraft*, 38(4):607–614, 2001.

[143] Y. Zeyada and R. A. Hess. Computer-aided assessment of flight simulator fidelity. *Journal of Aircraft*, 40(1):173–180, 2003.

[144] R. A. Hess. Rudder control strategies and force/feel system designs in transport aircraft. *Journal of Guidance, Control, and Dynamics*, 28(6):1251–1262, 2005.

[145] R. A. Hess. Theory for aircraft handling qualities based upon a structural pilot model. *Journal of Guidance, Control, and Dynamics*, 12(6):792–797, 1989.

[146] R. A. Hess and I. Sunyoto. Toward a unifying theory for aircraft handling qualities. *Journal of Guidance, Control, and Dynamics*, 8(4):40–46, 1985.

[147] A. I. Afloare and A. Ionita. Prediction of the handling qualities and pilot-induced oscillation rating levels. *INCAS Bulletin*, 6:3–13, 2014.

[148] R. A. Hess and R. Joyce. Analytical investigation of transport aircraft handling qualities. *In AIAA atmospheric flight mechanics conference*, 19–22, August 2013.

[149] O. L. Grant, K. A. Stol, A. Swain, and R. A. Hess. Handling qualities of a twin ducted-fan aircraft: An analytical evaluation. *Journal of Guidance, Control, and Dynamics*, 38(6):1126–1131, 2015.

[150] J. Gibson. The definition, understanding and fesign of aircraft handling qualities. *Delft University Press.*, 1997.

[151] G. D. Padfield. The making of helicopter flying qualities: a requirements perspective. *The Aeronautical Journal*, 102(1018):409–437, 1998.

[152] R. Hosman. *Pilot's perception and control of aircraft motions.* Delft University Press, 1996.

[153] R. Hosman, J. Schuring, and P. Van der Geest. Pilot model development for the manual balked landing maneuver. *AIAA modeling and simulation technologies conference and exhibit*, (AIAA-2005-5884), May 2005.

[154] R. Hosman and J. C. Van der Vaart. Effects of vestibular and visual motion perception on task performance. *Acta Psychologica*, 48(1):271–287, 1981.

[155] P. M. T. Zaal, D. M. Pool, M. Mulder, and M. M. Van Paassen. New types of target inputs for multi-modal pilot model identification. *In AIAA modeling and simulation technologies conference and exhibit*, pages 18–21, August 2008.

[156] M. Mulder, W. J. Kaljouw, and M. M. Van Paassen. Parameterized multi-loop model of pilot's use of central and peripheral visual motion cues. *AIAA modeling and simulation technologies conference and exhibit*, (AIAA-2005-5894), 2005.

[157] P. R. Grant, B. Yam, R. Hosman, and J. A. Schroeder. The effect of simulator motion on pilot's control behavior for helicopter yaw control tasks. In *AIAA modeling and simulation technologies conference.* AIAA, August 2005.

[158] E. L. Groen, M. H. Smaili, and R. J. Hosman. Perception model analysis of flight simulator motion for a decrab maneuver. *Journal of Aircraft*, 44(2):427–435, 2007.

[159] M. J. Griffin. The validation of biodynamic models. *Clinical Biomechanics*, 16(1):S81–S92, 2001.

[160] P. Masarati, G. Quaranta, A. Bernardini, and G. Guglieri. Voluntary pilot action through biodynamics for helicopter flight dynamics simulation. *Journal of Guidance, Control, and Dynamics*, 38(3):431–441, 2015.

[161] M. D. Pavel, M. Jump, B. Dang-Vu, P. Masarati, M. Gennaretti, A. Ionita, et al. Adverse rotorcraft pilot couplings - past, present and future challenges. *Progress in Aerospace Sciences*, 62:1–51, 2013.

[162] J. Venrooij, M. M. Van Paassen, M. Mulder, D. A. Abbink, M. Mulder, Van Der Helm, F. C., et al. A framework for biodynamic feedthrough analysis-part i: Theoretical foundations. *IEEE Transactions on Cybernetics*, 44(9):1686–1698, 2014.

[163] J. Venrooij, M. M. Van Paassen, M. Mulder, D. A. Abbink, M. Mulder, Van Der Helm, F. C., et al. A framework for biodynamic feedthrough analysis-part ii: Validation and application. *IEEE Transactions on Cybernetics*, 44(9):1699–1710, 2014.

[164] O. Dieterich, J. GÃ¶tz, Dang Vu, B. Haverdings, P. Masarati, and M. Pavel. *Adverse rotorcraft-pilot coupling: Recent research activities in Europe*.

[165] S. Kitazaki and M. J. Griffin. A modal analysis of whole-body vertical vibration, using a finite element model of the human body. *Journal of Sound and Vibration*, 200(1):83–103, 1997.

[166] M. R. Sirouspour and S. E. Salcudean. Suppressing operator-induced oscillations in manual control systems with movable bases. *IEEE Transactions on Control Systems Technology*, 11(4):448–459, 2003.

[167] S. SÃ¶vÃ©nyi and R. B. Gillespie. Cancellation of biodynamic feedthrough in vehicle control tasks. *IEEE Transactions on Control Systems Technology*, 15(6):1018–1029, 2007.

[168] S. Kitazaki and M. J. Griffin. Resonance behaviour of the seated human body and effects of posture. *Journal of biome-chanics*, 31(2):143–149, 1997.

[169] Y. Matsumoto and M. J. Griffin. Movement of the upper-body of seated subjects exposed to vertical whole-body vibration at the principal resonance frequency. *Journal of Sound and Vibration*, 215(4):743–762, 1998.

[170] W. H. Levison and C. B. Harrah. Biomechanical and performance response of man in six different directional axis vibration environments. Technical report AMRL-TR-77-71, Aerospace Medical Research Laboratory, 1977.

[171] G. Hike. A biomechanical pilot model for prediction of roll ratcheting. In *AIAA atmospheric flight mechanics conference*, pages 187–196. AIAA.

[172] Y. Matsumoto and M. J. Griffin. Modelling the dynamic mechanisms associated with the principal resonance of the seated human body. *Clinical Biomechanics*, 16(1):S31–S44, 2001.

[173] D. E. Johnston and B. L. Aponso. Design considerations of manipulator and feel system characteristics in roll tracking. *NASA CR-4111*, 1988.

[174] D. L. Raney, E. B. Jackson, and C. S. Buttrill. Simulation study of impact of aeroelastic characteristics on flying qualities of a high-speed civil transport. Technical report, NASA, 2002.

[175] D. L. Raney, E. B. Jackson, C. S. Buttrill, and W. M. Adams. The impact of structural vibration on flying qualities of a supersonic transport. In *AIAA atmospheric flight mechanics conference*. AIAA, August 2001.

[176] J. Venrooij, M. Mulder, M. M. van Paassen, M. Mulder, and D. A. Abbink. Relating biodynamic feedthrough to neuromuscular admittance. *SMC*, pages 1668–1673, October 2009.

[177] T. E. Coe, J. T. Xing, R. A. Shenoi, and D. Taunton. A simplified 3-d human body-seat interaction model and its applications to the vibration isolation design of high-speed marine craft. *Ocean Engineering*, 36(9):732–746, 2009.

[178] P. Masarati, G. Quaranta, L. Zaichik, Y. Yashin, P. Desyatnik, M. D. Pavel, et al. Biodynamic pilot modelling for aeroelastic a/rpc. In *European rotorcraft forum*, Moscow, Russia, 2013.

[179] Fabio Fruggiero, Alfredo Lambiase, Sotirios Panagou, and Lorenzo Sabattini. Cognitive human modeling in collaborative robotics. *Procedia Manufacturing*, 51:584–591, 2020.

[180] Behzad Sadrfaridpour, Hamed Saeidi, Jenny Burke, Kapil Madathil, and Yue Wang. Modeling and control of trust in human-robot collaborative manufacturing. In *Robust Intelligence and Trust in Autonomous Systems*, pages 115–141. Springer, 2016.

[181] Takenori Obo, Chu Kiong Loo, and Naoyuki Kubota. Robot posture generation based on genetic algorithm for imitation. In *2015 IEEE Congress on Evolutionary Computation (CEC)*, pages 552–557. IEEE, 2015.

[182] Markus Huber, Markus Rickert, Alois Knoll, Thomas Brandt, and Stefan Glasauer. Human-robot interaction in handing-over tasks. In *RO-MAN 2008-The 17th IEEE International Symposium on Robot and Human Interactive Communication*, pages 107–112. IEEE, 2008.

[183] Wolfram Erlhagen, Albert Mukovskiy, Estela Bicho, Giorgio Panin, Csaba Kiss, Alois Knoll, Hein Van Schie, and Harold Bekkering. Goal-directed imitation for robots: A bio-inspired approach to action understanding and skill learning. *Robotics and autonomous systems*, 54(5):353–360, 2006.

[184] Hemanth Manjunatha, Sri Sadhan Jujjavarapu, and Ehsan T Esfahani. Transfer learning of motor difficulty classification in physical human-robot interaction using electromyography. *Journal of Computing and Information Science in Engineering*, pages 1–32, 2022.

[185] Ruilin Chen, Xiaowei Jin, Shujin Laima, Yong Huang, and Hui Li. Intelligent modeling of nonlinear dynamical systems by machine learning. *International Journal of Non-Linear Mechanics*, 142:103984–103995, 2022. doi:10.1016/j.ijnonlinmec.2022.103984.

[186] Chaoxu Mu, Ke Wang, and Tie Qiu. Dynamic event-triggering neural learning control for partially unknown nonlinear systems. *IEEE Transactions on Cybernetics*, 52(4):2200–2213, 2020.

[187] William S Levine. *The Control Handbook (three volume set)*. CRC press, 2018.

[188] DL Kleinman. Optimal lineer control for systems with time delay and observation noise. *IEE Transactions on Automatic Control*, 14(4), 1969.

[189] Ronald A Hess. Structural model of the adaptive human pilot. *Journal of Guidance and Control*, 3(5):416–423, 1980.

[190] Sven Cremer, Sumit Kumar Das, Indika B Wijayasinghe, Dan O Popa, and Frank L Lewis. Model-free online neuroadaptive controller with intent estimation for physical human–robot interaction. *IEEE Transactions on Robotics*, 36(1):240–253, 2019.

[191] Adriano Scibilia, Nicola Pedrocchi, and Luigi Fortuna. Human control model estimation in physical human–machine interaction: A survey. *Sensors*, 22(5):1732–1758, 2022.

[192] Duane T McRuer and Henry R Jex. A review of quasi-linear pilot models. *IEEE transactions on human factors in electronics*, (3):231–249, 1967.

[193] Hyeong Ryeol Kam, Sung-Ho Lee, Taejung Park, and Chang-Hun Kim. Rviz: a toolkit for real domain data visualization. *Telecommunication Systems*, 60:337–345, 2015.

[194] Gavriel Salvendy. *Handbook of human factors*. John Wiley & Sons, 1987.

[195] Duane T McRuer, Raymond E Magdaleno, and George P Moore. A neuromuscular actuation system model. *IEEE Transactions on Man-Machine Systems*, 9(3):61–71, 1968.

[196] Edward N Bachelder and Bimal Aponso. Human pilot control adaptation: A physiological interpretation. *AIAA SCITECH 2022 Forum*, pages 2446–2458, 2022. doi:10.2514/6.2022-2446.

[197] Francisco J Valero-Cuevas, Heiko Hoffmann, Manish U Kurse, Jason J Kutch, and Evangelos A Theodorou. Computational models for neuromuscular function. *IEEE Reviews in Biomedical Engineering*, 2:110–135, 2009.

[198] Dimitri Bertsekas. *Dynamic programming and optimal control: Volume I*, volume 1. Athena Scientific, 2012.

[199] Arthur E Bryson and Yu-Chi Ho. *Applied optimal control: optimization, estimation, and control*. Routledge, 2018.

[200] Weiwei Li and Emanuel Todorov. Iterative linear quadratic regulator design for nonlinear biological movement systems. *Proceedings of the 1st International Conference on Informatics in Control, Automation and Robotics*, pages 222–229, 2004.

[201] Emanuel Todorov and Weiwei Li. A generalized iterative lqg method for locally-optimal feedback control of constrained nonlinear stochastic systems. *Proceedings of the 2005, American Control Conference*, pages 300–306, 2005.

[202] Weiwei Li and Emanuel Todorov. An iterative optimal control and estimation design for nonlinear stochastic system. *Proceedings of the 45th IEEE Conference on Decision and Control*, pages 3242–3247, 2006.

[203] Li, Weiwei and Todorov, Emanuel. Iterative linearization methods for approximately optimal control and estimation of non-linear stochastic system. *International Journal of Control*, 80(9):1439–1453, 2007.

[204] Kirill Zaychik, Frank Cardullo, and Gary George. A conspectus on operator modeling: past, present and future. *AIAA Modeling and Simulation Technologies Conference and Exhibit*, pages 6625–6640, 2006.

[205] Gisele Helena Barboni Miranda and Joaquim Cezar Felipe. Computer-aided diagnosis system based on fuzzy logic for breast cancer categorization. *Computers in Biology and Medicine*, 64:334–346, 2015.

[206] Ensieh Modiri Dovom, Amin Azmoodeh, Ali Dehghantanha, David Ellis Newton, Reza M Parizi, and Hadis Karimipour. Fuzzy pattern tree for edge malware detection and categorization in iot. *Journal of Systems Architecture*, 97:1–7, 2019.

[207] Marcus Wohler, Fabian Loy, and Axel Schulte. Mental models as common ground for human-agent interaction in cognitive assistant systems. *Proceedings of the International Conference on Human-Computer Interaction in Aerospace*, (20), 2014. doi:10.1145/2669592.2669686.

[208] Martin Gestwa and L Grigorie. Using fuzzy control for modeling the control behaviour of a human pilot. *Fuzzy Controllers, Theory and Applications*, pages 297–326, 2011.

[209] Hai-Tao Jiang, Xiao-dong Su, and Hui Li. Dynamic multi-attribute decision making based on advantage retention degree. *International Journal of Control and Automation*, 7(9):389–398, 2014.

[210] Mohammad Yazdi, Sahand Daneshvar, and Hashem Setareh. An extension to fuzzy developed failure mode and effects analysis (fdfmea) application for aircraft landing system. *Safety Science*, 98:113–123, 2017.

[211] Xichao Su, Yu Wu, Jingyu Song, and Peilong Yuan. A fuzzy path selection strategy for aircraft landing on a carrier. *Applied Sciences*, 8(5):779–796, 2018. doi:10.3390/app8050779.

[212] Seong-Hyeon Na and Gwang-Eun Lee. Fuzzy fmea for rotorcraft landing system. *Journal of the Korea Academia-Industrial Cooperation Society*, 22(1):751–758, 2021.

[213] P Stewart, D Gladwin, M Parr, and Jill Stewart. Multi-objective evolutionary fuzzy augmented flight control for an f16 aircraft. *Proceedings of the Institution of Mechanical Engineers, Part G: Journal of Aerospace Engineering*, 224(3):293–309, 2010.

[214] Geoffrey E Hinton and Ruslan R Salakhutdinov. Reducing the dimensionality of data with neural networks. *Science*, 313(5786):504–507, 2006.

[215] Ryota Mori and Shinji Suzuki. Neural network modeling of lateral pilot landing control. *Journal of Aircraft*, 46(5):1721–1726, 2009.

[216] RJ Jagacinski, JM Flach, and Lawrence Erlbaum. *Control theory for humans: Quantitative approaches to modeling performance*. CRC Press, 2004.

[217] W Tan, X Qu, and W Wang. Compared with human pilot model of neural networks and quasi-linearity in frequency domain. *Acta Aeronautica et Astronautica Sinica*, 24(6):4–12, 2003.

[218] Lin Cheng, Zhenbo Wang, Fanghua Jiang, and Junfeng Li. Adaptive neural network control of nonlinear systems with unknown dynamics. *Advances in Space Research*, 67(3):1114–1123, 2021.

[219] Zs J Viharos and Krisztián Balázs Kis. Survey on neuro-fuzzy systems and their applications in technical diagnostics and measurement. *Measurement*, 67:126–136, 2015.

[220] J-SR Jang. Anfis: adaptive-network-based fuzzy inference system. *IEEE Transactions on Systems, Man, and Cybernetics*, 23(3):665–685, 1993.

[221] Seniz Ertugrul. Predictive modeling of human operators using parametric and neuro-fuzzy models by means of computer-based identification experiment. *Engineering Applications of Artificial Intelligence*, 21(2):259–268, 2008.

[222] Li-Chih Ying and Mei-Chiu Pan. Using adaptive network based fuzzy inference system to forecast regional electricity loads. *Energy Conversion and Management*, 49(2):205–211, 2008.

[223] Muhammad Zaigham Abbas, Intisar Ali Sajjad, Babar Hussain, Rehan Liaqat, Akhtar Rasool, Sanjeevikumar Padmanaban, and Baseem Khan. An adaptive-neuro fuzzy inference system based-hybrid technique for performing load disaggregation for residential customers. *Scientific Reports*, 12(1):1–14, 2022.

[224] Engin Avci and Zuhtu Hakan Akpolat. Speech recognition using a wavelet packet adaptive network based fuzzy inference system. *Expert Systems with Applications*, 31(3):495–503, 2006.

[225] Liang-Ying Wei, Tai-Liang Chen, and Tien-Hwa Ho. A hybrid model based on adaptive-network-based fuzzy inference system to forecast taiwan stock market. *Expert Systems with Applications*, 38(11):13625–13631, 2011.

[226] Shirin Kordnoori, Arash Sharifi, and Hamed Shah-Hosseini. Human fall detection using neuro-fuzzy models based on ensemble learning. *Progress in Artificial Intelligence*, 11:1–14, 2022.

[227] Roderick Murray-Smith. A local model network approach to nonlinear modelling. *University of Strathclyde*, 1994. doi:10.48730/me80-tw49.

[228] Kayvan Aghabayk, Nafiseh Forouzideh, and William Young. Exploring a local linear model tree approach to car-following. *Computer-Aided Civil and Infrastructure Engineering*, 28(8):581–593, 2013.

[229] Mohammad R Salmanpour, Mojtaba Shamsaei, Abdollah Saberi, Ivan S Klyuzhin, Jing Tang, Vesna Sossi, and Arman Rahmim. Machine learning methods for optimal prediction of motor outcome in parkinson's disease. *Physica Medica*, 69:233–240, 2020.

[230] Hossein Iranmanesh, Mehdi Keshavarz, and Majid Abdollahzade. Predicting dust storm occurrences with local linear neuro fuzzy model: a case study in ahvaz city, iran. *International Conference on Soft Computing-MENDEL*, pages 158–167, 2016.

[231] Oliver Nelles. Local linear model trees for on-line identification of time-variant nonlinear dynamic systems. *International Conference on Artificial Neural Networks*, pages 115–120, 1996.

[232] Kaijun Xu. Visual scene simulation to civil aviation aircraft approaching and landing using dual fuzzy neural network. *International Conference on Network Computing and Information Security*, pages 275–280, 2012.

[233] Kai Jun Xu. Decisional autonomy of approach and landing phase for civil aviation aircraft using dual fuzzy neural network. *Advanced Materials Research*, 476:936–939, 2012.

[234] Kaijun Xu, Guangming Zhang, and Yang Xu. A dual fuzzy neuro controller using genetic algorithm in civil aviation intelligent landing system. *Advanced Science Letters*, 6(1):360–363, 2012.

[235] Qi-Dan Zhu, Hui Li, Meng-Zhu Yu, Zhi Zhang, and Xing-Wei Jiang. Landing risk evaluation of carrier-based aircraft based on bp neural network. *2012 Second International Conference on Instrumentation, Measurement, Computer, Communication and Control*, pages 1596–1601, 2012.

[236] Yann LeCun, Yoshua Bengio, and Geoffrey Hinton. Deep learning. *Nature*, 521(7553):436–444, 2015.

[237] Giorgio Nicola, Enrico Villagrossi, and Nicola Pedrocchi. Human-robot co-manipulation of soft materials: enable a robot manual guidance using a depth map feedback. *Proceedings of the 31st IEEE International Conference on Robot and Human Interactive Communication (RO-MAN)*, pages 498–504, 2022.

[238] Yago MR da Silva, Fabio AA Andrade, Lucas Sousa, Gabriel GR de Castro, João T Dias, Guido Berger, José Lima, and Milena F Pinto. Computer vision based path following for autonomous unammed aerial systems in unburied pipeline onshore inspection. *Drones*, 6(12):410–429, 2022.

[239] Adriano Scibilia, Nicola Pedrocchi, and Luigi Fortuna. Modeling of control delay in human-robot collaboration. *Proceedings of the 48th Annual Conference of the IEEE Industrial Electronics Society*, 2022. doi:10.1109/IECON49645.2022.9968477.

[240] Das Akash, Kumar Kumawat Piyush, and Dutt Chaturvedi Nitin. A study to target energy consumption in wastewater treatment plant using machine learning algorithms. *31st European Symposium on Computer Aided Process Engineering*, pages 1511–1516, 2021.

[241] Xiao-Dong Li, John KL Ho, and Tommy WS Chow. Approximation of dynamical time-variant systems by continuous-time recurrent neural networks. *IEEE Transactions on Circuits and Systems II: Express Briefs*, 52(10):656–660, 2005.

[242] Kyongmin Yeo and Igor Melnyk. Deep learning algorithm for data-driven simulation of noisy dynamical system. *Journal of Computational Physics*, 376:1212–1231, 2019.

[243] Yutaka Matsuo, Yann LeCun, Maneesh Sahani, Doina Precup, David Silver, Masashi Sugiyama, Eiji Uchibe, and Jun Morimoto. Deep learning, reinforcement learning, and world models. *Neural Networks*, 152:267–275, 2022.

[244] Richard S Sutton and Andrew G Barto. *Reinforcement learning: An introduction*. MIT press, 2018.

[245] Volodymyr Mnih, Koray Kavukcuoglu, David Silver, Andrei A Rusu, Joel Veness, Marc G Bellemare, Alex Graves, Martin Riedmiller, Andreas K Fidjeland, Georg Ostrovski, et al. Human-level control through deep reinforcement learning. *Nature*, 518(7540):529–533, 2015.

[246] Tie Zhang, Hanlei Sun, and Yanbiao Zou. An electromyography signals-based human-robot collaboration system for human motion intention recognition and realization. *Robotics and Computer-Integrated Manufacturing*, 77:102359–102374, 2022.

[247] Chengxi Li, Pai Zheng, Shufei Li, Yatming Pang, and Carman KM Lee. Ar-assisted digital twin-enabled robot collaborative manufacturing system with human-in-the-loop. *Robotics and Computer-Integrated Manufacturing*, 76:102321–102330, 2022.

[248] Yibing Wang, Long Wang, Jingqiu Guo, Ioannis Papamichail, Markos Papageorgiou, Fei-Yue Wang, Robert Bertini, Wei Hua, and Qinmin Yang. Ego-efficient lane changes of connected and automated vehicles with impacts on traffic flow. *Transportation Research part C: Emerging Technologies*, 138:103478–103503, 2022.

[249] Ryan Self, Moad Abudia, SM Nahid Mahmud, and Rushikesh Kamalapurkar. Model-based inverse reinforcement learning for deterministic systems. *Automatica*, 140:110242–110255, 2022.

[250] Giorgio Nicola and Stefano Ghidoni. Deep reinforcement learning for motion planning in human robot cooperative scenarios. *Proceedings of the 26th IEEE International Conference on Emerging Technologies and Factory Automation (ETFA)*, 2021. doi:10.1109/ETFA45728.2021.9613505.

[251] Julia Nilsson, Jonatan Silvlin, Mattias Brannstrom, Erik Coelingh, and Jonas Fredriksson. If, when, and how to perform lane change maneuvers on highways. *IEEE Intelligent Transportation Systems Magazine*, 8(4):68–78, 2016.

[252] Yaoqiong Du, Yizhou Wang, and Ching-Yao Chan. Autonomous lane-change controller via mixed logical dynamical. *Proceedings of the 17th International IEEE Conference on Intelligent Transportation Systems (ITSC)*, pages 1154–1159, 2014.

[253] Wei Liu, Seong-Woo Kim, Scott Pendleton, and Marcelo H Ang. Situation-aware decision making for autonomous driving on urban road using online pomdp. *2015 IEEE Intelligent Vehicles Symposium (IV)*, pages 1126–1133, 2015.

[254] Yingjun Ye, Xiaohui Zhang, and Jian Sun. Automated vehicle's behavior decision making using deep reinforcement learning and high-fidelity simulation environment. *Transportation Research Part C: Emerging Technologies*, 107:155–170, 2019.

[255] Abseen R Anya, Nagui M Rouphail, H Christopher Frey, and Bastian Schroeder. Application of aimsun microsimulation model to estimate emissions on signalized arterial corridors. *Transportation Research Record*, 2428(1):75–86, 2014.

[256] Tingting Li, Jianping Wu, and Ching-Yao Chan. Evolutionary learning in decision making for tactical lane changing. *2019 IEEE Intelligent Transportation Systems Conference (ITSC)*, pages 1826–1831, 2019.

[257] Simon Ulbrich and Markus Maurer. Towards tactical lane change behavior planning for automated vehicles. *Proceedings of the 18th International Conference on Intelligent Transportation Systems*, pages 989–995, 2015.

[258] Longsheng Jiang, Dong Chen, Zhaojian Li, and Yue Wang. Risk representation, perception, and propensity in an integrated human lane-change decision model. *IEEE Transactions on Intelligent Transportation Systems*, 23(12):23474–23487, 2022.

[259] Dale A Lawrence. Stability and transparency in bilateral teleoperation. *IEEE Transactions on Robotics and Automation*, 9(5):624–637, 1993.

[260] Braden P Murphy and Farshid Alambeigi. A surgical robotic framework for safe and autonomous data-driven learning and manipulation of an unknown deformable tissue with an integrated critical space. *Journal of Medical Robotics Research*, pages 2340001–2340016, 2023.

[261] Qing Gao, Jinyang Li, Yimin Zhu, Siyue Wang, Jingshu Liufu, and Jinguo Liu. Hand gesture teleoperation for dexterous manipulators in space station by using monocular hand motion capture. *Acta Astronautica*, 204:630–639, 2023.

[262] Krzysztof Adam Szczurek, Raul Marin Prades, Eloise Matheson, Jose Rodriguez-Nogueira, and Mario Di Castro. Mixed reality human-robot interface with adaptive communications congestion control for the teleoperation of mobile redundant manipulators in hazardous environments. *IEEE Access*, 10:87182–87216, 2022.

[263] Navvab Kashiri, Lorenzo Baccelliere, Luca Muratore, Arturo Laurenzi, Zeyu Ren, Enrico Mingo Hoffman, Malgorzata Kamedula, Giuseppe Francesco Rigano, Jorn Malzahn, Stefano Cordasco, et al. Centauro: A hybrid locomotion and high power resilient manipulation platform. *IEEE Robotics and Automation Letters*, 4(2):1595–1602, 2019.

[264] Shahin Sirouspour. Modeling and control of cooperative teleoperation systems. *IEEE Transactions on Robotics*, 21(6):1220–1225, 2005.

[265] A Rashidinejad, SKY Nikravesh, and HA Talebi. Nonlinear bilateral teleoperation with flexible-link slave manipulator. *Proceedings of the 3rd RSI International Conference on Robotics and Mechatronics (ICROM)*, pages 284–289, 2015.

[266] Shahin Sirouspour and Peyman Setoodeh. Multi-operator/multi-robot teleoperation: an adaptive nonlinear control approach. *Proceedings of the IEEE/RSJ International Conference on Intelligent Robots and Systems*, pages 1576–1581, 2005.

[267] Arash Ajoudani, Nikos Tsagarakis, and Antonio Bicchi. Tele-impedance: Teleoperation with impedance regulation using a body–machine interface. *The International Journal of Robotics Research*, 31(13):1642–1656, 2012.

[268] Adriano Scibilia, Marco Laghi, Elena De Momi, Luka Peternel, and Arash Ajoudani. A self-adaptive robot control framework for improved tracking and interaction performances in low-stiffness teleoperation. *Proceedings of the 18th International Conference on Humanoid Robots (Humanoids)*, pages 280–283, 2018. doi:10.1109/HUMANOIDS.2018.8625062.

[269] Huanqing Wang, Peter Xiaoping Liu, and Shichao Liu. Adaptive neural synchronization control for bilateral teleoperation systems with time delay and backlash-like hysteresis. *IEEE Transactions on Cybernetics*, 47(10):3018–3026, 2017.

[270] Yana Yang, Changchun Hua, and Xinping Guan. Adaptive fuzzy finite-time coordination control for networked nonlinear bilateral teleoperation system. *IEEE Transactions on Fuzzy Systems*, 22(3):631–641, 2013.

[271] Hyeonbeom Lee and H Jin Kim. Trajectory tracking control of multirotors from modelling to experiments: A survey. *International Journal of Control, Automation and Systems*, 15(1):281–292, 2017.

[272] Gabriel Hoffmann, Steven Waslander, and Claire Tomlin. Quadrotor helicopter trajectory tracking control. *AIAA Guidance, Navigation and Control Conference and Exhibit*, pages 7410–7424, 2008.

[273] Samir Bouabdallah, Andre Noth, and Roland Siegwart. Pid vs lq control techniques applied to an indoor micro quadrotor. *2004 IEEE/RSJ International Conference on Intelligent Robots and Systems (IROS)*, 3:2451–2456, 2004.

[274] Ian D Cowling, Oleg A Yakimenko, James F Whidborne, and Alastair K Cooke. Direct method based control system for an autonomous quadrotor. *Journal of Intelligent & Robotic Systems*, 60(2):285–316, 2010.

[275] Zachary T Dydek, Anuradha M Annaswamy, and Eugene Lavretsky. Adaptive control of quadrotor uavs: A design trade study with flight evaluations. *IEEE Transactions on Control Systems Technology*, 21(4):1400–1406, 2012.

[276] Michael A Henson and Dale E Seborg. Feedback linearizing control. *Nonlinear Process Control*, 4:149–231, 1997.

[277] Daewon Lee, H Jin Kim, and Shankar Sastry. Feedback linearization vs. adaptive sliding mode control for a quadrotor helicopter. *International Journal of Control, Automation and Systems*, 7(3):419–428, 2009.

[278] Abdellah Mokhtari, Nacer K M'Sirdi, Kamal Meghriche, and Abdelkader Belaidi. Feedback linearization and linear observer for a quadrotor unmanned aerial vehicle. *Advanced Robotics*, 20(1):71–91, 2006.

[279] Pedro Castillo, Pedro Albertos, Pedro Garcia, and Rogelio Lozano. Simple real-time attitude stabilization of a quad-rotor aircraft with bounded signals. *Proceedings of the 45th IEEE Conference on Decision and Control*, pages 1533–1538, 2006.

[280] Samir Bouabdallah and Roland Siegwart. Backstepping and sliding-mode techniques applied to an indoor micro quadrotor. *Proceedings of the 2005 IEEE International Conference on Robotics and Automation*, pages 2247–2252, 2005.

[281] İ Can Dikmen, Aydemir Arisoy, and Hakan Temeltas. Attitude control of a quadrotor. *Proceedings of the 4th International Conference on Recent Advances in Space Technologies*, pages 722–727, 2009.

[282] Patrick Adigbli, Christophe Grand, Jean-Baptiste Mouret, and Stephane Doncieux. Nonlinear attitude and position control of a micro quadrotor using sliding mode and backstepping techniques. In *7th European Micro Air Vehicle Conference (MAV07)*, pages 1–9, 2007.

[283] Tarek Madani and Abdelaziz Benallegue. Control of a quadrotor mini-helicopter via full state backstepping technique. *Proceedings of the 45th IEEE Conference on Decision and Control*, pages 1515–1520, 2006.

[284] Abhijit Das, Frank Lewis, and Kamesh Subbarao. Backstepping approach for controlling a quadrotor using lagrange form dynamics. *Journal of Intelligent and Robotic Systems*, 56(1):127–151, 2009.

[285] Bin Xian, Shizhang Wang, and Sen Yang. Nonlinear adaptive control for an unmanned aerial payload transportation system: theory and experimental validation. *Nonlinear Dynamics*, 98(3):1745–1760, 2019.

[286] Chih-Lyang Hwang and Hailay Berihu Abebe. Generalized and heterogeneous nonlinear dynamic multiagent systems using online rnn-based

finite-time formation tracking control and application to transportation systems. *IEEE Transactions on Intelligent Transportation Systems*, 23(8):13708–13720, 2021.

[287] Marilena D Pavel, Pierangelo Masarati, Massimo Gennaretti, Michael Jump, Larisa Zaichik, Binh Dang-Vu, Linghai Lu, Deniz Yilmaz, Giuseppe Quaranta, Achim Ionita, et al. Practices to identify and preclude adverse aircraft-and-rotorcraft-pilot couplings–a design perspective. *Progress in Aerospace Sciences*, 76:55–89, 2015.

[288] Bernard B. Munyazikwiye, Dmitry Vysochinskiy, Mikhail Khadyko, and Kjell G. Robbersmyr. Prediction of vehicle crashworthiness parameters using piecewise lumped parameters and finite element models. *Designs*, 2(4):43–59, 2018.

[289] PR Payne and EL Stech. Dynamic models of the human body technical report, sep. 1962-feb. 1964. Technical report, AMRL, 1969.

[290] Wael Abbas, Ossama B Abouelatta, Magdi El-Azab, Mamdouh Elsaidy, Adel A Megahed, et al. Optimization of biodynamic seated human models using genetic algorithms. *Engineering*, 2(09):710–720, 2010.

[291] Lin-An XU, Zhong-Hua LIU, Xiao-Ling LI, et al. Dynamic modeling and vibration characteristics of multi-dof upper part system of seated human body. *Chinese Journal of Engineering Design*, 15(4):244–249, 2008.

[292] Andrea Zanoni, Alessandro Cocco, and Pierangelo Masarati. Multibody dynamics analysis of the human upper body for rotorcraft–pilot interaction. *Nonlinear Dynamics*, 102(3):1517–1539, 2020.

[293] Masami Iwamoto, Yoshikatsu Kisanuki, Isao Watanabe, Katsuya Furusu, Kazuo Miki, and Junji Hasegawa. Development of a finite element model of the total human model for safety (thums) and application to injury reconstruction. *Proceedings of the International IRCOBI Conference*, pages 18–20, 2002.

[294] Philippe Vezin and Jean Pierre Verriest. Development of a set of numerical human models for safety. *Proceedings of the 19th International Technical Conference on the Enhanced Safety of Vehicles (ESV)*, (05–0163):16–32, 2005.

[295] K von Merten. Using humos2 model for the reconstruction of accidents with thoracical injuries. *Journal of Biomechanics*, 39(Supplement 1):S165–S175, 2006.

[296] M Toma, FEA Njilie, M Ghajari, and U Galvanetto. Assessing motorcycle crash-related head injuries using finite element simulations. *International Journal of Simulation Modelling*, 9(3):143–151, 2010.

[297] Doron Schwartz, Berkan Guleyupoglu, Bharath Koya, Joel D Stitzel, and F Scott Gayzik. Development of a computationally efficient full human body finite element model. *Traffic Injury Prevention*, 16(sup1):S49–S56, 2015.

[298] Stephen A Billings. *Nonlinear system identification: NARMAX methods in the time, frequency, and spatio-temporal domains*. John Wiley & Sons, 2013.

[299] EG Nepomuceno and SAM Martins. A lower bound error for free-run simulation of the polynomial narmax. *Systems Science & Control Engineering*, 4(1):50–58, 2016.

[300] Wilson Rocha Lacerda, Luan Pascoal Costa da Andrade, Samuel Carlos Pessoa Oliveira, and Samir Angelo Milani Martins. Sysidentpy: A python package for system identification using narmax models. *Journal of Open Source Software*, 5(54):2384, 2020.

[301] LUIS A Aguirre, Giovani G Rodrigues, and Cristiano RF Jácome. Identificaçao de sistemas nao lineares utilizando modelos narmax polinomiais–uma revisao e novos resultados. *SBA Controle e Automação*, 9(2):90–106, 1998.

[302] WR Junior, Samir Angelo Milani Martins, and Erivelton G Nepomuceno. Meta-model structure selection: Building polynomial narx model for regression and classification. *arXiv preprint arXiv:2109.09917*, 2021.

[303] Abolfazl Hashemi and Haris Vikalo. Accelerated orthogonal least-squares for large-scale sparse reconstruction. *Digital Signal Processing*, 82:91–105, 2018.

[304] Abd AlRahman R AlMomani, Jie Sun, and Erik Bollt. How entropic regression beats the outliers problem in nonlinear system identification. *Chaos: An Interdisciplinary Journal of Nonlinear Science*, 30(1), 2020.

[305] Alexander Kraskov, Harald Stögbauer, and Peter Grassberger. Estimating mutual information. *Physical review E*, 69(6):066138, 2004.

[306] Ronald DeVore, Boris Hanin, and Guergana Petrova. Neural network approximation. *Acta Numerica*, 30:327–444, 2021.

[307] Irina Higgins. Generalizing universal function approximators. *Nature Machine Intelligence*, 3(3):192–193, 2021.

[308] Kurt Hornik. Approximation capabilities of multilayer feedforward networks. *Neural networks*, 4(2):251–257, 1991.

[309] Anton Maximilian Schäfer and Hans-Georg Zimmermann. Recurrent neural networks are universal approximators. *International journal of neural systems*, 17(04):253–263, 2007.

[310] Guohao Shen, Yuling Jiao, Yuanyuan Lin, and Jian Huang. Approximation with cnns in sobolev space: with applications to classification. *Advances in Neural Information Processing Systems*, 35:2876–2888, 2022.

[311] Balázs Csanád Csáji et al. Approximation with artificial neural networks. *Faculty of Sciences, Etvs Lornd University, Hungary*, 24(48):7, 2001.

[312] Edward N Lorenz. Deterministic nonperiodic flow. *Journal of atmospheric sciences*, 20(2):130–141, 1963.

[313] Steven H Strogatz. Norbert wienerâs brain waves. In *Frontiers in mathematical biology*, pages 122–138. Springer, 1994.

[314] Floris Takens. Dynamical systems and turbulence. *Warwick, 1980*, pages 366–381, 1981.

[315] Matteo Candaten and Sergio Rinaldi. Peak-to-peak dynamics in food chain models. *Theoretical Population Biology*, 63(4):257–267, 2003.

[316] Gustav Feichtinger, Christian V Forst, and Carlo Piccardi. A nonlinear dynamical model for the dynastic cycle. *Chaos, Solitons & Fractals*, 7(2):257–271, 1996.

[317] Carlo Piccardi and Gustav Feichtinger. Peak-to-peak dynamics in the dynastic cycle. *Chaos, Solitons & Fractals*, 13(2):195–202, 2002.

[318] Carlo Piccardi. Parameter estimation for systems with peak-to-peak dynamics. *International Journal of Bifurcation and Chaos*, 18(03):745–753, 2008.

[319] Carlo Piccardi. Controlling chaotic oscillations in delay-differential systems via peak-to-peak maps. *IEEE Transactions on Circuits and Systems I: Fundamental Theory and Applications*, 48(8):1032–1037, 2001.

[320] Mohammad Karami, Mohammadreza Abbasi, and Gholamreza Vossoughi. Design of a continuous fractional-order nonsingular terminal sliding mode control with time delay estimation for fes control of human knee joint. In *2021 7th International Conference on Control, Instrumentation and Automation (ICCIA)*, pages 1–5. IEEE, 2021.

[321] Erwin R Boer and Robert V Kenyon. Estimation of time-varying delay time in nonstationary linear systems: an approach to monitor human operator adaptation in manual tracking tasks. *IEEE Transactions on Systems, Man, and Cybernetics-Part A: Systems and Humans*, 28(1):89–99, 1998.